HAL open science

Effective calculations in nonlinear geometric problems

Boris Thibert

To cite this version:

Boris Thibert. Effective calculations in nonlinear geometric problems. Mathematics [math]. Université Grenoble Alpes, 2015. tel-01884562

HAL Id: tel-01884562

https://hal.science/tel-01884562v1

Submitted on 2 Oct 2018

HAL is a multi-disciplinary open access archive for the deposit and dissemination of scientific research documents, whether they are published or not. The documents may come from teaching and research institutions in France or abroad, or from public or private research centers.

L'archive ouverte pluridisciplinaire **HAL**, est destinée au dépôt et à la diffusion de documents scientifiques de niveau recherche, publiés ou non, émanant des établissements d'enseignement et de recherche français ou étrangers, des laboratoires publics ou privés.

UNIVERSITÉ DE GRENOBLE

HABILITATION A DIRIGER DES RECHERCHES

Spécialité : **Mathématiques appliquées**

Arrêté ministériel : 23 novembre 1988

Présentée par

Boris Thibert

préparée au sein du **Laboratoire Jean Kuntzmann**
et de l'**École doctorale MSTII**

Effective calculations in nonlinear geometric problems

Habilation soutenue le **29 juin 2015** devant le jury composé de:

Mr. Joseph Fu
Professeur, Georgia University, Rapporteur
Mr. Bruno Levy
Directeur de Recherche, INRIA, Rapporteur
Mr. Gabriel Peyré
Directeur de Recherche, CNRS, Rapporteur
Éric Bonnetier
Professeur, Université Joseph Fourier, Grenoble, Examinateur
Mr. Simon Masnou
Professeur, Université Claude Bernard, Lyon , Examinateur
Hervé Pajot
Professeur, Université Joseph Fourier, Grenoble, Examinateur
Konrad Polthier
Professeur, Freie Universität, Berlin, Examinateur

Table of Contents

Introduction (in French) **1**

Introduction **9**

Publications **15**

1 Geometric inference using distance functions **17**
1.1 Distance functions, reach and μ-reach 19
1.2 Convergence of geodesics 23
1.3 Double offset regularity 29
1.4 Stability of curvature measures 33
1.5 Application in digital geometry 39

2 Generalized Voronoi Covariance Measure **45**
2.1 Background on distance-like functions and VCM 46
2.2 δ-Voronoi Covariance Measure 49
2.3 Computation and Experiments 51
2.4 Digital Voronoi Covariance Measure in $\mathbb{R}^3$ 51
2.5 Perspectives 53

3 Reflector problem and numerical optimal transport **55**
3.1 Intersection of confocal paraboloids of revolution 57
3.2 Other types of union and intersections 59
3.3 Computing the intersection of a power diagram with a sphere 60
3.4 Numerical resolution and semi-discrete optimal transport 61
3.5 Industrial design constraints 63
3.6 Perspectives 65

4 Convex Integration Theory and Smooth Fractals **67**
4.1 One-dimensional Convex Integration and corrugations 69
4.2 Construction of an embedding of the square flat torus 72
4.3 Smooth fractals 78
4.4 More images 81
4.5 Perspectives 82

Introduction

Je présente dans ce mémoire ma contribution à la géométrie numérique depuis mon arrivée à Grenoble en 2005 comme maître de conférences. Dans la continuité de mes travaux de thèse, j'ai travaillé sur des problèmes d'inférence géométrique ainsi que sur divers problèmes de modélisation de surfaces ayant des connections avec des domaines variés tels que le *transport optimal*, la *géométrie algorithmique* ou la *théorie de l'intégration convexe*. Le point commun de ma contribution dans ces domaines est le développement de calculs effectifs dans des problèmes géométriques. Dans tous les cas, le but est de certifier la construction d'objets géométriques, tels que des variétés ou des triangulations, ou d'estimer précisément des quantités reliées à la métrique, la courbure, ou d'autres invariants géométriques.

Les contraintes géométriques apparaissant dans des problèmes de modélisation de surface peuvent parfois s'exprimer avec des *équations aux dérivées partielles* (EDP). Cependant, les méthodes numériques standards, comme les méthodes d'éléments finis, ne permettent pas toujours d'obtenir une solution. J'ai travaillé ces dernières années sur des approches géométriques alternatives permettant de résoudre certaines EDP non linéaires. Je mentionne ci-dessous deux exemples :

— Le *problème du réflecteur en champ lointain* est un problème bien connu d'*optique anidolique* consistant à créer la surface d'un réflecteur avec une contrainte de préservation d'énergie. Le but est de créer un miroir qui envoie une source de lumière ponctuelle sur une cible de lumière prescrite à l'infini. Quand la source de lumière et la lumière cible sont modélisées par des densités de probabilité sur la sphère, ce problème est équivalent à une équation de type Monge-Ampère sur la sphère. En combinant une approche variationnelle venant du transport optimal avec des outils de géométrie algorithmique et une construction géométrique due à L. A. Caffarelli et V. Oliker, nous avons proposé une méthode efficace de résolution numérique de ce problème.

— Un autre exemple impliquant une EDP est celui de la réalisation d'un plongement isométrique du tore carré plat dans l'espace euclidien de dimension trois. Dans ce cas, la contrainte isométrique est exprimée par une EDP non linéaire impliquant le tenseur de métrique. L'outil théorique principal que nous avons utilisé est celui de la *théorie de l'intégration convexe*, qui a été développé par M. Gromov dans les années 70-80 pour résoudre de manière générale des systèmes différentiels sous-déterminés. Nous avons implémenté cet outil afin d'obtenir un algorithme de construction d'un plongement isométrique du tore carré plat dans l'espace ambiant.

Les méthodes numériques standards permettant de résoudre efficacement les EDP linéaires ne sont pas forcément adaptées à la résolution d'EDP non linéaires, et l'utilisation de méthodes alternatives peut s'avérer efficace. De même, certaines quantités géométriques, comme la courbure, sont bien définies sur des objets suffisamment réguliers, mais ne peuvent pas être définies directement en l'absence d'une telle régularité. Des approches alternatives, venant par exemple de *théorie géométrique de la mesure*, permettent de prendre en compte cette faible régularité. Dans mes recherches, j'ai été amené à considérer des objets géométriques ayant une régularité assez faible, comme des variétés plongées de classe C^1, des triangulations ou des nuages de points. J'ai aussi considéré différents types de bruits dans des problématiques d'inférence géométrique, qui doivent également être appréhendés avec des approches appropriées. Dans ce contexte, j'ai été amené à utiliser et à développer des outils de différents domaines, tels que la géométrie algorithmique, le transport optimal, l'analyse convexe et la théorie de l'intégration convexe, afin de résoudre des problèmes de modélisation de surface satisfaisant des contraintes géométriques, et de garantir les calculs effectués. Je mentionne ci-dessous trois exemples.

— Un des buts de l'inférence géométrique est d'estimer certaines quantités d'objets géométriques, à partir d'approximations qui peuvent avoir une faible régularité, comme des triangulations ou des nuages de point. En combinant et en établissant des propriétés de stabilité et de régularité des fonctions distances, nous avons obtenu un résultat de stabilité assez général des mesures de courbure de Federer. L'algorithme que nous proposons pour calculer ces mesures de courbure à partir d'un nuage de points est basé sur des outils classiques de géométrie algorithmique.
— Les fonctions distances à des compacts ont été beaucoup utilisées dans le contexte de l'inférence géométrique pour l'estimation de quantités géométriques d'une forme à partir d'un objet proche pour la distance de Hausdorff. Cependant, quand les données contiennent des points aberrants, l'hypothèse de proximité pour la distance de Hausdorff n'est pas satisfaite. Nous avons utilisé la *distance à une mesure*, qui est une fonction distance généralisée robuste aux points aberrants, pour estimer de manière robuste la géométrie d'une forme. Les calculs sur des nuages de points utilisent la notion de *diagramme de puissance*, qui est un outil central de géométrie algorithmique.
— La problématique du plongement isométrique est intrinsèquement liée à des problèmes de régularité. Un argument classique basé sur le Theorema

Egregium et sur la courbure de Gauss montre qu'un plongement isométrique du tore carré plat dans l'espace euclidien de dimension trois ne peut pas être de classe C^2. Cependant, le théorème de Nash-Kuiper implique qu'il est possible de réaliser un tel plongement avec une régularité C^1. La construction du plongement que nous proposons est basée sur la théorie de l'intégration convexe et a permis de révéler une structure inattendue, celle de *fractale lisse*. On peut remarquer que cette théorie a aussi été utilisée pour le paradoxe de Sheffer-Shnirelman, pour construire des solutions faibles non triviales de l'équation d'Euler incompressible. La théorie de l'intégration convexe peut être vue comme un outil permettant de construire des solutions paradoxales.

DESCRIPTION DES CHAPITRES

Chapitre 1: Inférence géométrique basée sur la fonction distance

Le but de l'inférence géométrique est de répondre à la question suivante: à partir d'un objet géométrique dans $\mathbb{R}^d$ connu uniquement à travers une approximation, comme par exemple un nuage de points, peut-on estimer de manière robuste ses propriétés topologiques et géométriques ? Les fonctions de distance à des compacts ont été abondemment utilisées ces quinze dernières années dans ce contexte, de par leurs propriétés de régularité et de stabilité. Dans ce chapitre, nous présentons plusieurs résultats d'inférence géométrique basés sur la fonction distance.

Nous avons établi avec André Lieutier un résultat de convergence de géodésiques sur des triangulations [13]. Plus précisément, étant donné une suite $(T_n)_{n\geq 0}$ de triangulations dont les points et les normales convergent vers ceux d'une surface S de classe C^2 dans l'espace euclidien de dimension trois, et une suite de courbes géodésiques C_n de T_n qui converge vers une courbe limite, nous montrons que la courbe limite est une géodésique de S sous une hypothèse de vitesse de convergence des normales et de vitesse de convergence des longueurs des arêtes des triangulations. Comme les géodésiques que nous considérons ne sont pas forcément des plus courts chemins, la preuve ne peut pas uniquement reposer sur des notions métriques et nous avons été amenés à introduire une notion de courbure géodésique discrète.

Nous avons étudié avec Frédéric Chazal, David Cohen-Steiner et André Lieutier la régularité des voisinages tubulaires et des "double offset" des compacts de $\mathbb{R}^d$ [5]. Le r-voisinage tubulaire d'un compact est l'ensemble des points à distance inférieure ou égale à r de K. Le double offset d'un compact est obtenu en prenant le r-voisinage tubulaire du compact, puis en prenant le t-voisinage tubulaire de l'adhérence de son complémentaire, avec $t < r$. Il est bien connu dans la communauté de Computer Aided Geometric Design qu'une forme peut être lissée en appliquant cette opération de "double offset". Dans le cas où un compact est à

μ-reach positif, qui est une hypothèse très faible de régularité, nous quantifions la régularité de son voisinage tubulaire et de son "double offset".

Nous utilisons ces résultats de régularité en inférence géométrique. Nous montrons que les mesures de courbure du voisinage tubulaire d'un compact K à μ-reach positif peuvent être estimées par les mesures de courbure d'un voisinage tubulaire d'un compact K' qui est proche de K au sens de Hausdorff [6]. Nous montrons comment calculer ces mesures de courbure sur une union de boules. Les mesures de courbures du voisinage tubulaire d'un compact K à μ-reach positif peuvent ainsi être approchées par celles du voisinage tubulaire d'un nuage de points.

En collaboration avec Jacques-Olivier Lachaud, nous avons considéré des problèmes d'inférence géométrique dans le contexte de la géométrie digitale, c'est à dire quand les formes sont digitalisées et approchées par des ensembles de voxels (*i.e.* pixels de dimension d) de taille h. Nous étudions la topologie du bord de l'ensemble digital et établissons un résultat de convergence d'intégration sur des ensembles digitaux [12].

Chapitre 2: Mesure de covariance de Voronoi généralisée

Les résultats d'inférence géométrique du premier chapitre découlent des propriétés de régularité et de stabilité (par rapport à la distance de Hausdorff) des fonctions de distance. Malheureusement, les données sont souvent perturbées par des points aberrants et l'hypothèse de proximité pour la distance de Hausdorff n'est pas toujours réaliste en pratique. Les fonctions *distance-like* ont été introduites récemment dans le contexte de l'inférence géométrique car elles possèdent les mêmes propriétés de régularité que les fonctions distances [CCSM11], à savoir elles sont Lipschitz et 1-semiconcaves. L'ensemble des fonctions distance-like contient les fonctions distances aux compacts, mais aussi d'autres fonctions comme les fonctions *distance à une mesure* qui sont robustes aux points aberrants [CCSM11].

La *mesure de covariance de Voronoi* (VCM) a été introduite dans [MOG11] pour l'estimation de normales, de courbures et d'arêtes vives. Elle est définie pour tout compact K et est stable pour la distance de Hausdorff, au sens où si deux compacts sont proches au sens de Hausdorff, alors leurs VCM sont également proches l'une de l'autre. De plus, la VCM d'une surface lisse contient de l'information sur le champ de vecteurs normal à la surface.

Avec Louis Cuel, Jacques-Olivier Lachaud and Quentin Mérigot, nous avons généralisé la mesure de covariance de Voronoi aux fonctions distance-like [7]. Plus précisément, nous associons à n'importe quelle fonction distance-like δ une mesure à valeur dans l'ensemble des tenseurs, notée δ-VCM. Nous montrons un résultat de stabilité du δ-VCM qui implique que l'on peut retrouver précisément les normales d'une sous-variété S de $\mathbb{R}^d$ à partir du δ-VCM, si δ est une distance à une mesure proche de la distance à la mesure de probabilité uniforme sur S (pour la distance de Wasserstein). Cette estimation est stable pour la distance de Hausdorff et robuste aux points aberrants. Nous proposons aussi un algorithme de calcul du δ-VCM, quand la fonction distance-like δ est encodée par un nuage de

points pondéré de petite taille, et nous l'utilisons pour l'estimation de normales et d'arêtes vives. Avec Louis Cuel et Jacques-Olivier Lachaud, nous avons également utilisé le VCM dans le contexte de la géométrie digitale [8].

Chapitre 3: Problème du réflecteur et transport optimal numérique

Dans le *problème du réffecteur en champ lointain*, les données sont la description d'une distribution de lumière émise par une source de lumière ponctuelle localisée à l'origine et une distribution de lumière souhaitée à l'infini, c'est à dire sur la sphère des directions. Si on modélise les deux distributions de lumière par des densités de probabilité μ sur la sphère source et ν sur la sphère cible, le problème du réflecteur en champ lointain peut se formuler comme une équation de Monge-Ampère généralisée sur la sphère. L'approche de L. A. Caffarelli and V. Oliker pour montrer l'existence d'une solution faible à ce problème est géométrique et fonctionne de la manière suivante [CO08] : ils approchent la mesure de probabilité cible ν par une suite de mesures discrètes $\nu_N = \sum_i \alpha_i \delta_{y_i}$ supportées par un ensemble fini de directions $Y = \{y_1, \ldots, y_N\}$. Ils montrent l'existence d'une solution du problème du réflecteur (semi-discret) entre μ et ν_N et montrent que cette solution converge vers une solution du problème original quand N tend vers l'infini. Plus récemment, il a été montré que le problème du réflecteur en champ lointain est équivalent à un problème de transport optimal sur la sphère pour le coût $c : \mathcal{S}^{d-1} \times \mathcal{S}^{d-1} \to \mathbb{R}$ défini par $c(x, y) := -\log(1 - \langle x|y\rangle)$ [GO03, Wan04].

PROBLÈME DU RÉFLECTEUR EN CHAMP LOINTAIN : Simulation de l'illumination à l'infini avec le moteur de rendu physiquement réaliste LUXRENDER. La mesure μ est uniforme et supportée par une demi-sphère. La mesure ν_N correspond à la discrétisation d'une image de Monge sur la sphère cible. Les expériences ont été réalisées avec $N = 1000$ à gauche et $N = 15000$ à droite.

Avec Pedro Machado Manhães de Castro et Quentin Mérigot, nous avons proposé une résolution numérique du problème du réflecteur dans le cas semi-discret [10].

En utilisant une formulation basée sur le transport optimal, nous transformons ce problème en un problème de maximisation concave. Notre algorithme nécessite le calcul de cellules de Laguerre sur la sphère, qui correspondent au c-sous-différentiel de la variable duale dans la formulation duale du transport optimal. Nous montrons que ces cellules de Laguerre peuvent être obtenues en intersectant un diagramme de puissance avec la sphère unité and montrons que la complexité de cette intersection est linéaire. Nous considérons également d'autres types de réflecteurs intervenant dans des problèmes d'optique anidolique, par exemple dans le *problème du réflecteur en champ proche*, où l'on souhaite éclairer des points dans l'espace et non pas des directions.

Avec André Julien, Dominique Attali and Quentin Mérigot, nous avons aussi proposé des heuristiques qui prennent en compte des contraintes de modélisation industrielles [1].

Chapitre 4: intégration convexe et fractales lisses

Une application f d'une variété riemannienne (M^n, g) dans un espace euclidien $\mathbb{E}^q = (\mathbb{R}^q, \langle ., . \rangle)$ est une isométrie si elle préserve les distances, *i.e.* si la longueur de chaque courbe $\gamma : [a, b] \to M^n$ de classe C^1 est égale à la longueur de son image $f \circ \gamma$. Si la métrique est donnée dans un système de coordonnées locales par $g = \sum_{i,j}^n g_{ij} \mathrm{d}x_i \mathrm{d}x_j$, la condition d'isométrie est équivalente au système non linéaire d'équations aux dérivées partielles

$$\langle \frac{\partial f}{\partial x_i}, \frac{\partial f}{\partial x_j} \rangle = g_{ij}, \quad 1 \leq i \leq j \leq n \tag{1}$$

de $s_n = \frac{n(n+1)}{2}$ équations. En 1954, J. Nash a surpris la communauté mathématique en montrant qu'il était possible de réaliser un plongement isométrique $f : (M^n, g) \to \mathbb{E}^q$ d'une variété riemannienne compacte si $q \geq n + 2$, mais seulement avec une régularité C^1 [Nas54]. Des arguments reposant sur la courbure empêchent d'avoir une régularité C^2 en général. En 1955, le théorème de Nash a été étendu par Kuiper à la codimension 1 [Kui55]. Le résultat de Nash et Kuiper a beaucoup de conséquences contre-intuitives, l'une d'entre elles étant que le tore carré plat $\mathbb{E}^2/\mathbb{Z}^2$ admet un plongement isométrique C^1 dans $\mathbb{E}^3$.

Le résultat de Nash et de Kuiper, ainsi que d'autres résultats géométriques, ont été revisités dans les années 70-80 par M. Gromov. Il a introduit le h-principe qui établit que beaucoup de *relations différentielles* se ramènent à des problèmes topologiques [GR70, Gro86] et a développé plusieurs outils pour résoudre ces relations différentielles, l'un d'entre eux étant la *théorie de l'intégration convexe*.

Avec Vincent Borrelli, Said Jabrane et Francis Lazarus, nous avons adapté la théorie de l'intégration convexe à la *relation différentielle des isométries* (1) afin d'obtenir un algorithme de construction d'un plongement isométrique du tore carré plat dans $\mathbb{E}^3$. Nous présentons des images d'un tel plongement. Cette visualisation, ainsi que la simplification de la construction, nous a amené à découvrir la notion de *fractales lisses*, qui est liée à la structure géométrique de l'application de Gauss (*i.e.* le champ de vecteurs normal) du plongement limite. Nous montrons que cette application de Gauss peut être obtenue par un produit infini de

rotations appliqué à un plongement initial. Bien que les coefficients des rotations soient intrinsèquement compliqués, le comportement asymptotique de ce produit est relativement simple et présente une certaine similarité avec la fonction de Weierstrass.

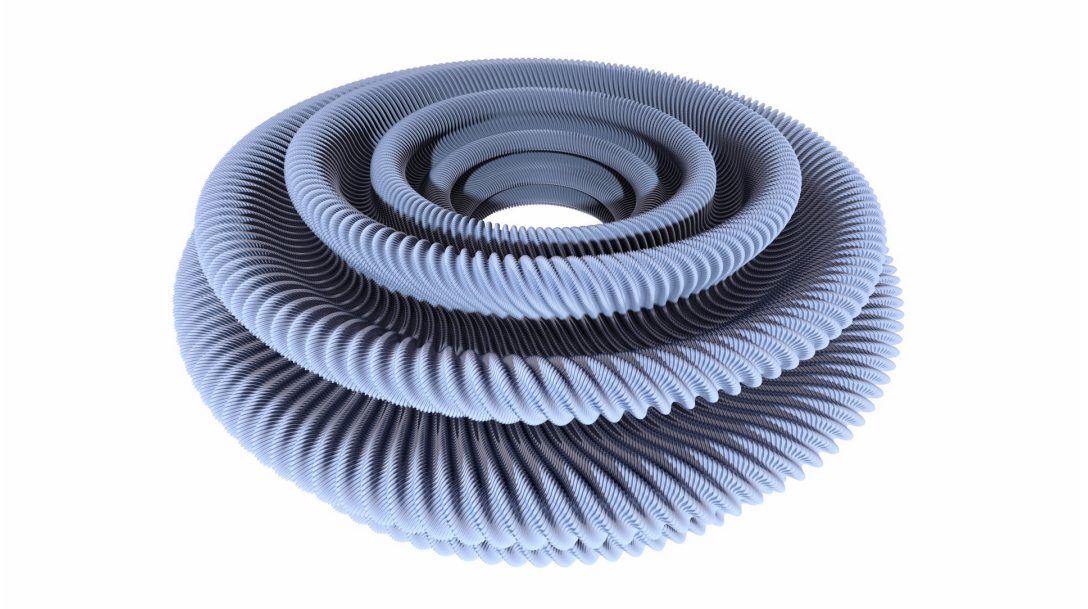

Image d'un plongement isométrique du tore carré plat dans $\mathbb{E}^3$

Introduction

In this dissertation, I present my contributions to numerical geometry since my arrival in Grenoble in 2005 as an Assistant Professor. I have been working in the field of *geometric inference* in the continuation of my PhD and also on different problems of surface modeling having connections with various domains such as *optimal transport*, *computational geometry* or *convex integration theory*. The common point to my contribution in these fields is the development of effective calculations in problems having a geometric flavor. In all the cases, the aim is to certify the construction of geometric objects, such as manifolds or triangulations, or to accurately estimate quantities related for example to the metric, the curvature, or any other geometric invariant.

The geometric constraints that appear in surface modeling can sometimes be expressed by *partial differential equations* (PDE). However standard numerical approaches, such as finite element methods, do not always provide a solution. I have investigated these last years alternative geometric approaches for numerically solving nonlinear geometric PDEs. I mention below two examples.

— The far-field reflector problem is a well-known inverse problem arising in nonimaging optics that consists in designing a reflector surface that satisfies an energy preservation constraint. The goal is to create a mirror that reflects a given point light source to a prescribed target light at infinity. When the source and target lights are modeled by two probability densities on the sphere, this problem amounts to solve a Monge-Ampere type equation on the sphere, which is a nonlinear PDE. By combining a variational approach from optimal transport, computational geometry and a geometric construction due to L. A. Caffarelli and V. Oliker, we have proposed an efficient method to numerically solve this problem.

— Another example involving a PDE is the realization of an isometric embedding of the square flat torus in the three dimensional Euclidean space. In that case, the isometric constraint is expressed by a nonlinear PDE system involving the metric tensor. Our main theoretical tool is the *convex integra-*

tion theory that has been developed by M. Gromov in the 70s-80s for solving underdeterminated differential systems. We have implemented this tool so as to get an algorithm for building isometric embeddings of the square flat torus in the ambient space.

The standard numerical methods that are efficient for solving linear PDEs may not be adapted when PDEs are not anymore linear. As mentioned above, the use of geometric approaches can then be helpful. Similarly, geometric quantities such as curvatures are well defined on "regular" objects, but cannot be defined directly when the regularity is too weak. Alternative approaches, coming for example from *geometric measure theory*, then allow to take into account this low regularity. In this dissertation, I consider geometric objects with low regularities, such as manifolds of class C^1, triangulations and even point sets. I also consider different kind of noises in geometric inference problems, that again need to be handled appropriately. In this context, I have been using and developing tools from different fields, such as computational geometry, optimal transport, convex analysis and convex integration in order to solve problems of surface modeling with prescribed geometric constraints and to provide certified effective estimations. I mention some examples below.

— In geometric inference, one often wants to estimate geometric quantities on shapes such as manifolds, from approximations that can have a low regularity, such as triangulations or point sets. By combining stability and regularity properties of distance functions, we prove a stability result for Federer's curvature measures. Our algorithm to compute these curvatures for finite point sets is using tools from computational geometry.

— Distance functions have been extensively used in the context of geometric inference to provide geometric estimations for a shape from an Hausdorff approximation. However, when the data are corrupted with *outliers*, the assumption of proximity for the Hausdorff distance is not satisfied. We have been using the *distance to a measure*, which is a generalized distance function robust to outliers, to provide robust estimation of the normals of a shape. The computations on a point set involves the *power diagram*, which is a central tool in computational geometry.

— The isometric embedding problematic is intrinsically related to regularity problems. A classical argument based on Theorema Egregium and the Gaussian curvature implies that an isometric embedding of the square flat torus in the three dimensional Euclidean space cannot be of class C^2. However, the Nash-Kuiper Theorem asserts that it is possible to realize such an embedding with a C^1 regularity. The construction that we propose is using the convex integration theory and has allowed to reveal the paradoxal notion of *smooth fractals*. Remark that this theory has also been used for the Scheffer–Shnirelman paradox, to provide non trivial weak solutions to the incompressible Euler equation. The convex integration theory can be seen as a tool to provide paradoxical solutions.

BRIEF OVERVIEW OF MY CONTRIBUTIONS

Chapter 1: Geometric inference using distance functions

The aim of geometric inference is to answer the following question: Given a geometric object in $\mathbb{R}^d$ that is only known through an approximation, such as a point set, can we get a robust estimation of its topological or geometric properties? Distance functions to compact sets have been extensively used in this context the last fifteen years, thanks to their regularity properties and Hausdorff stability properties. By Hausdorff stability, we mean that if two compact sets are close for the Hausdorff distance, then their distance functions are close for the supremum norm. In this chapter, we present several results of geometric inference that are based on distance functions.

Together with André Lieutier, we have provided a result of convergence of geodesics on triangulations [13] . More precisely, given a sequence $(T_n)_{n\geq 0}$ of triangulations whose points and normals converge to those of a surface S of class C^2 in the three dimensional space, and a sequence of geodesic curves C_n on T_n that is converging to a limit curve, we show that the limit curve is a geodesic of S under reasonable assumptions concerning the rate of convergence of the normals and of the edges of the triangulation. Since we consider geodesics that are not necessarily shortest paths, the proof cannot only rely on metric notions and we are led to introduce a discrete notion of geodesic curvature.

With my co-authors Frédéric Chazal, David Cohen-Steiner and André Lieutier, we have studied the regularity of the offset and double offset of compact sets of $\mathbb{R}^d$ [5]. The r-offset of a compact set K is the set of points that are at a distance less than r from K. The double offset of a compact set is obtained by offsetting it with a parameter r, then offsetting the closure of its complement with a parameter $t < r$. It is well known in the Computer Aided Geometric Design community that a shape can be smoothed using the double offset operation. Under the assumption that the compact set has positive μ-reach, which is a very weak regularity assumption, we quantify the regularity of its offset and double-offset.

We use these regularity results for curvature estimation. We show that the curvature measures of the offset of a compact set K with positive μ-reach can be estimated by the curvature measures of the offset of a compact set K' close to K in the Hausdorff sense [6]. We show how these curvature measures can be computed for finite unions of balls. The curvature measures of the offset of a compact set with positive μ-reach can thus be approximated by the curvature measures of the offset of a point-cloud sample.

Together with Jacques-Olivier Lachaud, we also have considered geometric inference problems in the context of digital geometry, namely when a shape of $\mathbb{R}^d$ is digitized and approximated by a set of voxels (*i.e.* d-dimensional pixels) of size h. We study the topology of the boundary of the digitization and provide a convergence result for digital integration [12].

Chapter 2: Generalized Voronoi Covariance Measure

The inference results of the first chapter derive from the regularity properties and from the Hausdorff stability of the distance function. Unfortunately, geometric data is usually corrupted with outliers, and the hypothesis of proximity for the Hausdorff distance is not realistic in practice. *Distance-like* functions have been recently introduced in the context of geometric inference because they possess the key regularity properties of the distance function: they are Lipschitz and their square are 1-semiconcave [CCSM11]. The set of distance-like functions contains distance functions, but also contains other functions such as *distances to measures* that are robust to outliers [CCSM11].

The *Voronoi Covariance Measure* (VCM) has been introduced in [MOG11] for normal, curvature and sharp features estimations. It is a tensor-valued measure associated to any compact set K. It has been shown to be Hausdorff stable, in the sense that if two compact sets are close in the Hausdorff sense, their VCM are also close to each other. Furthermore the VCM of a smooth surface encodes the normal vector field to this surface.

Together with Louis Cuel, Jacques-Olivier Lachaud and Quentin Mérigot, we have generalized the VCM to any distance-like function δ [7]. More precisely, we associate to any distance-like function δ a tensor-valued measures called the δ-Voronoi covariance measure (δ-VCM) and show its stability. As a consequence, it is possible to recover the normal vectors of a manifold S of $\mathbb{R}^d$ accurately from the δ-VCM, provided that δ is a distance to a measure close to the distance to the uniform probability measure on S (for the Wasserstein distance). This estimation is Hausdorff stable and robust to outliers. We also provide an algorithm to compute the δ-VCM, when the distance-like function δ is encoded by a weighted point set with small cardinality, and use it for normal, curvature and sharp features estimations. With Louis Cuel and Jacques-Olivier Lachaud [8] we have also used the VCM in the context of digital geometry and provided a convergent digital normal estimator.

Chapter 3: Reflector problem and numerical optimal transport

The *far-field reflector problem* is a well-known problem arising in nonimaging optics. The inputs are the description of the light distribution emitted by a punctual light source located at the origin and a desired target distribution of light at infinity, that is, on the sphere of directions. When the two light distributions can be modeled by a probability density μ on the source sphere and a probability density ν on the target sphere, the far-field reflector problem can be formulated as a generalized Monge-Ampère equation on the sphere. The approach of L. A. Caffarelli and V. Oliker to show the existence of a weak solution to this problem is geometric [CO08] and works as follows: they approximate the target probability measure ν by a sequence of discrete measures $\nu_N = \sum_i \alpha_i \delta_{y_i}$ supported on a finite set of directions $Y = \{y_1, \dots, y_N\}$. They show the existence of a solution to the (semi-discrete) far field reflector problem between μ and ν_N, and show that this solution converges to a solution of the original problem as N tends to

infinity. More recently, the far field reflector problem was shown to be equivalent to an optimal transport problem on the sphere [GO03, Wan04] for the cost $c : \mathcal{S}^{d-1} \times \mathcal{S}^{d-1} \to \mathbb{R}$ defined by $c(x, y) := -\log(1 - \langle x|y\rangle)$.

Together with Pedro Machado Manhães de Castro and Quentin Mérigot, we have proposed a numerical resolution of the reflector problem in the semi-discrete setting [10]. Using the optimal transport formulation, we cast this problem into a concave maximization problem. Our algorithm requires to calculate Laguerre cells on the sphere, that corresponds to the c-subdifferentials of the dual variable in the optimal transport formulation. We show that these Laguerre cells can be computed by intersecting a certain power diagram with the unit sphere and show that the complexity of this intersection is linear. We have also investigated other types of reflectors arising in nonimaging optics, for example in the *near field reflector problem*, where one wants to illuminate points in the space instead of directions.

Together with André Julien, Dominique Attali and Quentin Mérigot, we have also proposed heuristics that take into account industrial design constraints on the reflector surface [1].

FAR-FIELD REFLECTOR PROBLEM: Simulation of the illumination at infinity using the physically accurate raytracer engine LUXRENDER. The measure μ is supported on half the source sphere and is uniform. The measure ν_N is discretizing the measure of an image of Monge projected on the target sphere. The experiments were done with $N = 1,000$ on the left and $N = 15,000$ on the right.

Chapter 4: Convex Integration Theory and Smooth Fractals

A map f from a Riemannian manifold (M^n, g) into a Euclidean space $\mathbb{E}^q = (\mathbb{R}^q, \langle ., . \rangle)$ is an isometry if it preserves length, that is the length of every C^1 curve $\gamma : [a, b] \to M^n$ is equal to the length of its image $f \circ \gamma$. Suppose that, in some local

coordinate system, the metric is given by $g = \sum_{i,j}^{n} g_{ij} \mathrm{d}x_i \mathrm{d}x_j$, then the isometric condition is equivalent to a system of nonlinear PDE

$$\langle \frac{\partial f}{\partial x_i}, \frac{\partial f}{\partial x_j} \rangle = g_{ij}, \quad 1 \leq i \leq j \leq n$$

of $s_n = \frac{n(n+1)}{2}$ equations. In 1954, Nash surprised the mathematical community by showing that it was possible to realize an isometric embedding $f : (M^n, g) \to \mathbb{E}^q$ of a Riemannian manifold, but only with a C^1 regularity [Nas54], provided that $q \geq n + 2$. This C^1 regularity cannot be improved to C^2 in general since the curvature tensor would then provide obstructions to the existence of isometric maps. Shortly after, the theorem of Nash was extended by Kuiper to the codimension 1 [Kui55]. The result of Nash and Kuiper has many counterintuitive consequences, one of them being that the square flat torus $\mathbb{E}^2/\mathbb{Z}^2$ admits a C^1 isometric embedding into $\mathbb{E}^3$.

The result of Nash and Kuiper, as well as other geometric results, was revisited in the 70s and 80s by Gromov. He introduced the h-principle that states that many *partial differential relations* reduce to topological problems [GR70, Gro86] and he developed several tools to solve partial differential relations, one of them being the convex integration theory.

Together with Vincent Borrelli, Said Jabrane and Francis Lazarus, we have adapted the convex integration theory to the *differential relation for isometries* so as get an algorithm for the construction of an isometric embedding of the square flat torus in $\mathbb{E}^3$. We provide images of such an embedding. This visualization, as well as the simplification of the construction, led us to discover the notion of *Smooth Fractals*, which is related to the geometric structure of the Gauss map (*i.e.* the normal vector field) of the limit isometric embedding. We show that this Gauss map can be obtained as an infinite product of rotations applied to the Gauss map of an initial embedding. Although the coefficients of the rotations are intrinsically complicated, the asymptotic behavior of this product is fairly simple and bears a formal similarity with the Weierstrass function.

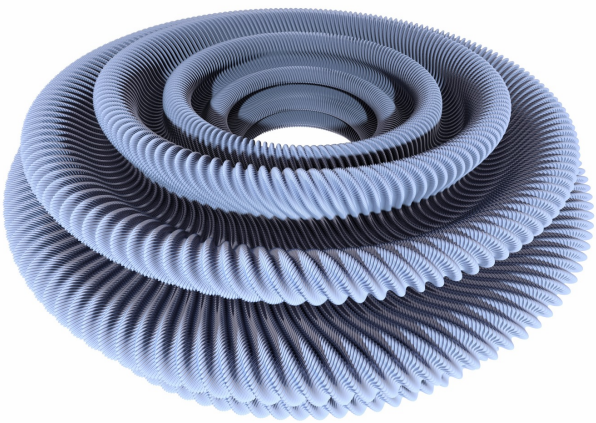

Image of an isometric embedding of the square flat torus in $\mathbb{E}^3$

Publications

Here is the list of publications written after my PhD. I will not present in this manuscript the articles [15, 14, 11, 16, 9].

[1] Julien André, Dominique Attali, Quentin Mérigot, and Boris Thibert. Far-field reflector problem under design constraints. *International Journal of Computational Geometry and Applications*, to appear.

[2] Vincent Borrelli, Saïd Jabrane, Francis Lazarus, and Boris Thibert. Flat tori in three-dimensional space and convex integration. *Proceedings of the National Academy of Sciences*, 109(19):7218–7223, 2012.

[3] Vincent Borrelli, Saïd Jabrane, Francis Lazarus, and Boris Thibert. The nash-kuiper process for curves. *Actes du séminaire de théorie spectrale et géométrie*, 30:1–19, 2012.

[4] Vincent Borrelli, Saıd Jabrane, Francis Lazarus, and Boris Thibert. Isometric embeddings of the square flat torus in ambient space. *Ensaios Matematicos*, 24:1–91, 2013.

[5] Frédéric Chazal, David Cohen-Steiner, André Lieutier, and Boris Thibert. Shape smoothing using double offsets. In *Proceedings of the 2007 ACM symposium on Solid and physical modeling*, pages 183–192. ACM, 2007.

[6] Frédéric Chazal, David Cohen-Steiner, André Lieutier, and Boris Thibert. Stability of curvature measures. In *Computer Graphics Forum*, volume 28, pages 1485–1496. Wiley Online Library, 2009.

[7] Louis Cuel, Jacques-Olivier Lachaud, Quentin Mérigot, and Boris Thibert. Robust geometry estimation using the generalized voronoi covariance measure. *SIAM Journal on Imaging Sciences*, to appear.

[8] Louis Cuel, Jacques-Olivier Lachaud, and Boris Thibert. Voronoi-based geometry estimator for 3d digital surfaces. In *Discrete Geometry for Computer Imagery*, volume 8668 of *Lecture Notes in Computer Science*, pages 134–149. Springer International Publishing, 2014.

[9] Michael P Cusack, Boris Thibert, Dale E Bredesen, and Gabriel Del Rio. Efficient identification of critical residues based only on protein structure by network analysis. *PloS one*, 2(5):e421, 2007.

[10] Pedro Machado Manhães De Castro, Quentin Mérigot, and Boris Thibert. Intersection of paraboloids and application to minkowski-type problems. In *30th Annual Symposium on Computational Geometry, SOCG'14, Kyoto, Japan, June 08 - 11, 2014*, page 308, 2014.

[11] Franck Hétroy, Cédric Gérot, Lin Lu, and Boris Thibert. Simple flexible skinning based on manifold modeling. In *International Conference on Computer Graphics Theory and Applications (GRAPP)*, 2009.

[12] Jacques-Olivier Lachaud and Boris Thibert. Properties of gauss digitized shapes and digital surface integration. Submitted, 2014.

[13] André Lieutier and Boris Thibert. Convergence of geodesics on triangulations. *Computer Aided Geometric Design*, 26(4):412–424, 2009.

[14] Damien Rohmer, Marie-Paule Cani, Stefanie Hahmann, and Boris Thibert. Folded paper geometry from 2d pattern and 3d contour. In *Eurographics 2011 (short paper)*, pages 21–24, 2011.

[15] Kenneth Rose, Alla Sheffer, Jamie Wither, Marie-Paule Cani, and Boris Thibert. Developable surfaces from arbitrary sketched boundaries. *Computer Graphics Forum*, 2007.

[16] Boris Thibert, Dale E Bredesen, and Gabriel del Rio. Improved prediction of critical residues for protein function based on network and phylogenetic analyses. *BMC bioinformatics*, 6(1):213, 2005.

Chapter 1

Geometric inference using distance functions

The purpose of geometric inference is to answer the following problem: Given a geometric object in $\mathbb{R}^d$ that is only known through an approximation, such as a point set, can we get a robust estimation of its topological or geometric properties? This problematic is motivated by certain applications arising in different domains such as medical imaging, reverse engineering, life sciences, cultural object scans, metrology, etc, where point sets are acquired by sensors from a 3D shape. We can be interested in recovering topological properties, such as the number of connected components, the genus, Betti numbers or geometric properties, such as the curvatures, the normals, etc. Two kind of questions then arise: can we define geometric notions, such as normals or curvatures, on non-smooth objects such as point sets ? Under which assumption do these notions approximate their continuous counterparts on the underlying object ?

The distance function to a compact set has been widely used in geometric inference, because it encodes geometric information on the compact set, it provides a projection map that allows the comparison with other geometric shapes, and it is Hausdorff stable (this will be detailed below). In this context, the notion of *sets with positive reach*, introduced and first studied by Federer [Fed59], is central. Sets with positive reach share important properties with convex sets and smooth manifolds. Originally, they were introduced because it is possible to generalize on those sets a notion of curvature due to Steiner, Minkowski and Weyl [Wey39].

A compact set K of $\mathbb{R}^d$ is said to have a reach greater than $r > 0$, if every point $x \in \mathbb{R}^d$ at a distance strictly less than r from K admits a unique projection on K (*i.e.* has a unique closest point on K). The set of points at a distance less than r from a compact set K is called r-offset or r-tubular neighborhood. The projection map defined on an offset of a compact set K with positive reach allows one to compare the compact set K with an Hausdorff approximation of it. This projection map has been used in many situations, for example to show convergence results for the curvature measures of a sequence of triangulations converging to a smooth manifold [Fu93a]. It has also been used by to get quantitative estimations of the

normals [MT04] and of the curvature measures [CSM06] of a smooth manifold from a triangulation close to it in the Hausdorff sense. Note that a notion of anisotropic curvature measure allowing an estimation of principal curvatures and principal directions was also introduced in [CSM06].

Over the last ten years, distance functions to compact sets have also been successfully used to recover the topology or approximate the geometry of a shape from a compact set close to it with respect to the Hausdorff distance. It is clear that two compact sets can be very close in the Hausdorff sense and have drastically different topological and geometric properties. However, it has been shown that properties measured on offsets are more stable. For example, the topology of a submanifold can be recovered from a union of balls of radius r centered at points that are close to the sub-manifold [NSW08]. Another example concerns compact sets that satisfy the very weak assumption of having positive μ-reach: the topology of the offsets of a compact set with positive μ-reach can be recovered from the offsets of a compact set which is close in the Hausdorff sense [CCSL09b]. Note that the notion of positive μ-reach is a relaxed version of the notion of positive reach, which is Hausdorff stable (in a sense that will be made clear later). It has also been used to show that the normal cone of the offset of a compact set with positive μ-reach is close to the normal cone of an offset of a compact set Hausdorff close [CCSL09a].

Contribution.

— **Convergence of geodesics (Section 1.2).** In the joint work [13] with André Lieutier, we consider the following problem: Given a sequence $(T_n)_{n\geq 0}$ of triangulations whose points and normals converge to those of a C^2-surface S of the three dimensional space, if C_n is a geodesic of T_n and if $(C_n)_{n\geq 0}$ converges to a curve, we want to know if the limit curve is a geodesic. The result is straightforward and positive when the geodesics C_n are shortest paths, but does not hold in general. We exhibit a counter-example. We also prove a result of convergence with additional assumptions concerning the rate of convergence of the normals and of the edges of the triangulation. This result is applied to different subdivision schemes, thus validating an existing algorithm that builds geodesics on subdivision surfaces [PTSB01].

— **Double offset regularity (Section 1.3).** It is well known in the Computer Aided Geometric Design community that a shape can be smoothed using the double offset operation. The double offset of a compact set is obtained by offsetting it with a parameter r, then offsetting the closure of its complement with a parameter $t < r$. Under the assumption that the shape has positive μ-reach, a simple combination of results from [Fed59] and [Fu85] implies that the boundary of the double offset is of class $C^{1,1}$. Together with Frédéric Chazal, David Cohen-Steiner and André Lieutier, we worked on the offset and double offset regularity [5]. We give an explicit lower bound on the reach of a compact set with positive μ-reach and also provide an estimation of the curvature of its double offset.

— **Stability of curvature measure (Section 1.4).** We address with Frédéric Chazal, David Cohen-Steiner and André Lieutier the problem of curvature

estimation from sampled compact sets [6]. We show that the gaussian, mean or anisotropic curvature measures of the offset of a compact set K with positive μ-reach can be estimated by the same curvature measures of the offset of a compact set K' close to K in the Hausdorff sense. We show how these curvature measures can be computed for finite unions of balls. The curvature measures of the offset of a compact set with positive μ-reach can thus be approximated by the curvature measures of the offset of a point-cloud sample.

— **Digital geometry (Section 1.5).** We consider with Jacques-Olivier Lachaud geometric inference problems in the context of digital geometry [12], namely when a shape X of $\mathbb{R}^d$ is digitized and represented by a set of voxels (*i.e.* d-dimensional pixels) of size h. We assume that the boundary of X has positive reach. We show the boundary $\partial_h X$ of the Gauss digitization is close to the boundary of the shape in the Hausdorff sense in any dimension, thus extending a 2D result [Lac06]. Furthermore, the boundary $\partial_h X$ is not a $d-1$-dimensional manifold in general. We show that the non-manifoldness of the Gauss digitized boundary $\partial_h X$ may only occur in "small parts". The restriction to $\partial_h X$ of the projection map onto ∂X being not injective, we show the non-injective part is negligible, thus providing a convergence result for digital integration.

Before detailing my contribution in Sections 1.2, 1.3, 1.4 and 1.5, we briefly recall in Section 1.1 important properties of distance functions and related notions that are central in the context of geometric inference.

1.1 DISTANCE FUNCTIONS, REACH AND μ-REACH

Many results in geometric inference rely on the distance function and on the reach of a compact set. We recall in this section the most important properties used later in the context of geometric inference.

1.1.1 — Sets with positive reach

Distance functions. The distance function to a compact subset K of $\mathbb{R}^d$ is the function on $\mathbb{R}^d$ defined by the formula $\mathrm{d}_K(x) := \min_{p\in K} \|p-x\|$. Remark that d_K encodes entirely the compact set K since $K = \mathrm{d}_K^{-1}(\{0\})$. Note also that d_K is 1-Lipschitz and is thus, by Rademacher theorem, differentiable almost everywhere for the Lebesgue measure. For any positive number r, we denote by K^r the r-offset of K, defined by $K^r := \{x \,|\, \mathrm{d}_K(x) \leq r\}$. The set K^r is also often called the tubular neigborhood of K of size r.

Proposition 1.1. *Let x be a point in the complement $\mathbb{R}^d \setminus K$ of K. The following three statements are equivalent*

(i) *d_K^2 is differentiable at the point x ;*
(ii) *d_K is differentiable at the point x ;*
(iii) *x has a unique projection p on K.*

Moreover, if one of this statement holds we have:

$$\nabla d_K^2(x) = 2(x-p) \quad \textit{and} \quad \nabla d_K(x) = \frac{x-p}{\mathrm{d}_K(x)}.$$

The medial axis of K, denoted by $\mathrm{Med}(K)$, is the set where the projection is not unique. This set, or variants of it, plays an important role in computational geometry, in reconstruction problems and in geometric inference.

The following property, stating that the distance function is semiconcave, is fundamental in this chapter and will also play a central role in the following chapter with the generalized distance-like functions.

Lemma 1.2. *The squared distance function to a compact set K is 1-semiconcave. More precisely, for every $x \in \mathbb{R}^d$ the function $k_x : \mathbb{R}^d \to \mathbb{R}$ defined by*

$$k_x(y) := \|y-x\|^2 - \mathrm{d}_K^2(y)$$

is convex.

Sets with positive reach. The notion of sets with positive reach generalizes the notions of smooth sub-manifolds and convex sets of the Euclidean space and offers a natural framework allowing a definition of curvature measures. The Steiner-Minkowski formula states that the volume of an ε-offset of a convex body in the Euclidean space is a polynomial of degree d in ε. The Weyl tube formula shows that the volume of an ε-offset of a submanifold of $\mathbb{R}^d$ is also a polynomial, provided ε is small enough [Wey39]. Herbert Federer extended the tube formula to sets with positive reach. He also introduced a local version of the tube formula, allowing a consistent definition of *curvature measures* [Fed59].

DEFINITION 1.3. The reach of a compact set $K \subseteq \mathbb{R}^d$ is the maximum radius r such that the offset K^r does not intersect the medial axis $\mathrm{Med}(K)$, or equivalently

$$\mathrm{reach}(K) = \max\{r \geq 0;\ \mathrm{d}_K \text{ is differentiable in } K^r\}$$

The set K is said to have positive reach if $\mathrm{reach}(K) > 0$.

Convex sets have infinite reach. The reach of an embedded C^2 submanifold of $\mathbb{R}^d$ is bounded by $1/\rho$, where ρ is the maximal principal curvature of the submanifold. One important fact about sets with positive reach is the existence of a projection map

$$\mathrm{p}_K : K^r \to K$$

defined on the r-offset K^r, where $r < \mathrm{reach}(K)$. This map is a practical tool because it allows to compare the compact set K with an object which is Hausdorff close. Furthermore, this map is Lipschitz:

Lemma 1.4. *Let K be a compact set with reach R and $r < R$. Then the projection map p_K is $\frac{R}{R-r}$-Lipschitz in the offset K^r.*

Combined with Proposition 1.1, this lemma directly implies that d_K is of class $C^{1,1}$ in the set $K^{r_2} \setminus K^{r_1}$ where $0 < r_1 < r_2 < \mathrm{reach}(K)$ and d_K^2 is of class $C^{1,1}$ on K^r, where $r < \mathrm{reach}(K)$.

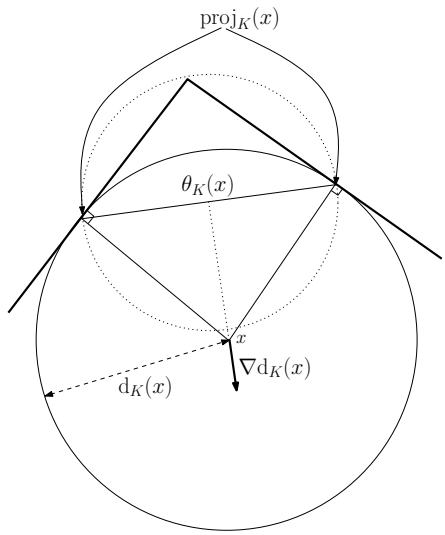

Figure 1.1: A 2-dimensional example with 2 closest points.

1.1.2 — The generalized gradient and its flow.

The distance function d_K is not differentiable on $\mathrm{Med}(K)$. However, it is possible to define a *generalized gradient* function $\nabla \mathrm{d}_K : \mathbb{R}^d \to \mathbb{R}^d$ that coincides with the usual gradient of d_K at points where d_K is differentiable. In the geometric inference community, this generalized gradient, as well as its flow, was introduced by André Lieutier [Lie04]. We note that it was also known in the more general context of semiconcave functions (see [Pet07] for instance).

Generalized gradient. For any point $x \in \mathbb{R}^d \setminus K$, we denote by $\mathrm{proj}_K(x)$ the set of points in K closest to x (Figure 1.1):

$$\mathrm{proj}_K(x) = \{y \in K \mid d(x, y) = d(x, K)\}$$

Note that $\mathrm{proj}_K(x)$ is a non empty compact set. There is a unique smallest closed ball $\sigma_K(x)$ enclosing $\mathrm{proj}_K(x)$ (cf. Figure 1.1). We denote by $\theta_K(x)$ the center of $\sigma_K(x)$ and by $\mathcal{F}_K(x)$ its radius. The point $\theta_K(x)$ can equivalently be defined as the point on the convex hull of $\mathrm{proj}_K(x)$ nearest to x. For $x \in \mathbb{R}^d \setminus K$, the generalized gradient $\nabla \mathrm{d}_K(x)$ is defined as follows:

$$\nabla \mathrm{d}_K(x) = \frac{x - \theta_K(x)}{\mathrm{d}_K(x)}.$$

It is natural to set $\nabla \mathrm{d}_K(x) = 0$ for $x \in K$. For $x \in \mathbb{R}^d \setminus K$, $\|\nabla \mathrm{d}_K(x)\|$ is the cosine of the (half) angle of the smallest cone with apex x that contains $\mathrm{proj}_K(x)$. Note that the generalized gradient at the point x corresponds to the orthogonal projection of 0 onto the Clarke subgradient ([Cla90] and [CCSL09a, Lemma 5.2]).

Gradient flow. The map $x \mapsto \|\nabla \mathrm{d}_K(x)\|$ is lower semicontinuous. Although $\nabla \mathrm{d}_K$ is not continuous, it is shown that Euler schemes using $\nabla \mathrm{d}_K$ converge uni-

formly, when the integration step decreases, towards a continuous flow $\mathcal{C} : \mathbb{R}^+ \times \mathbb{R}^d \to \mathbb{R}^d$. The integral line of this flow starting at a point $x \in \mathbb{R}^d$ can be parameterized by arc length $s \mapsto \mathcal{C}(t(s), x)$. It is possible to express the value of d_K at the point $\mathcal{C}(t(l), x)$ by summing along the integral line with length l downstream point x:

$$\mathrm{d}_K\left(\mathcal{C}(t(l), x)\right) = \mathrm{d}_K(x) + \int_0^l \|\nabla \mathrm{d}_K(\mathcal{C}(t(s), x)\| ds \tag{1.1}$$

It is proven in [Lie04] that the functions $\mathcal{F}_K$ and R_K are increasing along the trajectories of the flow. The Integration Flow Formula (1.1) is one of the main technical tools used in [CL05, CCSL09b, CCSL09a] to prove stability results and is also a key ingredient of [5].

Critical point theory. The *critical points* of d_K are defined as the points x for which $\nabla \mathrm{d}_K(x) = 0$. Note that this notion of critical point is the same as the one considered in the setting of non smooth analysis [Cla90] and Riemannian geometry [Gro93]. The topology of the offsets K^r of a compact set K are closely related to the critical values of d_K [Gro93] (*i.e.* the values of its distance function at critical points). The *weak feature size* of K, or $\mathrm{wfs}(K)$, is defined as the minimum distance between K and the set of critical points of d_K. Notice that $\mathrm{wfs}(K)$ may be equal to 0. Nevertheless, $\mathrm{wfs}(K)$ is non zero for a large class of compact sets including polyhedrons and piecewise analytic sets [CL05]. Furthermore, $\mathrm{wfs}(K)$ may be viewed as the "minimum size of the topological features" of the set K:

Lemma 1.5 ([CL05]). *If $0 < r, s < \mathrm{wfs}(K)$ then K^r and K^s are homeomorphic. The same holds for the complements of K^r and K^s. The same also holds for the boundaries ∂K^r and ∂K^s that are topological $(n-1)$-dimensional manifolds.*

1.1.3 — Hausdorff stability and μ-reach

Haudorff stability. The *Hausdorff distance* $d_H(K, K')$ between two compact sets K and K' in $\mathbb{R}^d$ is the minimal number r such that $K \subset K'^r$ and $K' \subset K^r$. The distance function is Hausdorff stable since one has $d_H(K, K') = \sup_{x \in \mathbb{R}^d} |\mathrm{d}_K(x) - \mathrm{d}_{K'}(x)|$. This Hausdorff stability does not hold anymore for the projection p_K and $\mathrm{p}_{K'}$ and for the gradients $\nabla \mathrm{d}_K$ and $\nabla \mathrm{d}_{K'}$. However, it has been shown in [CCSL09b] that if a point x of $\mathbb{R}^d$ is far enough from K, then one can bound from below $\|\nabla \mathrm{d}_K(x)\|$ by using the generalized gradient of $\mathrm{d}_{K'}$, provided that $d_H(K, K')$ is small. Roughly speaking, the norm of the gradient can be estimated by the norm of the gradient of an Hausdorff approximation. This motivates the definitions of μ-reach and critical function introduced in [CCSL09b].

Sets with positive μ-reach. Remark that d_K is differentiable at a point x if and only if the norm of its generalized gradient at the point x is equal to 1. Hence the reach of a compact set K can be seen as the maximal offset value r for which every point $x \in K^r$ satisfies $\|\nabla \mathrm{d}_K(x)\| = 1$. Using this remark, one can define a parameterized notion of reach, the μ-reach.

DEFINITION 1.6. Let $\mu > 0$. The μ-reach of a compact set K is the maximal offset value r for which every point $x \in K^r$ satisfies $\|\nabla \mathrm{d}_K(x)\| \geq \mu$:

$$\mathrm{reach}_\mu(K) = \sup\left\{r,\ \forall x \in K^r\ \|\nabla \mathrm{d}_K(x)\| \geq \mu\right\}.$$

Note that the 1-reach coincides with the reach introduced by Federer [Fed59].

DEFINITION 1.7 (critical function). Given a compact set $K \subset \mathbb{R}^d$, its *critical function* $\chi_K : (0, +\infty) \to \mathbb{R}_+$ is the real function defined by:

$$\chi_K(r) = \inf_{x \in \mathrm{d}_K^{-1}(r)} ||\nabla \mathrm{d}_K(x)||$$

We note that the infimum can be replaced by a minimum since $\|\nabla \mathrm{d}_K\|$ is lower semicontinuous and $\mathrm{d}_K^{-1}(r)$ is compact. It also results from the compactness of $\mathrm{d}_K^{-1}(r)$ that $r \mapsto \chi_K(r)$ is lower semicontinuous. The critical function is in some sense "stable" with respect to small (measured by Hausdorff distance) perturbations of a compact set, precisely [CCSL09b]:

Theorem 1.8 (critical function stability theorem)**.** *Let K and K' be two compact sets of $\mathbb{R}^d$ and $d_H(K, K') \leq \varepsilon$. For all $r \geq 0$, we have:*

$$\inf\{\chi_{K'}(u) \,|\, u \in I(r, \varepsilon)\} \leq \chi_K(r) + 2\sqrt{\frac{\varepsilon}{r}}$$

where $I(r, \varepsilon) = [r - \varepsilon, r + 2\chi_K(r)\sqrt{\varepsilon r} + 3\varepsilon]$

The claim of Theorem 1.8 can be read as $\chi_K(r) \geq \inf\{\chi_{K'}(u) \,|\, u \in I(r, \varepsilon)\} - 2\sqrt{\frac{\varepsilon}{r}}$ and says that a lower bound on the critical function of a compact set K' yields a lower bound on the critical function of "nearby" (for Hausdorff distance) compact sets K. In particular, if a set K' of measured points is known to lie within some Hausdorff distance of a physical object represented by the unknown compact set K, the critical function of K' gives, by Theorem 1.8, a lower bound on the critical function of the partially known physical object K. Since the computation of the critical function of a point set is straightforward [CCSL09b], this implies that a lower bound on the critical function of a compact set can be estimated from a point set which is Hausdorff close.

1.2 CONVERGENCE OF GEODESICS

A shortest path is a curve on a surface with minimal length among all the curves connecting two given points. A geodesic is a curve on a surface whose length does not decrease if it is perturbed in a small neighborhood of any point. A shortest path is clearly a geodesic, but the converse is not true.

Various applications of the computation of geodesics have been considered. For example, the heart's left ventricle can be modeled by a family of embedded surfaces; a muscular fiber of the central region of the left ventricle has particular properties and can be considered as a geodesic of one of those surfaces [Mou03, Str79]. The computation of geodesics appears in the simulation of several physical

processes. In the fabrication of composite parts by filament winding, the filament must ideally wind along geodesics. The computation of radar cross sections involves the simulation of creeping rays which follow geodesics of the object. Since triangulations are widely used for surface modeling, it is natural to consider the modeling of geodesics on surfaces approximated by triangulations. Many algorithms have been proposed for the computation of shortest paths on triangulations [KS98, PC05]. Concerning geodesics [PTSB01] have also proposed an algorithm that builds geodesics on triangulations.

A simple calculation shows that if a sequence $(T_n)_{n\in\mathbb{N}}$ of triangulations converges in Hausdorff distance to S, if the normals of T_n also converge to the normals of S, then the limit curve of a sequence of shortest paths is a shortest path of S [HPW06, MS05]. However, as we will see later, this result does not hold anymore for geodesics. This is due to the fact that a shortest path is a notion that only depends on the distance and is therefore a quantity of order 1. On the contrary, because of the local characterization, a geodesic is a notion of order 2 and involves the curvature. Hence, the result of convergence of [HPW06] cannot be used in some applications. For example, in the modeling of the human heart, the curves modeling the fibers are closed and are not shortest paths [Mou03]. Furthermore, this result cannot be used to validate the algorithm given in [PTSB01], where the authors build a sequence of geodesics on approximating triangulations that are not shortest paths in general.

Contributions. We first show that the result of convergence for shortest paths cannot be applied to geodesics, by providing a counter-example. In a second step, we provide a positive result of convergence for geodesics on triangulations. We suppose, as for the result with shortest paths given in [HPW06], that the points and the normals of the triangulation converge to those of a smooth surface. We also add an assumption on the convergence speed of the normals and of the length edges of the sequence of triangulations. We assume that the edge lengths cannot converge faster to zero than the angles between the normals (in a sense that will be precized later). The proof relies on a notion of discrete geodesic curvature.

We then apply these results to sequences of triangulations that follow subdivision schemes, such as for example Catmull-Clark schemes or subdivision schemes for splines (of degree greater than or equal to three) or Bézier polygons. In particular, our results validate the algorithm of [PTSB01] that builds geodesics on subdivision surfaces.

1.2.1 — Geodesics on triangulations

Let C be a polygonal curve of a triangulation T. We suppose that C is a geodesic of T, namely that it minimizes locally the distance. The curve C is clearly a straight line on each triangle. When C crosses an edge of T at a point p, which is not a vertex of T, then the incident and refracted angles of C on T at p are equal. If C passes through a vertex p of T, then it is a little more tricky: the polygonal curve C separates the set of the triangles of T containing p into two connected regions r_1 and r_2 (see Figure 1.3). If one denotes by $\alpha_p^{r_1}$ the sum of the angles $\alpha_i^{r_1}$ of the

triangles of region r_1 at p (*resp.* by $\alpha_p^{r_2}$ the sum of the angles $\alpha_i^{r_2}$ of the triangles of region r_2 at p), one has

$$\alpha_p^{r_1} \geq \pi \quad \text{and} \quad \alpha_p^{r_2} \geq \pi. \tag{1.2}$$

Remark that if a geodesic traverses a vertex p of T, then the sum of the angles of the triangles of T at the vertex p is greater than 2π, namely $\alpha_p^{r_1} + \alpha_p^{r_2} \geq 2\pi$. We can also notice that if $\alpha_p^{r_1} + \alpha_p^{r_2} > 2\pi$, then the geodesic cannot be extended uniquely beyond p: there exist two distinct polygonal curves C_1 and C_2 containing p and q that satisfy Equation (1.2) are geodesics.

1.2.2 — Counter-example

We show in Figure 1.2 a sequence of triangulations that converges in normals and in distance to the plane. However a sequence of geodesics C_n of T_n does not converge to a geodesic of the plane. The construction is done as follows: The triangulation overlaps the horizontal plane $\mathbb{R}^2 \times \{0\}$ outside the large circle and inside the small one. In the ring between the two circles, it is made of 4^n identical small "roof shaped" bumps detailed on the right of Figure 1.2. The points d_n^1, d_n^2, p_n and m_n are on the plane $\mathbb{R}^2 \times \{0\}$ while the points t_n^1 and t_n^2 stand at some height above the plane. The faces $d_n^1 t_n^1 d_n^2$, $p_n t_n^2 m_n$, $d_n^1 t_n^1 t_n^2 m_n$ and $d_n^2 t_n^1 t_n^2 p_n$ are planar and all make a slope s_n with $\mathbb{R}^2 \times \{0\}$. If we take $s_n = \frac{3}{2^n}$, one has, for each $n \in \mathbb{N}$, $\beta_1 + \beta_2 + \beta_3 + \beta_4 > \pi$. Thus the polygonal curve C_n wrapped around the outer circle is a geodesic. Remark that the length of the edge $m_n p_n$ is of order $1/4^n$ and is therefore converging faster to 0 than the slope s_n.

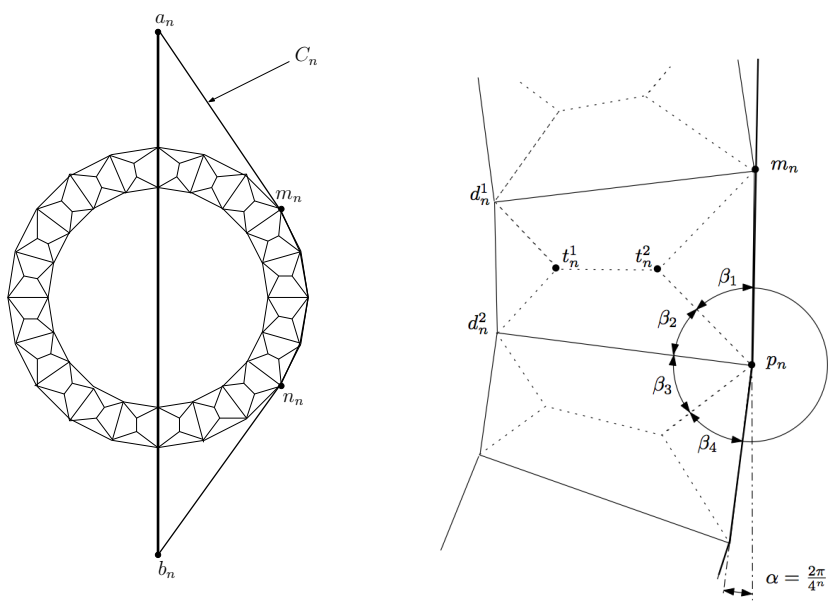

Figure 1.2: Triangulation T_n and geodesic C_n seen from above: on the left we see the whole surface; the region in the dashed quadrangle is depicted on the right

Observe that the sequence $(T_n)_{n\in\mathbb{N}}$ of triangulations converges towards the

plane in the Hausdorff sense. Furthermore the normals of T_n tend to the normals of the plane. The shortest path on T_n between the point a_n and b_n is the straight line. However, the line $a_n m_n n_n b_n$ (denoted by C_n), wrapped around the circle between m_n and n_n is a local minimum, that is a geodesic, between a_n and b_n. These geodesics converge in the Hausdorff sense towards a curve C composed of two lines and an arc of circle. We can notice that the triangulations T_n and the curves C_n satisfy all the assumptions of the result of [HPW06], except that C_n is a geodesic (and not a shortest path). However the limit curve C is not a geodesic. This counter-example implies that the convergence in distance and in normals of T_n to S is not sufficient to expect a result of convergence for geodesic.

1.2.3 — Convergence towards a geodesic

The main result is the following theorem, whose proof will be sketched in Section 1.2.5. Roughly speaking, if the points and normals of the triangulation T_n converge to those of a surface S and if the edge lengths do not converge faster to zero than the angles between the normals, then geodesics of T_n converge to geodesics of S.

Theorem 1.9 ([13]). *Let S be a smooth surface of $\mathbb{R}^3$, let r denote the reach of S and let $(T_n)_{n\in\mathbb{N}}$ be a sequence of triangulations. Let K, $\widetilde{K}$, θ_{min} be positive constants and let $(d_n)_{n\in\mathbb{N}}$ be a sequence of real numbers converging to 0. Suppose that for every n:*

a) T_n belongs to the r-offset S^r of S;

b) for every $m \in T_n$ $\|m - \mathrm{p}_S(m)\| \leq d_n$, where p_S is the projection onto S.

c) for every $m \in T_n$, the angle between any triangle Δ containing m and the tangent plane $T_{\mathrm{p}_S(m)}S$ of S at $\mathrm{p}_S(m)$ is smaller than $\frac{K}{2^n}$;

d) the lengths of the edges of T_n are greater than $\frac{\widetilde{K}}{2^n}$;

e) all the angles of T_n are greater than θ_{min};

Let $(C_n)_{n\in\mathbb{N}}$ be a sequence of polygonal curves $C_n : [0,1] \to \mathbb{R}^3$ with uniform parametrization such that C_n is an interior geodesic of T_n and $\mathrm{p}_S(C_n)$ does not intersect the boundary of S. If $(C_n)_{n\in\mathbb{N}}$ converges towards a curve C in the sup norm sense in $\mathbb{R}^3$, then C is of class C^2 and is a geodesic of S.

1.2.4 — Application to subdivision surfaces

Corollary 1.10 is a general result that can be easily applied to several subdivision schemes. Let $(P_n)_{n\in\mathbb{N}}$ be a sequence of parameterized triangulations $P_n : [0,1]^2 \to \mathbb{R}^3$ that is converging to a parameterized smooth surface $f : [0,1]^2 \to \mathbb{R}^3$. The parameter domain $[0,1]^2$ of each P_n can be triangulated so that P_n is linear on each triangle of $[0,1]^2$. We say that the parameter domain of P_n is a triangular grid if its vertices are $p_n^{i,j} = \left(\frac{i}{2^n}, \frac{j}{2^n}\right)$ (where $i,j \in \{0,..2^n\}$) and the edges are $p_n^{i,j}p_n^{i+1,j}$, $p_n^{i,j}p_n^{i,j+1}$ and $p_n^{i,j}p_n^{i+1,j+1}$. We say that $(P_n)_{n\in\mathbb{N}}$ uniformly converges to a function f with rate of convergence $\frac{1}{2^n}$ if

$$\exists N \in \mathbb{N},\ \exists K \in \mathbb{R},\ n > N \ \Rightarrow \sup_{(u,v)\in[0,1]^2} \|P_n(u,v) - f(u,v)\| \leq \frac{K}{2^n}.$$

We say that $(P_n)_{n\in\mathbb{N}}$ uniformly converges in derivative to f with rate of convergence $\frac{1}{2^n}$ if there exists $K > 0$ and $N \in \mathbb{N}$, such that for any $n > N$:

$$\sup_{\substack{i\in\{0,..,2^n-1\}\\ j\in\{0,..,2^n\}}} \left\| 2^n \left[P_n\left(\frac{i+1}{2^n}, \frac{j}{2^n}\right) - P_n\left(\frac{i}{2^n}, \frac{j}{2^n}\right)\right] - \frac{\partial f}{\partial u}\left(\frac{i}{2^n}, \frac{j}{2^n}\right)\right\| \leq \frac{K}{2^n},$$

$$\text{and} \quad \sup_{\substack{i\in\{0,..,2^n\}\\ j\in\{0,..,2^n-1\}}} \left\| 2^n \left[P_n\left(\frac{i}{2^n}, \frac{j+1}{2^n}\right) - P_n\left(\frac{i}{2^n}, \frac{j}{2^n}\right)\right] - \frac{\partial f}{\partial v}\left(\frac{i}{2^n}, \frac{j}{2^n}\right)\right\| \leq \frac{K}{2^n}.$$

One obtains the following corollary.

Corollary 1.10. *Let $(P_n)_{n\in\mathbb{N}}$ be a sequence of parametrized triangulations $P_n : [0,1]^2 \to \mathbb{R}^3$and $f : [0,1]^2 \to \mathbb{R}^3$ be a parametrized surface of class C^2, such that:*

a) the parameter domain of each P_n is a triangular grid,
b) $(P_n)_{n\in\mathbb{N}}$ uniformly converges to f with rate of convergence $\frac{1}{2^n}$,
c) $(P_n)_{n\in\mathbb{N}}$ uniformly converges in derivative to f with rate of convergence $\frac{1}{2^n}$,
d) f is regular, i.e. $\forall (u,v) \in [0,1]^2\ \frac{\partial f}{\partial u}(u,v) \wedge \frac{\partial f}{\partial v}(u,v) \neq 0$.

Let $(C_n)_{n\in\mathbb{N}}$ be a sequence of polygonal curves $C_n : [0,1] \to \mathbb{R}^3$ with uniform parametrization such that C_n is an interior geodesic of P_n. If $(C_n)_{n\in\mathbb{N}}$ converges in the sup norm sense towards a curve C which is interior to S, then C is of class C^2 and is a geodesic of S.

This corollary allows to show directly convergence of geodesics for several subdivision surfaces, for example subdivision schemes of splines of arbitrary degree (greater than or equal to 3) or Bézier polygons. It also works for Catmull-Clark schemes, if the limit curve does not contain extraordinary vertices.

1.2.5 — Sketch of proof of Theorem 1.9

The idea of the proof is the following: loosely speaking, we show that if a triangulation T_n is "almost planar", then any geodesic C_n on T_n is "not turning too much". When projected onto tangent planes to S, it is even turning much less. Using this fact allows to show that a kind of local discrete curvature of C_n is very small. This is sufficient to show that the limit curve of C_n is of class $C^{1,1}$ in $\mathbb{R}^3$. Using the fact that the limit curve lies on S allows to conclude that it is a geodesic of class C^2. More precisely:

Let $C_n : [0,1] \to \mathbb{R}^3$ be a polygonal parameterized curve of T_n linear on each triangle of T_n. Let us take two parameters $0 \leq t_a < t_b \leq 1$. We denote by $l(C_n, t_a, t_b)$ the length of C_n between t_a and t_b. The *total curvature* of C_n between t_a and t_b is given by:

$$TC_{3D}(C_n, t_a, t_b) = \sum_{p_n \text{ vertex of } C_n([t_a,t_b])} \beta^{3D}_{dev}(p_n),$$

where $\beta^{3D}_{dev}(p)$ is the deviation angle of C_n at the vertex p (see Figure 1.3). Here, the deviation angle of a polygonal curve $p_1, .., p_n$ at the vertex p_i is the angle $\angle \overrightarrow{p_{i-1}p_i}, \overrightarrow{p_ip_{i+1}}$. We now introduce the tangential curvature, which is a kind of discrete geodesic curvature of C_n on T_n relatively to S. The *tangent total curva-*

ture of C_n with respect to S between t_a and t_b is defined by

$$TC^{TS}_{Tan}(C_n, t_a, t_b) = \sum_{p_n \text{ vertex of } C_n([t_a,t_b])} \beta^{TS}_{dev}(p_n),$$

where $\beta^{TS}_{dev}(p_n)$ is the deviation angle of the orthogonal projection of $C_n([t_a, t_b])$ onto the plane $T_{\mathrm{p}_S(p_n)}S$ tangent to S at the vertex $\mathrm{p}_S(p_n)$ (see Figure 1.3).

We now need two preliminary lemmas. Intuitively, Lemma 1.11 implies that angle deviation tends to 0, but its projection onto the plane tangent to S tends faster to 0. Lemma 1.12 states that if the curve C_n does not turn too much and if its length is not too long, then C_n cannot intersect too many edges of T_n.

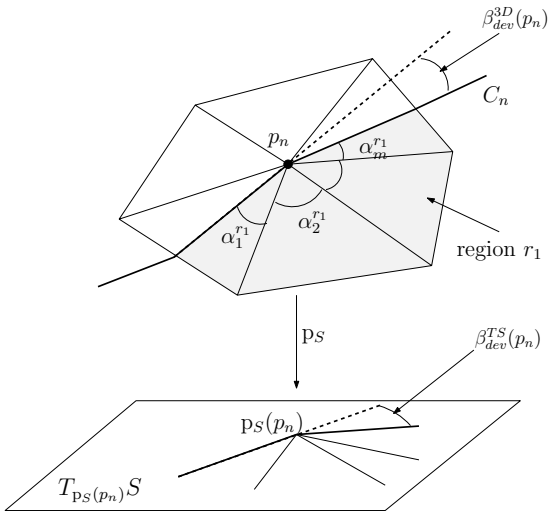

Figure 1.3: Deviation angle of a geodesic and of its orthogonal projection

Lemma 1.11. *There exists K_1 such that for every n, if C_n is a geodesic of T_n and p_n is a vertex of C_n, one has:*

$$\beta^{3D}_{dev}(p_n) \leq K_1\, \alpha_n, \quad \textit{and} \quad \beta^{TS}_{dev}(p_n) \leq K_1\, \alpha_n^2,$$

where α_n is the maximal angle between all the triangles of T_n containing p_n and $T_{\mathrm{p}_S(p_n)}S$.

Lemma 1.12. *There exists a constant K_2, such that the number of intersection $\sharp(C_n, t_a, t_b)$ between $C_n([t_a, t_b])$ and the edges of T_n satisfies*

$$\sharp(C_n, t_a, t_b) \leq K_2 \left[1 + \; TC^{TS}_{Tan}(C_n, t_a, t_b) + 2^n\, l(C_n, t_a, t_b)\right].$$

The proof is now divided into the following steps.

Step 1. By combining the two previous lemmas, we have the following circular inequality:

$$\begin{aligned} TC^{TS}_{Tan}(C_n, t_a, t_b) &\leq K_1\, \alpha_n^2\, \sharp\,(C_n, t_a, t_b) \\ &\leq K_1\, K_2\, \alpha_n^2\, \left[1 + \; TC^{TS}_{Tan}(C_n, t_a, t_b) + 2^n\, l(C_n, t_a, t_b)\right]. \end{aligned}$$

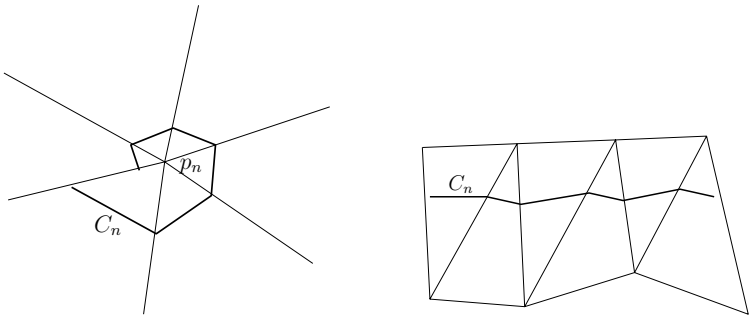

Figure 1.4: The number of intersections $\sharp C_n$ depends on $TC^{TS}_{Tan}(C_n)$ and $l(C_n)$.

Therefore, for some constants K_3 and K_4 independant of t_a and t_b, one has

$$TC^{TS}_{Tan}(C_n, t_a, t_b) \leq \frac{K_3}{2^n} l(C_n, t_a, t_b) + \frac{K_4}{4^n}. \tag{1.3}$$

Step 2. By using again the same lemmas, one can show that for some constant K and K':

$$TC_{3D}(C_n, t_a, t_b) \leq K\ l(C_n, t_a, t_b) + K'\ \frac{1}{2^n}. \tag{1.4}$$

Step 3. Using this last equation, we prove that the limit curve C is of class $C^{1,1}$. For this, we proceed as follows. We first show that the sequence $\left(\frac{dC_n}{dt^+}\right)_{n\geq 0}$ is bounded and is a Cauchy sequence. We deduce that the lengths and the slopes $\frac{dC_n}{dt^+}$ of C_n converge. We then deduce that C is of class C^1 and that $\left(\frac{dC_n}{dt^+}\right)_{n\geq 0}$ converges to $\frac{dC}{dt}$. We finally show that $\frac{dC}{dt}$ is Lipschitz-continuous.

Step 4. We consider a point $p_0 = C(t_0)$. In this step, using Equations (1.3) and (1.4), we prove that $\mathrm{p}_{T_{C(t_0)}S} \circ C$ is twice differentiable at t_0 and that $(\mathrm{p}_{T_{C(t_0)}S} \circ C)''(t_0) = 0$. Here $\mathrm{p}_{T_{C(t_0)}S}$ denotes the orthogonal projection on the plane tangent to S at $C(t_0)$. One can show that this implies that C is of class C^2, then that it has zero geodesic curvature and then that it is a geodesic of S.

Remark that the projection map p_S onto S is used all along the proof, and in particular its Lipschitz constant in an offset of S in Step 4.

1.3 DOUBLE OFFSET REGULARITY

In Computer Aided Geometric Design (CAGD) applications, *blending* or *filleting* operators consist in "*rounding*" sharp edges and corners of objects. It may be motivated by aesthetic or ergonomy, constrained by manufacturing processes such as machining or moulding, or required by functional issues such as structural or aerodynamical behaviour. A widely used geometric definition, illustrated on Figure 1.5 consists in the so called *blends by rolling ball* [RR86].

Figure 1.5 shows on the left a simple solid, made of the union of two "boxes". In the middle, concave edges have been rounded, while, on the right, all edges have been rounded. Starting from the solid on the left, the rounding of concave edges can be defined by the following fictive operation. Assuming the solid to be

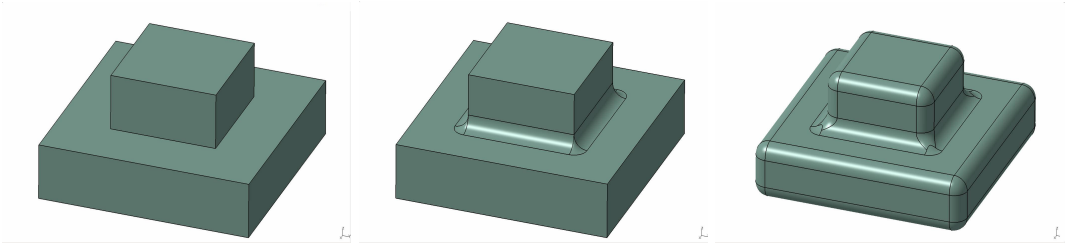

Figure 1.5: Smoothing by double offset illustrated on a simple CAD model

made of a hard material (like steel) one embed it in a bloc of wax. Then one uses a spherical ball of given radius to remove as much wax as possible to obtain the solid on the middle of the figure.The remaining solid is said to be the initial one *rounded from the outside by a rolling ball*. The rounding of convex edges can be obtained by applying the same fictive process to the complement of the solid: one build the complement of the part in the middle out of a hard material, fill it with wax and remove (from the inside!) as much wax as possible with a spherical ball. Taking again the complement of the resulting solid yields the solid on the right of Figure 1.5 . This definition of rounding is rather natural if one's intent is to design a part which have to be machined by a spherical tool (or whose mold has to be machined by a spherical tool). In many situations, this rounding process produces solids with smooth boundaries.

Contributions. We consider here a similar smoothing done by a double offset operation. The double offset of a compact set is obtained by offsetting it with a parameter r, then offsetting the closure of its complement with a parameter $t < r$. Given a compact set K with positive μ-reach, we quantify the reach of $\overline{\mathbb{R}^d \setminus K^r}$ and of the boundary of $K^{r,t} := \overline{\mathbb{R}^d \setminus K^r}^t$. We also provide estimations on the Hausdorff distance between ∂K, ∂K^r and $\partial K^{r,t}$ and show that ∂K^r and $\partial K^{r,t}$ are isotopic hypersurfaces.

1.3.1 — Complements of offsets

Let $K \subset \mathbb{R}^d$ be a compact set with positive μ-reach. It can be easily deduced, by using a result of Joseph Fu [Fu85, Corollary 3.4] that that the closure $\overline{\mathbb{R}^d \setminus K^r}$ of the complement of the offset of K has positive reach, for any value $0 < r < \mathrm{reach}_\mu(K)$. The main result of [5] is the following theorem that provides an explicit lower bound on this reach. Moreover, one gives a lower bound for the critical function of K^r.

Theorem 1.13 ([5]). *For $r \in (0, r_\mu)$, one has*

$$\mathrm{reach}(\overline{\mathbb{R}^d \setminus K^r}) \geq \mu r \tag{1.5}$$

Moreover the critical function of $\overline{\mathbb{R}^d \setminus K^r}$ is lower bounded for any $t \in (\mu r, r)$:

$$\chi_{\overline{\mathbb{R}^d \setminus K^r}}(t) \geq \frac{2\mu r - t(1+\mu^2)}{t(1-\mu^2)}. \tag{1.6}$$

The bound on the reach is tight. We provide in Figure 1.6 an example of compact set K with positive μ-reach such that $\mathrm{reach}(\overline{\mathbb{R}^d \setminus K^r}) = \mu r$.

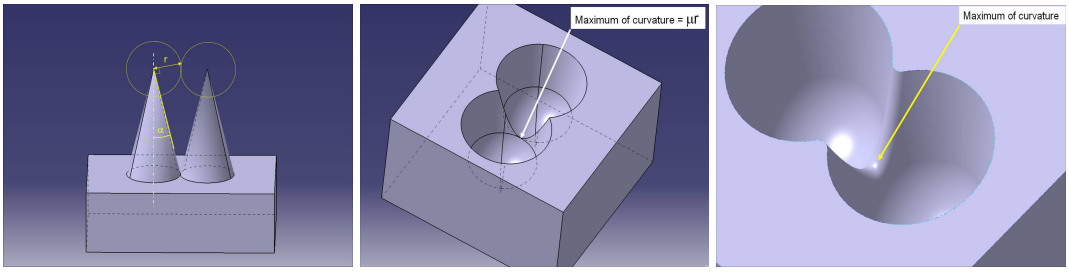

Figure 1.6: Tightness of the bound : in the first image, we can visualize a compact K (here we take $\mu = \sin\alpha$); the complement $\overline{\mathbb{R}^d \setminus K^r}$ of its offset in the second one (where $r = \frac{h}{\cos\alpha}$); In the last image, we visualize $K^{r,t}$ where $t < \mu r$ and $\mu = \sin\alpha$.

Example of Figure 1.6: Let $\alpha \in (0, \pi/2)$, $h > 0$, $P_1 = (h, 0, \frac{h}{\tan\alpha})$, $P_2 = (-h, 0, \frac{h}{\tan\alpha})$, $I_1 = (h, 0, 0)$ and $I_2 = (-h, 0, 0)$. Let C_i be the cone of axis $(P_i I_i)$, with vertex P_i and angle α. Let K be the compact set defined as (see top of Figure 1.6) the union of the rectangular box whose top face is in the plane $z = 0$, together with the two cones delimited by C_1, C_2 and the plane $z = 0$. An easy computation shows that $\mathrm{reach}_\mu(K) = 0$ for $\mu > \sin\alpha$ and $\mathrm{reach}_\mu(K) = +\infty$ for $\mu \leq \sin\alpha$. The two cones C_1 and C_2 intersect along a curve C in the plane $y = 0$. If $r \leq \frac{h}{\cos\alpha}$, then the r-offsets of C_1 and C_2 intersect in the plane $y = 0$ along a curve that is a translation of the curve C. Let $Q = (0, 0, 0)$. By Meusnier's theorem, the radius of curvature of C at P is given by $h \tan\alpha$. Therefore we have

$$\mathrm{reach}(\overline{\mathbb{R}^d \setminus K^r}) = \min(r, h\tan\alpha).$$

If we now take $r = \frac{h}{\cos\alpha}$, one has that $\mathrm{reach}(\overline{\mathbb{R}^d \setminus K^r}) = \mu r$, for $\mu = \sin\alpha$.

SKETCH OF PROOF. Let $x \in (K^r \setminus K)$. We denote by $\mathrm{proj}_K(x)$ the set of nearest neighbors of $x \in \overline{\mathbb{R}^d \setminus K^r}$, d the distance from x to $\overline{\mathbb{R}^d \setminus K^r}$ and y the center of the ball of smallest radius $l \geq 0$ enclosing $\mathrm{proj}_K(x)$. To obtain the inequalities of the theorem, we establish and compare an upper and a lower bound of $\mathrm{d}_K(y)$.

Step 1. Using the convexity of the function $k_x(z) := \|z - x\|^2 - \mathrm{d}_K^2(z)$, one shows $k_x(y) = d^2 - l^2 - \mathrm{d}_K^2(y) \leq d^2 - r^2$, from which on gets

$$\mathrm{d}_K^2(y) \geq r^2 - l^2.$$

Step 2. We consider the flow line of $\nabla \mathrm{d}_K$ issued from y and denote by $\tilde{y}$ the first intersection point of this trajectory with the sphere centered on x and of diameter d. Using the Flow Integration Formula (1.1) and the fact that the norm of the gradient is strictly increasing along the flow line, one gets

$$\mathrm{d}_K(y) \leq r - \tilde{l}\mu,$$

where $\tilde{l}$ is the length of the flow line in between y and $\tilde{y}$.

Step 3. We deduce from the two previous equations that $r^2 - l^2 \leq (r - \tilde{l}\mu)^2$. Let θ be the angle between $y - x$ and any vector joining x to a point of Γ. From the relations $l = d \sin\theta$ and $\tilde{l} \geq d(1 - \cos\theta)$, a simple computation shows that if $d < \mu r$, then $\theta = 0$. The conclusion follows from the fact that $\cos\theta = \|\nabla \mathrm{d}_{\overline{\mathbb{R}^d \setminus K^r}}(x)\|$. A simple calculation then gives Equation (1.6). □

We can also deduce from the Flow Integration Formula (1.1) an upper bound on the Hausdorff distance between ∂K and ∂K^r. Note that the bound of Theorem 1.14 is tight, as illustrated in Figure 1.14.

Theorem 1.14 (Offset distance theorem [5])**.** *Let K be a compact set and let $\mu > 0$, $r > 0$ be such that $r < \mathrm{reach}_\mu(K)$. Then*

$$d_H(\partial K, \partial K^r) < \frac{r}{\mu}.$$

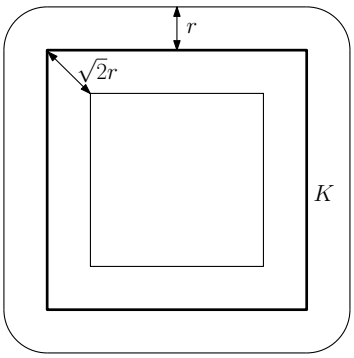

Figure 1.7: The boundary of the r-offset of a square K in the plane is at Hausdorff distance $\sqrt{2}r$ of K. For $\mu = \frac{\sqrt{2}}{2}$, $\mathrm{reach}_\mu(K) > 0$ and this example shows the tightness of the bound in Theorem 1.14

1.3.2 — Smoothness of double offsets

Let $K \subset \mathbb{R}^d$ be a compact set. For $0 < d < r$, the (r, d)-double offset $K^{r,t}$ of K is the set of points that are at distance t of $\overline{\mathbb{R}^d \setminus K^r}$:

$$K^{r,t} = \overline{\mathbb{R}^d \setminus K^r}^t = \{x \in \mathbb{R}^d \colon d(x, \overline{\mathbb{R}^d \setminus K^r}) \leq t\}$$

Since the distance function d_V to a compact set V with positive reach is differentiable with non-zero Lipschitz gradient on the offset V^t, where $t < \mathrm{reach}(V)$, one obtains the following result.

Theorem 1.15 (Double offset theorem [5])**.** *If $r < \mathrm{reach}_\mu(K)$ for some value $\mu > 0$ and if $t < \mu r$ then $\partial K^{r,t}$ is a smooth $C^{1,1}$-hypersurface. Moreover,*

$$\mathrm{reach}(\partial K^{r,t}) \geq \min(t, \mu r - t)$$

which implies that the smallest of the principal radii of curvature at any point of $\partial K^{r,t}$ is at least $\min(t, \mu r - t)$.

One also gets an estimation on the Hausdorff distance between $\partial K^{r,t}$ and ∂K and also show that ∂K^r and $\partial K^{r,t}$ are isotopic.

Proposition 1.16 ([5]). *If $r < \mathrm{reach}_\mu(K)$ for some value $\mu > 0$ and if $0 < t < \mu r$ then*

$$d_H(\partial K^{r,t}, \partial K) \leq \frac{r}{\mu} - t$$

Theorem 1.17 (Offsets isotopy theorem [5]). *For $r < \mathrm{reach}_\mu(K)$ and $0 < t < \mu r$, ∂K^r and $\partial K^{r,t}$ are isotopic hypersurfaces.*

1.4 STABILITY OF CURVATURE MEASURES

We address the problem of curvature estimation from sampled compact sets. Let us first recall a question of John Milnor [Mil93]: *In what sense do two sets have to be close to each other, in order to guarantee that their curvature measures are close to each other?* We provide here a partial answer to this question.

Contribution. We show that the curvature measures (anisotropic or not) of the offset of a compact set K with positive μ-reach can be estimated by the same curvature measures of the offset of a compact set K' close to K in the Hausdorff sense. Hence a Hausdorff proximity is sufficient to answer the question of John Milnor. However, the stability does not concern the sets themselves but their offset. Since the curvature measures can be computed for finite unions of balls, the curvature measures of the offset of a compact set with positive μ-reach can thus be approximated by the curvature measures of the offset of a point-cloud sample.

1.4.1 — Curvature measures and normal cycle of sets with positive reach

Curvature measures have been defined for sets with positive reach by Herbert Federer and have been generalized by Joseph Fu to a wide class of compact sets, containing in particular triangulations, semialgebraic sets and subanalytic sets [Fu93b, Fu94], using the *normal cycle theory* introduced by Peter Wintgen and Martina Zähoe [Win82, Zäh86]. Although we only deal here with compact sets with positive reach, we introduce the definition based on normal cycle, because it is useful in the proofs.

We first need to introduce the definition of invariant forms of the tangent bundle $T\mathbb{R}^d$ of $\mathbb{R}^d$. We identify the tangent bundle $T\mathbb{R}^d$ with $E \times F$, where E is the base space and F is the fiber. Let $J : E \to F$ be the canonical isomorphism between E and F. We endow $T\mathbb{R}^d$ with the dot product $< (e, f), (e', f') >=< e, e' > + < J^{-1}(f), J^{-1}(f') >$. At any point (m, ξ) of $ST\mathbb{R}^d = \{(m, \xi) \in E \times F,\ \|\xi\| = 1\}$, we consider an orthonormal frame $(e_1, ..., e_{d-1})$ of the space orthogonal to $J^{-1}(\xi)$ and we take $\epsilon_i = J(e_i)$. We build the (d-1)-differential form:

$$\Omega = (e_1^* + t\epsilon_1^*) \wedge ... \wedge (e_{d-1}^* + t\epsilon_{d-1}^*),$$

where u^* denotes the 1-form defined by $u^*(x) =< u, x >$. One can show that this form does not depend on the chosen orthonormal frame. The coefficient of t^k is a

(d-1)-form denoted by ω_k. One can show that each ω_k is invariant under the action of the orthogonal group.

Let now V be a set with positive reach. We define the set:

$$S(V) = \{(p,n) \in \mathbb{R}^d \times \mathbb{S}^{d-1},\ p \in \partial V \text{ and } n \in \mathcal{N}(p)\},$$

where $\mathcal{N}(p) = \{n \in \mathbb{S}^{d-1}, \exists t > 0,\ \mathrm{p}_V(p+tn) = p\}$ is the normal cone of V at p. One can show that $S(V)$ is a Lipschitz (d-1)-manifold. The normal cycle $N(V)$ of V is then by definition the $(d-1)$-current on $\mathbb{R}^d \times \mathbb{R}^d$ defined for every (d-1)-differential form ω by:

$$N(V)(\omega) = \int_{S(V)} \omega.$$

DEFINITION 1.18. Let V be compact set of $\mathbb{R}^d$ with positive reach. The kth-curvature measure of V, denoted by Φ_V^k associates to each measurable function f on $\mathbb{R}^d$ the real number:

$$\Phi_V^k(f) = N(V)(\bar{f}\ \omega_k),$$

where $\bar{f}$ is defined on $\mathbb{R}^d \times \mathbb{R}^d$ by $\bar{f}(p,n) = f(p)$.

Remark that our definition is slightly different from the classical one. More precisely, in the particular case where $f = 1_B$ is the characteristic function of a Borel set B, one recovers the usual notion of curvature measure [Fed59]. We have extended the definition to any (Lipschitz) function, because it is a natural framework allowing to state stability results. One can show that if V is the volume enclosed by an hypersurface ∂V, then $\Phi_V^k(1_B)$ is the integral over $\partial V \cap B$ of the k-th symmetric function of the principal curvatures of ∂V. In dimension 3, Φ_V^1 and Φ_V^2 are respectively the integral of twice the mean curvature and the integral of the gaussian curvature:

$$\Phi_V^2(1_B) = \int_{B\cap\partial V} G(p)dp \quad and \quad \Phi_V^1(1_B) = \int_{B\cap\partial V} H(p)dp,$$

where $H(p)$ an $G(p)$ denote respectively the gaussian and twice the mean curvature of ∂V at p.

Anisotropic curvature measures have also been introduced in [CSM06]. The authors associate to every pair of vectors X and Y of $\mathbb{R}^d$ a differential form $\omega^{X,Y}$ of $\mathbb{R}^d \times \mathbb{R}^d$. They then define the anisotropic curvature measure H_V of a geometric set V that associates to every (Lipschitz) function $f : \mathbb{R}^d \to \mathbb{R}$ the bilinear form

$$\mathrm{H}_V(f)\ :\ (X,Y) \mapsto N(C)(\bar{f}\omega^{X,Y}).$$

In the particular case where V is the volume enclosed by a C^2 compact hypersurface, $\mathrm{H}_V(1_B)$ is just the integral over $B \cap \partial V$ of a symmetric bilinear form $\mathrm{II}_{\partial V}$ related to the second fundamental form of ∂V. More precisely, this form $\mathrm{II}_{\partial V}$ coincides with the second fundamental form of ∂V on the tangent plane of V and vanishes on its orthogonal complement. For any Borel set B of $\mathbb{R}^d$, one has:

$$\mathrm{H}_V(1_B) = \int_{B\cap\partial V} \mathrm{II}_{\partial V}(p)dp.$$

Now, let K be a compact set whose μ-reach is greater than $r > 0$. Then $V = \overline{\mathbb{R}^d \setminus K^r}$ has a reach greater than μr. It is then possible to define the extended notions of curvature measures of K^r [RZ03, RZ05] by:

$$\Phi^k_{K^r}(f) = (-1)^k \Phi^k_V(f) \quad \text{and} \quad \mathrm{H}_{K^r}(f) = -\mathrm{H}_V(f).$$

1.4.2 — Stability of the curvature measures of the offsets

We compare here the curvature measures of the offsets of two compact sets, provided that the two compact sets are close in the Hausdorff sense and have positive μ-reach (Theorem 1.19). This result is obviously using the regularity of the offset of a compact set with positive μ-reach established in the previous section. Beyond that, it is worth noting that the smoothness of its double offset quantified in Theorem 1.15, is central in the proof.

We recall that the covering number $\mathcal{N}(A, t)$ of a compact set A is the minimal number of closed balls of radius t needed to cover A. Given a function $f : \mathbb{R}^d \to \mathbb{R}$, we let $\|f\|_\infty := \max_{x \in \mathbb{R}^d} |f(x)|$ and denote $\mathrm{Lip} f := \max_{x \neq y} |f(x) - f(y)|/\|x - y\|$ its Lipschitz constant, which can be infinite. We define the bounded-Lipschitz norm by $\|f\|_{\mathrm{BL}} := \|f\|_\infty + \mathrm{Lip}(f)$.

Theorem 1.19 ([6]). *Let K and K' be two compact sets of $\mathbb{R}^d$ whose μ-reaches are greater than r. We suppose that the Hausdorff distance $\epsilon = d_H(K, K')$ between K and K' is less than $\frac{r\mu\,(2-\sqrt{2})}{2} \min(\mu, \frac{1}{2})$. For any function $f : \mathbb{R}^d \to \mathbb{R}$, one has:*

$$|\Phi^i_{K^r}(f) - \Phi^i_{K'^r}(f)| \leq k(r, \mu, d, f)\ \|f\|_{\mathrm{BL}}\ \sqrt{\epsilon},$$

and

$$\|\overline{H}_{K^r}(f) - \overline{H}_{K'^r}(f)\| \leq k(r, \mu, d, f)\ \|f\|_{\mathrm{BL}}\ \sqrt{\epsilon},$$

where $k(r, \mu, d, f)$ only depends on f through the covering number $\mathcal{N}(\mathrm{spt}(f)^{O(\sqrt{\epsilon})}, \mu r/2)$ and $\mathrm{spt}(f) = \{x \in \mathbb{R}^d,\ f(x) \neq 0\}$.

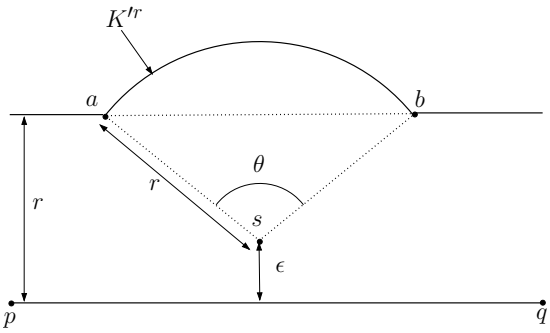

Figure 1.8: Tightness of the bound of Theorem 1.19: we take $K = [p, q]$ and $K' = [p, q] \cup \{s\}$, where s is at a distance ϵ from K. We have $d_H(K, K') = \epsilon$ and the total curvature θ of K'_r between a and b satisfies $\theta = 2 \arccos\left(\frac{r-\epsilon}{r}\right) = O\left(\sqrt{\epsilon}\right)$.

Remark that the upper bound in $\sqrt{\varepsilon}$ of Theorem 1.19 is sharp. Furthermore, one may notice that one can estimate locally the curvature: if we take the function $f(x) = \max(1 - \|x - c\|/r, 0)$ equal to 1 at a point $c \in \partial K'^r$ that radially decreases in

a “small" ball $\mathbb{B}$ of radius r and vanishes out of $\mathbb{B}$, then we can get local information about the curvature of K'^r from the curvature of K^r in the neighborhood of c.

We also note that the conclusion of the theorem may be rephrased by saying that the *bounded Lipschitz distance* between the curvature measures of K^r and K'^r is bounded by $O(\sqrt{\epsilon})$. The bounded Lipschitz distance between measures is similar to the 1-Wasserstein distance, except that it applies to general signed measures whereas Wasserstein distance is limited to probability measures.

A similar stability result has been obtained in [CCSM10]. They also show that the bounded Lipschitz distance between the curvature measures of K^r and K'^r is bounded by $O(\sqrt{\varepsilon})$. The main differences are that our result also applies to anisotropic curvature measures, whereas [CCSM10] is only limited to the usual curvature measures. On the other hand, the stability result for curvature measures in [CCSM10] derives from a stability result for so-called boundary measures, which holds without any assumptions on the underlying compact set, whereas ours requires to assume a lower bound on the μ-reach. While the two results seem related at first sight, the proof techniques are drastically different.

Theorem 1.19 assumes that both the compact sets K and K' have sufficiently large μ-reach. Nevertheless, in practical settings, particularly when dealing with point clouds, such an hypothesis is never satisfied. Using a variant of Theorem 1.8, it is still possible to approximate the curvature measures of the offsets of a compact set with positive μ-reach from any sufficiently close approximation of it.

Theorem 1.20 ([6]). *Let K and K' be two compact subsets of $\mathbb{R}^d$ such that $\mathrm{reach}_\mu(K') > r$. Assume that the Hausdorff distance $\varepsilon = d_H(K, K')$ between K and K' is such that $\varepsilon < \frac{\mu^2}{60+9\mu^2} r$. Then the conclusions of Theorem 1.19 also hold.*

1.4.3 — Computation of the curvature measures of $3D$ point clouds

When the compact set K is a finite point set in $\mathbb{R}^3$ it is possible to provide explicit formula for the curvature measures. The boundary of K^r is a spherical polyhedron: its faces are spherical polygons; its edges are circle arcs contained in the intersection of pairs of spheres of radius r with centers in K; its vertices belong to the intersection of three spheres of radius r with centers in K. Moreover, the combinatorial structure of ∂K^r is in one-to-one correspondence with the boundary of the α-shape of K [Ede93]. To get the experimental results below we used a half-edge data structure for boundaries of union of balls designed based upon the α-complex data structure of the library CGAL [Cga].

Let C be a cell of ∂K_r (*i.e.* a face, an edge or a vertex). A simple calculation shows that for $i \in \{1, 2\}$, $\Phi^i_{K^r}(1_C)$ is proportional to either the area, or the length, or the Dirac measure of C (depending on if C is a face or an edge or a vertex). One has $\Phi^i_{K^r}(1_C) = \varphi^i_{K^r}(C)\ \mathcal{H}^l(C)$, where l is the dimension of C. As a consequence, once computed on each cell C of ∂K^r, the values $\varphi^i_{K^r}(1_C)$ can simply be stored by adding an extra information to the elements of the data structure representing ∂K^r. For each vertex v of ∂K^r and $0 < r_1 < r_2$, we define $f_v : \mathbb{R}^3 \to \mathbb{R}$ by $f_v(x) = 1$ if $\|x - v\| \leq r_1$, $f_v(x) = 0$ if $\|x - v\| > r_2$ and $f_v(x) = 1 - \frac{\|x-v\|-r_1}{r_2-r_1}$ otherwise.

ALGORITHM

Input: a $3D$ point cloud K, a radius r and two values $0 < r_1 < r_2$
Output: an estimated curvature value on each vertex of ∂K^r

1. Compute ∂K^r
2. For each cell C (faces, edges, vertices) of ∂K^r compute $\varphi^1_{K^r}(C)$ and $\varphi^2_{K^r}(C)$.
3. For each vertex v of ∂K^r, we approximate $\Phi^1_{K^r}(f_v)$ and $\Phi^2_{K^r}(f_v)$ using a piecewise constant approximation of f_v.

In Figures 1.9 and 1.10 below, the curvatures are then represented on the boundary of the α-shape (for $\alpha = r$) of the point clouds where each triangle is colored according to the curvature value of its corresponding vertex in ∂K^r and to the colorbar on the right of Figure 1.9. Note that the color values are different for the different examples (since the extrema values are different). This algorithm can be easily adapted to calculate the anisotropic curvature measures for a finite set of points. In particular, this allows to estimate the principal curvatures and principal directions from a point set.

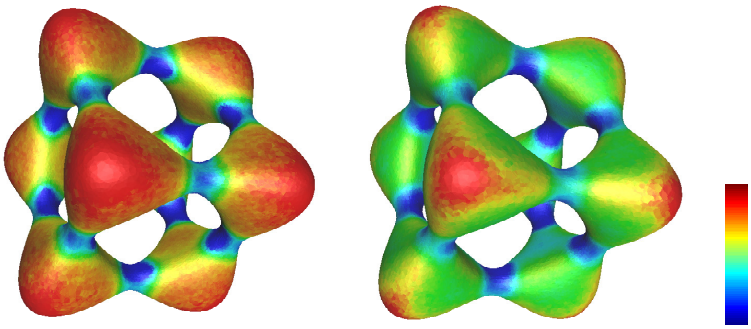

Figure 1.9: The Gauss (left) and mean (right) curvatures computed on the offset of a point set sampled around a smooth surface. The colors are related to the values of the curvature according to the colorbar on the right, the blue color corresponding to the lowest values.

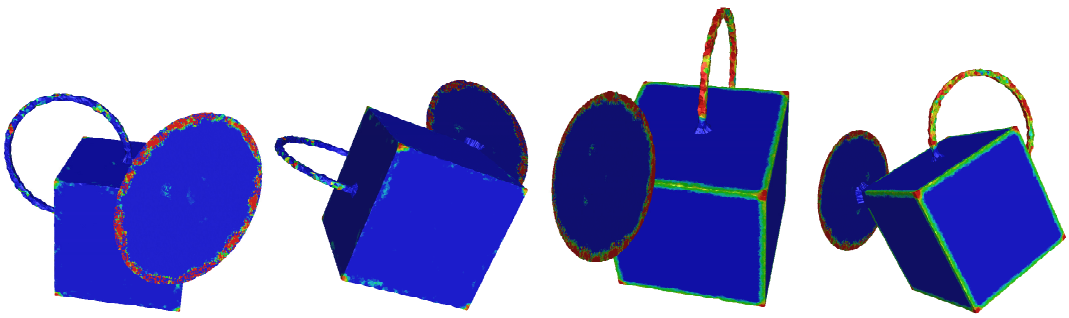

Figure 1.10: The Gauss (two first) and mean (two last) curvatures computed on the offset of a point cloud sampled around a non-manifold set union of a cube with a disc and a circle. As expected, the vertices and the boundary of the disc have a large Gaussian curvature.

1.4.4 — Sketch of proof of Theorem 1.19

We give here the sketch of the proof by comparing the two offsets K^r and K'^r globally. In [6], we compare these two offsets locally (*i.e.* in a Borel set B that contains the support of the function f), which gives a better bound on the error. The proof is therefore more complicated since a second current (related to the boundary of $B \cap \partial K'^{r,t}$, where B is a Borel set) appears in Equation (1.7).

The proof can now be divided into three steps: in the first step, we show that the problem can be carried onto the double offsets (that are smooth); in a second step, we compare the normal cycles of the double offsets; in the last step, we combine Step 1 and Step 2 to show that the curvature measures of the two offsets are close. Let K and K' be two compact sets with positive μ-reach that satisfy all the assumptions of Theorem 1.19.

Step 1: Carrying the problem into the double offsets
First note that $\overline{\mathbb{R}^d \setminus K^r}$ and $\overline{\mathbb{R}^d \setminus K'^r}$ have positive reach. We introduce the map:

$$\begin{array}{rccc} F_{-t}: & \mathbb{R}^d \times \mathbb{R}^d & \to & \mathbb{R}^d \times \mathbb{R}^d \\ & (p,n) & \mapsto & (p - tn, n) \end{array}.$$

If V is any compact set with positive reach and $t < \mathrm{reach}(V)$, the map F_{-t} induces naturally a one-to-one correspondence between the support of the normal cycle of the offset V^t and the support of the normal cycle of V. In particular, this map allows to send simultaneously the normal cycles of $K^{r,t}$ and $K'^{r,t}$ to respectively the normal cycles of K^r and K'^r. More precisely, one has:

$$N(\overline{\mathbb{R}^d \setminus K^r}) - N(\overline{\mathbb{R}^d \setminus K'^r}) = F_{-t\sharp}(N(K^{r,t}) - N(K^{r,t})),$$

where $F_{-t\sharp}$ denotes the push-forward for currents. Therefore, in order to compare the normal cycles of $\overline{\mathbb{R}^d \setminus K^r}$ and $\overline{\mathbb{R}^d \setminus K'^r}$, it is sufficient to compare the normal cycles of the double offsets $K^{r,t}$ and $K'^{r,t}$.

Step 2: Comparison of the normal cycles of the double offsets
In order to compare the normal cycles of $K^{r,t}$ and $K'^{r,t}$, we first need to compare their (geometric) supports in $\mathbb{R}^d \times \mathbb{R}^d$. Using the Flow Integration Formula (1.1), one first shows that the Hausdorff distance between $\partial K^{r,t}$ and $\partial K'^{r,t}$ is less than ϵ/μ. Using a result of [CCSL09a] one also shows that the difference between the normals of $\partial K^{r,t}$ and $\partial K'^{r,t}$ is bounded by $30\sqrt{\epsilon/(\mu t)}$. Hence the (geometric) supports of $N(K^{r,t})$ and $N(K'^{r,t})$ are close to each other. Let us take $t = \mu r/2$. Since the reach of $\partial K^{r,t}$ is larger than t (Theorem 1.15), the projection map $\mathrm{p}_{\partial K^{r,t}}$ onto $\partial K^{r,t}$ is then defined on the offset $U_t := (\partial K^{r,t})^t$. Since $\partial K'^{r,t} \subset U_t$, the map $\mathrm{p}_{\partial K^{r,t}}$ induces a one-to-one map between $\partial K'^{r,t}$ and $\partial K^{r,t}$. We now define

$$\begin{array}{rccc} \psi: & U_t \times \mathbb{R}^d & \to & \mathrm{spt}\left(N\left(K_{r,t}\right)\right) \\ & (x,n) & \mapsto & (\mathrm{p}_{\partial K^{r,t}}(x), n_{\mathrm{p}_{\partial K^{r,t}}(x)}) \end{array}.$$

Using the affine homotopy between ψ and the identity, the homotopy Lemma [Fed69, 4.1.9 page 363-364] allows to show that $N(K^{r,t})$ and $N(K'^{r,t})$ are close. More pre-

cisely

$$N(K^{r,t}) - N(K'^{r,t}) = \partial R, \tag{1.7}$$

where ∂R is the boundary of a particular d-rectifiable R current whose support $\mathrm{spt}(R)$ has a d-volume bounded by $\mathcal{H}^d(\mathrm{spt}(R)) \leq k(r,\mu,d)\mathcal{H}^{d-1}(\partial K'^{r,t})\sqrt{\varepsilon}$, where $\mathcal{H}^k$ denotes the k-dimensional Hausdorff measure and $k(r,\mu,d)$ is a constant that only depends on r, μ and d.

Step 3
Let us take an invariant form ω_k. By combining previous equations, one has:

$$\phi^k_{\mathbb{R}^d\setminus K^r}(f) - \phi^k_{\mathbb{R}^d\setminus K'^r}(f) = N(\overline{\mathbb{R}^d \setminus K^r})(\bar{f}\omega_k) - N(\overline{\mathbb{R}^d \setminus K'^r})(\bar{f}\omega_k) = F_{-t\sharp}\partial R(\bar{f}\omega_k).$$

We show that F_{-t} is $\sqrt{1+t^2}$-Lipschitz. Since ω_k and $\mathrm{d}\omega_k$ are uniformly bounded by a constant depending on the dimension, $\mathrm{Lip}(\bar{f}) = \mathrm{Lip}(f)$, one gets by Stokes theorem:

$$|\phi^k_{\mathbb{R}^d\setminus K^r}(f) - \phi^k_{\mathbb{R}^d\setminus K'^r}(f)| \leq k(r,\mu,d)\ \|f\|_{\mathrm{BL}}\ \mathcal{H}^{d-1}(\partial K'^{r,t})\ \sqrt{\epsilon},$$

The previous inequality still holds for K^r and K'^r. To conclude the proof, we use the bound on $\mathcal{H}^{d-1}(\partial K'^{r,t})$ in terms of covering number of K^r [CCSM10].

1.5 APPLICATION IN DIGITAL GEOMETRY

In some applications, a real object or a scene is known through a digital image, that is a union of voxels. Since the digitization process aims to be as faithful as possible to the real data, it is very natural to look at topological and geometric properties that can be inferred from digital data for rather elementary digitization processes. Here we consider the problem of estimating properties of the boundary ∂X of a compact set of $\mathbb{R}^d$ from the boundary $\partial_h X$of its Gauss digitization at a scale h.

A voxel of size $h > 0$, denoted by $\mathrm{Vox}_h(z)$, is a closed cube of size h aligned with the axis of $\mathbb{R}^d$ and centered in $z \in h\mathbb{Z}^d$. Given a compact domain $X \subset \mathbb{R}^d$ and a sampling grid step $h > 0$, the *Gauss digitization* of X is the point set $X_h = X \cap h\mathbb{Z}^d$, the associated digital set is $\mathrm{D}_h X := \cup_{x\in X_h}\mathrm{Vox}_h(x)$. The boundary of the Gauss digitization of X is denoted $\partial_h X := \partial(\mathrm{D}_h X)$.

The inference of topological properties has been extensively studied especially in the 2D case, when the shape is R-regular (*i.e.* when its boundary has positive reach) mainly with morphological tools [Pav82, Ser82, GL95, LCG98, SK05]. The extension to non R-regular shapes appears quite challenging. Fewer works address the case of d-dimensional images, for $d \geq 3$. One underlying reason is that topology preservation cannot be achieved in general already for $d = 3$. Stelldinger and Köthe [SK05, Theorem 3] exhibit an example of shape whose boundary is of class $C^{1,1}$, but whose Gauss digitization has non-manifold boundary, even for small h. Concerning geometric inference in $\mathbb{R}^3$, there are many methods that estimate the area of the boundary of a shape from its digitization, but few of them come with guarantee. Even for methods that have been shown to be convergent,

such as methods based on the estimation of the volume of an offset [SLS07] or statistical methods [LYZ+10], there is no error bound, hence the convergence speed is unknown.

Contribution. Using classical properties of distance functions to compact sets, we provide geometric inference results in the context of digital geometry [12]. We first connect the notion of *R-regularity* well used in digital geometry [GL95, LCG98, Pav82, Ser82] to the notion of *reach*. We consider a compact domain X of $\mathbb{R}^d$ whose boundary has positive reach. We establish that ∂X and $\partial_h X$ are Hausdorff close to each other whatever the dimension (this result was previously only known in dimension 2). We then show that "places" where $\partial_h X$ is non manifold may only occur where the normal vector is almost aligned with some digitization axis, and the limit angle decreases with h. Finally, we study the restriction to $\partial_h X$ of the projection map $\mathrm{p}_{\partial X}$ onto ∂X. Since it is not an homeomorphism, we estimate the size of the set of points on ∂X for which this map is not one-to-one, and show that it tends to zero with h. This allows us to show a convergence result for digital integration.

1.5.1 — R-regularity, reach and Hausdorff proximity

R-regularity and positive reach The R-regularity property was independently proposed by Pavlidis [Pav82] and Serra [Ser82]. Gross, Conrad and Latecki introduced the similar definition of *par(R)-regularity* in [GL95]. A closed ball $\mathrm{iob}(x, R)$ of radius R is an *inside osculating ball* of radius R to ∂X at point $x \in \partial X$ if $\partial X \cap \partial \mathrm{iob}(x, R) = \{x\}$ and $\mathrm{iob}(x, R) \subseteq X^\circ \cup \{x\}$, where X° is the interior of X. A closed ball $\mathrm{oob}(x, R)$ of radius R is an *outside osculating ball* of radius R to ∂X at point $x \in \partial X$ if $\partial X \cap \partial \mathrm{oob}(x, R) = \{x\}$ and $\mathrm{oob}(x, R) \subseteq (\mathbb{R}^d \setminus X) \cup \{x\}$. A set X is *par(R)-regular* if there exist an outside and an inside osculating ball of radius R at each $x \in \partial X$ [LCG98]. In the case where X is a d-dimensional object, the reach of ∂X and the R-regularity of X are related as follows.

Lemma 1.21 ([12]). *Let X be a d-dimensional compact domain of $\mathbb{R}^d$. Then*

$$\mathrm{reach}(\partial X) \geq R \quad \Longleftrightarrow \forall R' < R \quad X \textit{ is } \mathrm{par}(R')\text{−regular}.$$

Hausdorff distance between ∂X and its digital counterpart The following theorem is valid for arbitrary dimensions, thus extending a result in 2D [Lac06, Lemma B.9]. For $x \in \partial X$, we denote by $n(x, l)$ the segment of length $2l$, centered on x and aligned with the normal vector at x. Using the projection map, this result is straightforward.

Proposition 1.22 ([12]). *Let X be a compact domain of $\mathbb{R}^d$ such that the reach of ∂X is greater than R. Then, for any digitization step $0 < h < 2R/\sqrt{d}$, the Hausdorff distance between sets ∂X and $\partial_h X$ is less than $\sqrt{d}h/2$. More precisely:*

$$\forall x \in \partial X, \exists y \in \partial_h X, \|x - y\| \leq \frac{\sqrt{d}}{2} h \textit{ and } y \in n(x, \frac{\sqrt{d}}{2} h), \tag{1.8}$$

$$\forall y \in \partial_h X, \exists x \in \partial X, \|x - y\| \leq \frac{\sqrt{d}}{2} h \textit{ and } y \in n(x, \frac{\sqrt{d}}{2} h). \tag{1.9}$$

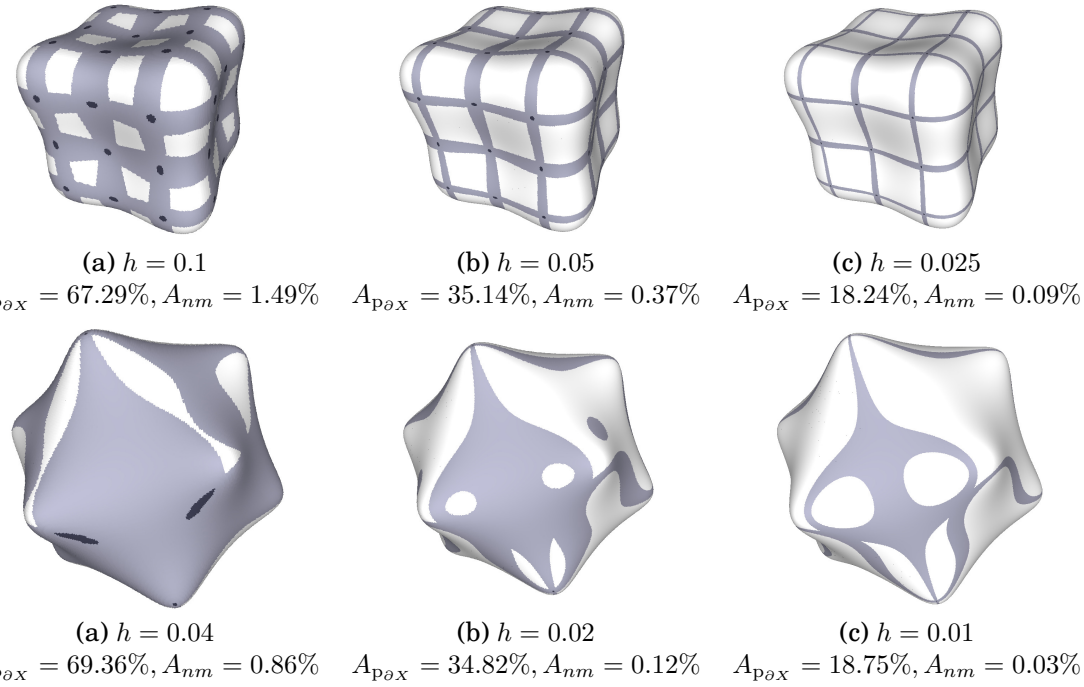

(a) $h = 0.1$
$A_{\mathrm{p}_{\partial X}} = 67.29\%, A_{nm} = 1.49\%$

(b) $h = 0.05$
$A_{\mathrm{p}_{\partial X}} = 35.14\%, A_{nm} = 0.37\%$

(c) $h = 0.025$
$A_{\mathrm{p}_{\partial X}} = 18.24\%, A_{nm} = 0.09\%$

(a) $h = 0.04$
$A_{\mathrm{p}_{\partial X}} = 69.36\%, A_{nm} = 0.86\%$

(b) $h = 0.02$
$A_{\mathrm{p}_{\partial X}} = 34.82\%, A_{nm} = 0.12\%$

(c) $h = 0.01$
$A_{\mathrm{p}_{\partial X}} = 18.75\%, A_{nm} = 0.03\%$

Figure 1.11: Illustration of Theorem 1.23 and Theorem 1.24 on several Gauss digitizations of two polynomial surfaces (top row displays a Goursat's smooth cube and bottom row displays Goursat's smooth icosahedron). Zones in dark grey indicates the surface parts where the Gauss digitization might be non manifold (Theorem 1.23); their relative area is denoted by A_{nm}. Zones in light grey (and dark grey) indicates the surface parts where projection $\mathrm{p}_{\partial X}$ might not be an homeomorphism (Theorem 1.24); their relative area is denoted by $A_{\mathrm{p}_{\partial X}}$. Clearly, both zones tends to area zero as the gridstep gets finer and finer, while parts where digitization might not be manifold are much smaller than parts where $\mathrm{p}_{\partial X}$ might not be homeomorphic.

1.5.2 — Manifoldness of the boundary of Gauss digitized sets in $\mathbb{R}^3$

We show in the following result that only places of ∂X with a normal very close to some axis direction may induce a non-manifold place in the h-boundary (dark grey zones in Figure 1.11). Even better, if the shape is not flat at these places, these zones tend to area zero with finer digitization gridsteps.

Theorem 1.23 ([12]). *Let X be some compact domain of $\mathbb{R}^3$ whose boundary has positive reach and $h < 0.178\mathrm{reach}(\partial X)$. Let y be a point of $\partial_h X$ and C_h be a 2-cell of $\partial_h X$ containing y. If $C_h \cap \partial X = \emptyset$ or if there exists $p \in C_h \cap \partial X$ such that the angle α_y between C_h and the normal to ∂X at p satisfies $\alpha_y \geq 1.2h/R$, then $\partial_h X$ is homeomorphic to a 2-disk around y.*

IDEA OF THE PROOF. The proof relies on the determination of necessary conditions for the presence of *crossed* configurations in the digitized set $\mathrm{D}_h(X)$. There are two kind of crossed configurations.

i) *crossed 8-configuration*: Let p be the point common to eight voxels. We say that there is a *crossed 8-configuration* around p if either only two voxels (out of the eight voxels) belong to $\mathrm{D}_h(X)$ and only share p or if only two voxels (out of the eight voxels) do not belong to $\mathrm{D}_h(X)$ and only share p.

ii) *crossed 4-configuration*: Let e be the edge common to four voxels. We say that there is a *crossed 4-configuration* around p if only two voxels (among the four voxels) belong to $\mathrm{D}_h(X)$ and only share the edge e.

A digital set without crossed configuration is a 2-manifold [Lat97]. The proof is then a technical calculation showing that under the assumptions of the theorem, there is no crossed configuration. □

1.5.3 — Non-homeomorphic part of the projection map

We assume that $h \leq R/\sqrt{d}$, which implies by Proposition 1.22 that the Hausdorff distance between ∂X and $\partial_h X$ is less than $R/2$. Therefore the projection map $\mathrm{p}_{\partial X}$ on ∂X is well defined on $\partial_h X$. However, this map is not one-to-one in general. We show here that the subset of ∂X for which $\mathrm{p}_{\partial X}$ is not injective from $\partial_h X$, otherwise said the part of ∂X with multiplicity greater than one through projection, is small. We define the following set

$$\mathrm{mult}(\partial X) = \{x \in \partial X, \text{s.t. } \exists y_1, y_2 \in \partial_h X, y_1 \neq y_2, \mathrm{p}_{\partial X}(y_1) = \mathrm{p}_{\partial X}(y_2) = x\}. \quad (1.10)$$

Theorem 1.24 ([12]). *If $h \leq R/\sqrt{d}$, then one has*

$$\mathcal{H}^{d-1}(\mathrm{mult}(\partial X)) \leq K_1(h)\, \mathcal{H}^{d-1}(\partial X)\, h,$$

where

$$K_1(h) = \frac{4d^2}{R} + O(h) \leq \frac{d^2\, 3^{d+1}}{R}.$$

Here the constant appearing in $O(h)$ only involves the dimension d and the reach R.

IDEA OF THE PROOF. Let $\mathrm{p}' : \partial_h X \to \partial X$ be the restriction to $\partial_h X$ of the projection $\mathrm{p}_{\partial X}$ onto ∂X. Proposition 1.22 implies that p' is surjective. However, it may not be injective in general. We introduce the set $\mathrm{mult}(\partial_h X) = \mathrm{p}'^{-1}(\mathrm{mult}(\partial X))$. Clearly, the map

$$\mathrm{p}' : \partial_h X \setminus \mathrm{mult}(\partial_h X) \to \partial X \setminus \mathrm{mult}(\partial X)$$

is one-to-one. For any point $x \in \partial X$, we denote by $\mathbf{n}(x)$ the outward unit normal vector to ∂X at x and by $\mathbf{n}_h(y)$ the outward unit normal vector to $\partial_h X$ at y. The outline of the proof is the following:

i) We show that the scalar products between normals of $\partial_h X$ and ∂X is always greater than $-2\sqrt{d}h/R$.

ii) We show that $\mathrm{mult}(\partial X) \subset \mathrm{p}'(P(h))$, where

$$P(h) := \{y \in \partial_h X,\ \langle \mathbf{n}(\mathrm{p}'(y)) | \mathbf{n}_h(y) \rangle \leq 0\}.$$

iii) We show that the $d-1$ jacobian of p' at y is approximately $|\langle \mathbf{n}(\mathrm{p}'(y)) | \mathbf{n}_h(y) \rangle|$,

hence the jacobian of its restriction to $P(h)$ is in $O(h)$.

iv) We conclude that $\mathcal{H}^{d-1}(\mathrm{mult}(\partial X))$ is in $O(h)$.

□

1.5.4 — Digital surface integration

We introduce a digital surface integral and show its convergence. Let $\mathrm{D}_h Z = \cup_{z\in Z}\mathrm{Vox}_h(z)$ be a digital set, namely a union of voxels centered in a point set $Z_h \subset h\cdot\mathbb{Z}^d$. The boundary of this digital set, denoted by $\partial_h Z = \cup_{z\in Z_h}$ is composed of $d-1$ facets.

DEFINITION 1.25. Let $f:\mathbb{R}^d\to\mathbb{R}$ be an integrable function and $\hat{\mathbf{n}}$ be a digital normal estimator. We define the *digital surface integral* by

$$\mathrm{DI}_h(f,\mathrm{D}_h Z,\hat{\mathbf{n}}) := \sum_{c \text{ is a } d-1 \text{ facet of } \partial_h Z} h^{d-1} f(\dot{c})|\hat{\mathbf{n}}(\dot{c})\cdot\mathbf{n}(\dot{c})|,$$

with $\mathbf{n}(\dot{c})$ the trivial normal to the $(d-1)$-cell c.

We recall that the bounded-Lipschitz norm of a function $f:\mathbb{R}^d\to\mathbb{R}$ is given by $\|f\|_{\mathrm{BL}} := \|f\|_\infty + \mathrm{Lip}(f)$. Given a normal estimator $\hat{\mathbf{n}}$ defined on $\partial_h X$, we define the error of the normal estimation by

$$\|\hat{\mathbf{n}}-\mathbf{n}\|_{\mathrm{est}} := \sup_{y\in\partial_h X}\|\mathbf{n}(\mathrm{p}_{\partial X}(y)) - \hat{\mathbf{n}}(y)\|.$$

We prove the convergence of the digital surface integral.

Theorem 1.26 ([12]). *Let X be a compact domain whose boundary has positive reach R. For $h \le \frac{R}{\sqrt{d}}$, the digital integral is convergent towards the integral over ∂X. More precisely, for any integrable function $f:\mathbb{R}^d\to\mathbb{R}$, one gets*

$$\left|\int_{\partial X} f(x)dx - \mathrm{DI}_h(f,\mathrm{D}_h(X),\hat{\mathbf{n}})\right| \le k(R,d)\ \mathcal{H}^{d-1}(\partial X)\ \|f\|_{\mathrm{BL}}\left(h + \|\hat{\mathbf{n}}-\mathbf{n}\|_{\mathrm{est}}\right)$$

where the constant $k(R,d)$ only depends on the dimension d and the reach R.

IDEA OF THE PROOF. Let $\mathrm{p}':\partial_h X\to\partial X$ be the restriction to $\partial_h X$ of the projection $\mathrm{p}_{\partial X}$ onto ∂X. The proof is decomposed as follows

— We first show that the multiplicity of p' is bounded almost everywhere for the (d-1)-Hausdorff measure.

— Since the set where the projection p' is not one-to-one is negligible (Theorem 1.24), we deduce from the general coarea formula that

$$\int_{\partial X} f(x)dx \approx \int_{\partial_h X} f(\mathrm{p}'(y))\mathrm{Jac}(\mathrm{p}')(y)dy,$$

where $\mathrm{Jac}(\mathrm{p}')$ is the $d-1$ jacobian of p'.

— From the relation $\mathrm{Jac}(\mathrm{p}')(y) \approx |\langle\mathbf{n}(\mathrm{p}'(y))|\mathbf{n}_h(y)\rangle|$, where $\mathbf{n}(\mathrm{p}'(y))$ is the normal to ∂X at the point $\mathrm{p}'(y)$ and $\mathbf{n}_h(y)$ is the normal of a $d-1$ face of $\partial_h X$

containing y, we deduce

$$\int_{\partial X} f(x)dx \approx \int_{\partial_h X} f(\mathrm{p}'(y))|\left\langle \mathbf{n}(\mathrm{p}'(y))|\mathbf{n}_h(y)\right\rangle|dy.$$

— Finally, we approximate this integral on each $d-1$ face. The Lipschitz constant appears here, coming from triangle inequalities.

□

Chapter 2

Generalized Voronoi Covariance Measure

Most of the stability properties mentioned in the first chapter derive from the regularity properties and from the Hausdorff stability of the distance function, namely if K and L are Hausdorff-close, then d_K and d_L are uniformly close. Unfortunately, geometric data is usually corrupted with outliers, and the hypothesis of Hausdorff noise is not realistic in practice.

Distance-like functions have been recently introduced in the context of geometric inference because they possess the key regularity properties of the distance function: they are Lipschitz and their square are 1-semiconcave [CCSM11]. The set of distance-like functions contains distance functions, but also contains other functions such as *distances to measures* that are robust to outliers [CCSM11]. Loosely speaking, the underlying idea of using distance to measures in the context of geometric inference is to replace compact sets by measures supported on compact sets and to work with distances to measures that are resistant to outliers (*i.e.*, not sensitive to isolated parts whose measure is "small").

In the particular case where one takes the uniform measure on a point set K, the distance to the measure is called the k-*distance* of K and can be computed using the notion of Power Diagram. Unfortunately it is not computable in practice since the number of cells appearing in the Power Diagram is of the order of $\binom{n}{k}$, where n is the number of points in K. To palliate this problem, a computable k-distance that approximates well the k-distance to K, called the witnessed k-distance, has been introduced in [GMM13].

There are many methods for normal or curvature estimation from point sets. Classical principal component analysis methods try to estimate normal vectors by fitting a tangent plane. In contrast, Voronoi-based methods try to fit the normal cones to the underlying shape, either geometrically [AB99, DS06] or using covariance matrices of Voronoi cells [ACSTD07, MOG11]. In the latter case, the normal estimation is given by the eigenvector corresponding to the largest eigenvalue of the covariance matrix. A tensor-valued measure, which is called the *Voronoi Co-*

variance Measure (VCM), has been defined for any compact set K [MOG11]. This tensor relies on the distance function to the compact set K. It is Hausdorff stable, in the sense that if two compact sets are close in the Hausdorff sense, their VCM are also close to each other. Furthermore the VCM of a smooth surface encodes the normal vector field to this surface. As a consequence, the geometric information extracted from the VCM of a point set which is Hausdorff close to a surface provides an estimation of the normal vector field of the smooth surface.

Contributions With my PhD student Louis Cuel, Jacques-Olivier Lachaud (who was co-advising Louis Cuel) and Quentin Mérigot, we have extended the notion of Voronoi Covariance Measure of a compact set [7]. More precisely, we associate to any distance-like function δ a tensor-valued measures called the δ-Voronoi covariance measure (δ-VCM). We show its stability: if a distance-like function δ approximates well the distance function to a compact set K, then the δ-VCM is close to the VCM of K. When applied to a point cloud P approximating a surface S of $\mathbb{R}^3$, this implies that one can recover the normal vectors of S accurately from δ, if δ is the k-distance to P. This estimation is Hausdorff stable and robust to outliers.

The distance to a measure of a point cloud being not computable in practice, we replace it by the witnessed k-distance. We show that the associated VCM still well approximates the VCM of the underlying surface, which opens the door to practical computations using the notion of Power Diagram. We show on various examples that the δ-VCM provides a very robust normal estimator resilient to Hausdorff noise and to outliers. We also use the δ-VCM to estimate curvatures and sharp features. Finally, with Louis Cuel and Jacques-Olivier Lachaud [8] we also use the VCM in the context of digital geometry and provide a convergent digital normal estimator.

Before detailing our contribution in Sections 2.2, 2.3 and 2.4, we briefly recall definitions and properties of distance-like functions and VCM.

2.1 BACKGROUND ON DISTANCE-LIKE FUNCTIONS AND VCM

We first recall some basics on distance-like functions, distance to measures and k-distances [CCSM11].

Distance-like functions A function $\delta : \mathbb{R}^d \to \mathbb{R}^+$ is called *distance-like* if it is proper (i.e. $\lim_{\|x\|\to\infty} \delta(x) = \infty$) and if δ^2 is 1-semiconcave (i.e. $\delta^2(.) - \|.\|^2$ is concave). These two properties imply that δ is 1-Lipschitz.

Distance functions to compact sets are clearly distance-like. Other typical examples central in this chapter are the power distances. Given a point cloud P and a family of non-negative weights $(\omega_p)_{p\in P}$, the *power distance* to P is the distance-like function δ_P defined by

$$\delta_P(x) := \left(\min_{p\in P} \left(\|x-p\|^2 + \omega_p\right)\right)^{1/2}. \tag{2.1}$$

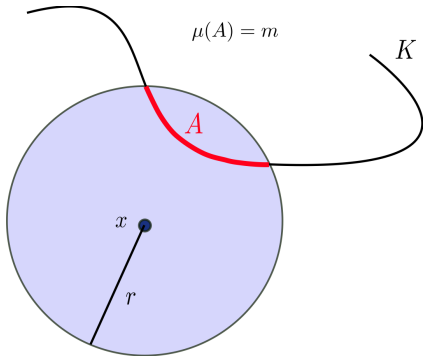

Figure 2.1: Distance to a measure. We suppose here that the measure μ is supported on a compact set K. The quantity $\delta_{\mu,m}(x)$ is the minimal radius r such that $\mathrm{B}(x,r) \cap K$ has a mass m.

When the weights are all zero, the power distance is nothing but the distance function to the point set P. Remark also that a power distance induces a decomposition of the space into a family of convex polyhedra, called power cells, on which the function δ_P^2 is quadratic. The power cell of a point p in P is defined by

$$\mathrm{Pow}_P(p) = \{x \in \mathbb{R}^d; \forall q \in P, \|x-p\|^2 + \omega_p \leq \|x-q\|^2 + \omega_q\}.$$

When the weight vector ω vanishes, we recover the notion of Voronoi cell. Note that the Power Diagram is an important notion in computational geometry that will also be central in the next chapter.

Distance to a measure The distance to a measure is defined for any probability measure μ on $\mathbb{R}^d$. The underlying idea is to replace a compact set by a (uniform) measure on it. Hence an outlier in a compact set K will have an importance related to its mass.

DEFINITION 2.1. Let μ be a probability measure on $\mathbb{R}^d$ and m_0 a regularization parameter in $(0,1)$. The distance to the measure μ is defined for every point x in $\mathbb{R}^d$ by

$$\mathrm{d}_{\mu,m_0}(x) := \left(\frac{1}{m_0}\int_0^{m_0} \delta_{\mu,m}^2(x)\mathrm{d}m\right)^{1/2}, \tag{2.2}$$

where $\delta_{\mu,m}(x) = \inf\{r \geq 0,\ \mu(\mathrm{B}(x,r)) \geq m\}$.

The distance to the measure is distance-like and has been shown to be resilient to wasserstein noise. More precisely, one has [CCSM11, Theorem 3.5]

$$\left\|d_{\mu,m_0} - d_{\mu',m_0}\right\|_\infty \leq \frac{1}{\sqrt{m_0}}\,\mathrm{W}_2(\mu,\mu'),$$

where W_2 is the 2-Wasserstein distance between measures and $\|.\|_\infty$ is the sup norm.

Point cloud case Let $P \subset \mathbb{R}^d$ be a finite point set with n points, $k \in (0, n)$ a real number and $m_0 = k/n$. The *k-distance to P*, denoted by $d_{P,k}$, is the distance to the uniform probability measure on P for the parameter m_0. In the particular case where k is an integer, a simple calculation shows that for every point x in $\mathbb{R}^d$

$$d^2_{P,k}(x) = \frac{1}{k} \sum_{p_i \in \mathrm{NN}_{P,k}(x)} \|x - p_i\|^2 ,$$

where $\mathrm{NN}_{P,k}(x)$ are the k nearest neighbors of x in P. The k-distance $d_{P,k}$ is a power distance. More precisely, if we denote $\mathrm{Bary}_{P,k}$ the set of isobarycenters of k distinct points in P, one has

$$\forall x \in \mathbb{R}^d \quad d^2_{P,k}(x) = \min_{b \in \mathrm{Bary}_{P,k}} \left(\|x - b\|^2 + \omega_b \right) ,$$

where the weight is given by $\omega_b = \frac{1}{k} \sum_{p_i \in \mathrm{NN}_{P,k}(b)} \|b - p_i\|^2$.

Voronoi Covariance Measure The *Voronoi Covariance Measure* is a tensor-valued measure that depends on an offset parameter $R > 0$ [MOG11]. It associates to any measurable function $\chi : \mathbb{R}^d \to \mathbb{R}$ the positive semi-definite matrix defined by

$$\mathcal{V}_{d_K,R}(\chi) = \int_{K^R} (x - p_K(x)) \otimes (x - p_K(x)).\chi(p_K(x))\mathrm{d}x,$$

where $\mathbf{v} \otimes \mathbf{w}$ denotes the $d \times d$ matrix whose entries are defined by $(\mathbf{v} \otimes \mathbf{w})_{ij} = v_i w_j$.

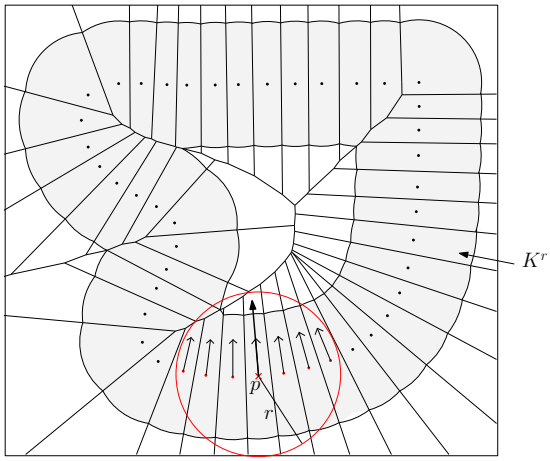

Figure 2.2: VCM of a point set K in $\mathbb{R}^2$. Here χ is the characteristic function of the ball $\mathrm{B}(p, r)$ centered in p and of radius r. $\mathcal{V}_{d_K,R}(\chi)$ is an integral over all the Voronoi cells of the points of $K \cap \mathrm{B}(p, r)$. The eigenvector corresponding to the largest eigenvalue of $\mathcal{V}_{d_K,R}(\chi)$ is shown and is capturing the normal of an underlying smooth curve (Courtesy of Louis Cuel).

This tensor encodes geometric information on the compact set K. In the particular case where S is a smooth compact surface of $\mathbb{R}^3$ with exterior unit normal

$\mathbf{n}$, if R is chosen small enough, one has the following expansion as $r \to 0$:

$$\left\| \mathcal{V}_{d_S,R}(\mathbf{1}_{\mathrm{B}(p,r)}) - \frac{2\pi}{3} R^3 r^2 \left[\mathbf{n}(p) \otimes \mathbf{n}(p)\right] \right\|_{\mathrm{op}} = O(r^3), \tag{2.3}$$

where $\|.\|_{\mathrm{op}}$ is the operator norm. Furthermore, it has been shown that if two compact sets are Hausdorff close, then their VCM are close. Hence, under reasonable assumptions, an eigenvector associated to the highest eigenvalue of $\mathcal{V}_{\mathrm{d}_K,R}(\chi)$ gives an estimation of the normal direction of S at the point p if K is a point set Hausdorff close to S and χ is a function supported on a small ball centered in p.

2.2 δ-VORONOI COVARIANCE MEASURE

We extend the notion of Voronoi Covariance Measure of a compact set. We associate to any distance-like function δ a tensor-valued measure called the *δ-Voronoi Covariance Measure* or δ-VCM.

DEFINITION 2.2 (δ-VCM [7]). The *δ-Voronoi Covariance Measure* is a tensor-valued measure. It associates to any measurable function $\chi : \mathbb{R}^d \to \mathbb{R}$ the positive semi-definite matrix defined by

$$\mathcal{V}_{\delta,R}(\chi) := \int_{\delta^R} \mathbf{n}_\delta(x) \otimes \mathbf{n}_\delta(x).\chi\left(x - \mathbf{n}_\delta(x)\right) \mathrm{d}x, \tag{2.4}$$

where $\delta^R := \delta^{-1}((-\infty, R])$ and $\mathbf{n}_\delta(x) := \frac{1}{2}\nabla\delta^2(x)$.

By the 1-semiconcavity property of distance-like functions, this vector field $\mathbf{n}_\delta$ is defined at almost every point of $\mathbb{R}^d$. The tensor $\mathcal{V}_{\delta,R}(\chi)$ is a convolution of a tensor with the function χ that localizes the calculation on the support of χ. Intuitively, if χ is the indicatrix of a ball $\mathrm{B} \subset \mathbb{R}^d$, then the VCM $\mathcal{V}_{\delta,R}(\chi)$ is the integral of $\mathbf{n}_\delta \otimes \mathbf{n}_\delta$ over the set of points of δ^R whose projection lie in the ball B.

The following lemma shows that computing the VCM of a power distance amounts to computing the covariance matrix of the intersection of each power cell with a ball, and can thus be implemented using the notion of Power Diagram (efficiently implemented in CGAL [Cga]).

Lemma 2.3 ([7]). *Let (P, ω) be a weighted point cloud. For any measurable function $\chi : \mathbb{R}^d \to \mathbb{R}$, one has*

$$\mathcal{V}_{\delta_P,R}(\chi) = \sum_{p \in P} \chi(p)\ M_p, \tag{2.5}$$

where

$$M_p := \int_{C_p} (x-p) \otimes (x-p) \mathrm{d}x \tag{2.6}$$

is the covariance matrix of $C_p := \mathrm{Pow}_P(p) \cap \mathrm{B}(p, (R^2 - \omega_p)^{1/2})$ and $\mathrm{B}(p, (R^2 - \omega_p)^{1/2})$ is the ball centered in p of radius $(R^2 - \omega_p)^{1/2}$).

Stability of the δ-VCM Our main theoretical result is Theorem 2.4, which asserts in a quantitative way that if a distance-like function δ is uniformly close to

the distance function to a compact set, then the δ-VCM is close to the VCM of this compact set. Informally, this theorem shows that one can recover geometric information about a compact set using an approximation of its distance function by a distance-like function. We recall that the bounded-Lipschitz norm of bounded Lischitz function function $f : \mathbb{R}^d \to \mathbb{R}$ is given by $\|f\|_{\mathrm{BL}} = \|f\|_\infty + \mathrm{Lip}(f)$.

Theorem 2.4 ([7]). *Let K be a compact set and δ a distance-like function. For any bounded Lipschitz function $\chi : \mathbb{R}^d \longrightarrow \mathbb{R}$, one has*

$$\|\mathcal{V}_{\delta,R}(\chi) - \mathcal{V}_{d_K,R}(\chi)\|_{\mathrm{op}} \leq C \ \|\chi\|_{\mathrm{BL}} \, \|\delta - d_K\|_\infty^{\frac{1}{2}},$$

where C is a constant that only depends on R, d and $\mathrm{diam}(K)$.

A notable feature of this theorem is that the constant in the upper bound only depends on the diameter of K and not on its local geometry or on its regularity. In practice choosing a test function χ supported in a small ball allows one to recover local information from the δ-VCM.

SKETCH OF PROOF. We have to bound the quantity

$$\int_{K^R} (x - p_K(x)) \otimes (x - p_K(x)).\chi(p_K(x))\mathrm{d}x - \int_{\delta^R} \mathbf{n}_\delta(x) \otimes \mathbf{n}_\delta(x).\chi\left(x - \mathbf{n}_\delta(x)\right) \mathrm{d}x.$$

The idea is to compare the two integrals on the common set $E = K^{R-\varepsilon}$ where $\varepsilon = \|\delta - d_K\|_\infty$ and to show that remaining parts are negligible.

— We first show that $K^{R-\varepsilon} \subset \delta^R \subset K^{R+\varepsilon}$, from which one can show that

$$\mathcal{H}^d(\delta^R \setminus E) = O(\|\delta - d_K\|_\infty) \quad \text{and} \quad \mathcal{H}^d(K^R \setminus E) = O(\|\delta - d_K\|_\infty).$$

— We then bound the integrand. Since d_K^2 and δ^2 are 1-semiconcave, the two functions $\mathbf{n}_\delta$ and $\mathbf{n}_{\mathrm{d}_K}(x) := x - \mathrm{p}_K(x) = \frac{1}{2}\nabla(\|x\|^2 - \mathrm{d}_K^2(x))$ are the gradient of two convex functions [CCSM11]. Using a result that bounds the L^1-norm of the gradient of convex functions, one gets

$$\int_E \|x - \mathrm{p}_K(x) - \mathbf{n}_\delta(x)\|\mathrm{d}x = \int_E \|\mathbf{n}_{\mathrm{d}_K}(x) - \mathbf{n}_\delta(x)\|\mathrm{d}x = O(\|\delta - d_K\|_\infty^{\frac{1}{2}}).$$

— We then conclude by injecting χ and using triangle inequalities. In this step appear the sup norm $\|\chi\|_\infty$ and the Lipschitz constant $\mathrm{Lip}(\chi)$.

□

Stability for the VCM using the k-distance Using the fact that the distance to a measure is resilient to outliers, we show that our δ-VCM, where δ is a distance to a measure or a k-distance, is robust to outliers. Although this result can hold for measures supported in $\mathbb{R}^d$, we choose to state it for uniform measures on surfaces of $\mathbb{R}^3$, so as to give a better intuition.

Corollary 2.5 ([7]). *Let P be a point set with n points, S a surface of $\mathbb{R}^3$, μ_P and μ_S be the uniform probability measures on P and S respectively. There exists $k > 0$*

such that

$$\|\mathcal{V}_{d_{P,k},R}(\chi) - \mathcal{V}_{d_S,R}(\chi)\|_{\mathrm{op}} \leq C \ \|\chi\|_{\mathrm{BL}} \ W_2(\mu_S, \mu_P)^{\frac{1}{4}},$$

where $d_{P,k}$ is the k-distance function to K and the constant C depends on S and R.

Remark this result can be easily extended to any dimension d and also to the case where the measure μ_S supported on the compact set S has a dimension at most l (*i.e.* there exists a constant α_S such that $\mu_S(\mathrm{B}(p,r)) \geq \alpha_S r^l$). Remark also that one can get a similar result if we replace the k-distance by the witnessed k-distance, which is computable in practice.

2.3 COMPUTATION AND EXPERIMENTS

We proposed an algorithm to compute an approximation of the VCM of a power distance. Let (P, ω) be a weighted point cloud that defines a distance-like function δ_P. In practice we replace the unit ball by a convex polyhedron. The input of our algorithm (summarized in Algorithm 1) is a weighted point cloud, a radius R and an approximation of the unit ball by a convex polyhedron B. Using Lemma 2.3, we compute an approximation of the cell C_p by $C_p^B := \mathrm{Pow}_P(p) \cap (p + (R^2 - \omega_p)^{1/2} B)$ and we also compute exactly $M_p^B = \int_{C_p^B} (x-p) \otimes (x-p) \mathrm{d}x$.

Algorithm 1 Computation of the measure $\mathcal{V}_{\delta_P,R}$ supported on P.

Require: $P \subseteq \mathbb{R}^d$ point cloud, $R > 0$, $B =$ approximation of $\mathrm{B}(0,1)$
  Computation of the power diagram $(\mathrm{Pow}_P(p))_{p \in P}$
  for all $p \in P$ **do**
    $C_p^B \leftarrow \mathrm{Pow}_P(p) \cap (p + (R^2 - \omega_p)^{1/2} B)$
    $\Delta_p^1, \ldots, \Delta_p^{k_p} \leftarrow$ decomposition of C_p^B into tetrahedra
    $M_p^B \leftarrow \sum_{i=1}^{k_p} \int_{\Delta_p^i} (x-p) \otimes (x-p) \mathrm{d}x$
  end for
  return $(M_p^B)_{p \in P}$.

In practice, we choose for the power distance the witnessed k-distance. Remark that one can also try other power distances [7]. Once we have the measure $(M_p^B)_{p \in P}$, we compute for each point q in P an approximation of the covariance matrix $\mathcal{V}_{\delta_P,R}(\chi_q^r)$, where χ_q^r is the characteristic function of the ball $\mathrm{B}(q,r)$. We use it for normal estimation and also feature detection in noisy point sets (Figures 2.3 and 2.4). The estimations are very robust in practice.

2.4 DIGITAL VORONOI COVARIANCE MEASURE IN $\mathbb{R}^3$

We also have adapted the Voronoi Covariance Measure in digital geometry [8]. The VCM also provides accurate results in this context, in particular on normal estimation (see Figure 2.5). Let $\mathrm{D}_h Z = \cup_{z \in Z} \mathrm{Vox}_h(z)$ be a digital set, where $Z_h \subset h\mathbb{Z}^3$ is set of points. We denote by $\partial_h Z$ the boundary of $\mathrm{D}_h Z$. We define the digital

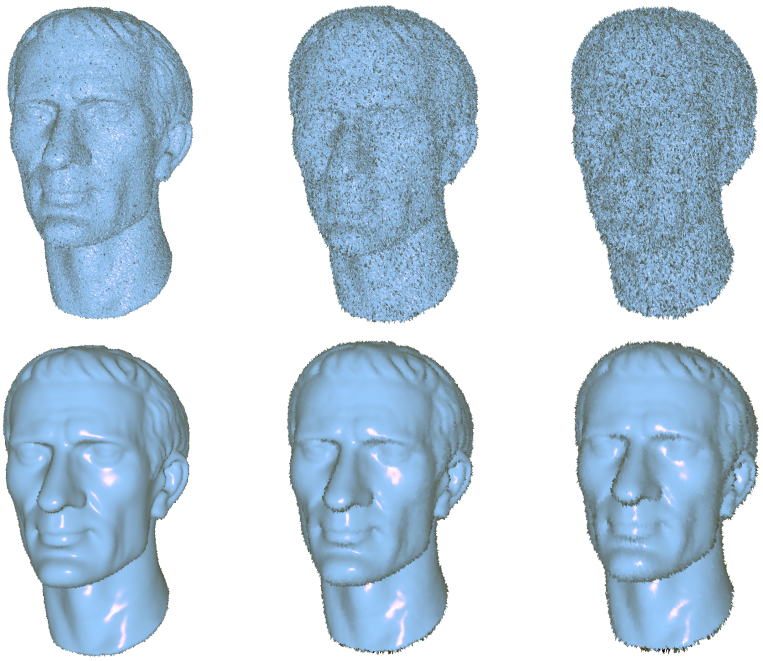

Figure 2.3: Rendering of "caesar" data using triangle normal (top row) and estimated δ-VCM normal (bottom row) where δ is the witnessed k-distance. Rendering with Phong shading, parameters $R = 0.04\mathrm{D}$, $r = 0.04\mathrm{D}$, $k = 30$, where D is the diameter of the original shape. From left to right, all the vertices are moved randomly at a distance less $0.02\mathrm{D}$, $0.04\mathrm{D}$ and $0.06\mathrm{D}$.

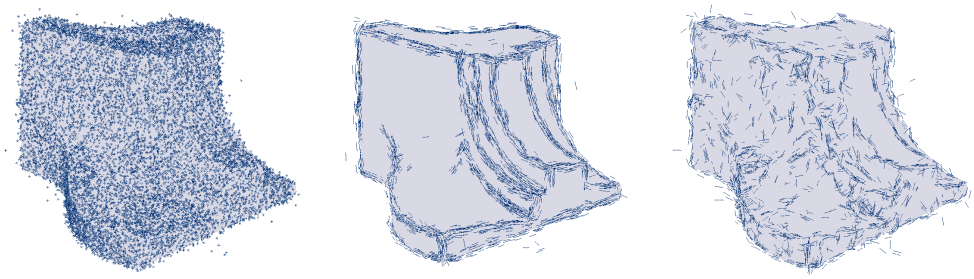

Input δ-VCM VCM

Figure 2.4: Edge detection on a noisy fandisk of diameter D: 98% of the points are moved at a distance at most $0.05\mathrm{D}$ and 2% are moved at a distance at most $0.25\mathrm{D}$ (Input). The results are computed with the parameters $R = 0.06\mathrm{D}$ and $r = 0.02\mathrm{D}$. In the middle, we have the δ-VCM, where δ is the witnessed k-distance (with $k = 30$). On the right, we have the results with the VCM.

VCM of $\mathrm{D}_h Z$ that associates to any measurable function $\chi : \mathbb{R}^d \to \mathbb{R}$ the matrix

$$\widehat{\mathcal{V}}_{\mathrm{D}_h Z, R}(\chi) := \sum_{x \in \Omega_h^R} h^3 (x - p_{P_h}(x)) \otimes (x - p_{P_h}(x)) \chi(p_{P_h}(x)),$$

where $P_h := \partial_h Z \cap h(\mathbb{Z} + \frac{1}{2})^3$ is the set of vertices of $\partial_h Z$; $\Omega_h^R = \{x \in P_h^R \cap h(\mathbb{Z} + \frac{1}{2})^3, \mathrm{Vox}_h(x) \subset P_h^R\}$ is the set of centers of voxels entirely contained in the R-

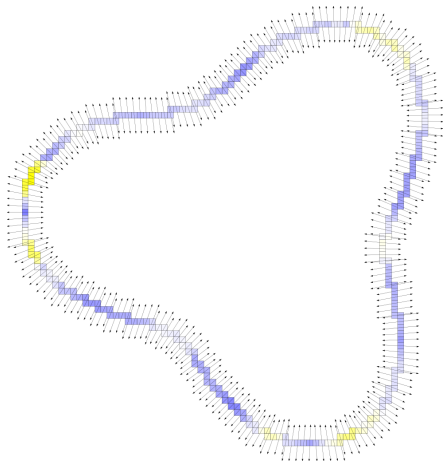

Figure 2.5: Normal estimation of digital set. The computation is made with the Dgtal library

offset P_h^R of P_h. We define the *normal direction estimator* $\widehat{n}_{r,R}(p_0)$ at a point p_0 as the direction of an eigenvector associated to the largest eigenvalue of $\widehat{\mathcal{V}}_{Z_h,R}(\chi_r)$, where χ_r is a Lipschitz function that is equal to 1 on $\mathrm{B}(p_0, r)$, equal to 0 outside $\mathrm{B}(p_0, r + r^{\frac{3}{2}})$ and that linearly interpolates in $\mathrm{B}(p_0, r + r^{\frac{3}{2}}) \setminus \mathrm{B}(p_0, r)$. One obtains in particular the following convergence result.

Corollary 2.6 ([8]). *Let X be a compact domain of $\mathbb{R}^3$ whose boundary ∂X is a C^2 surface. Let $a, b \in \mathbb{R}^+$, $r = ah^{\frac{1}{4}}$ and $R = bh^{\frac{1}{4}}$. Then the angle between the normal $N(p_0)$ to S at p_0 and the direction $\widehat{n}_{r,R}(p_0)$ satisfies*

$$\left(\widehat{n}_{r,R}\widehat{(p_0), n}(p_0)\right) \leq C_S\, h^{\frac{1}{8}}.$$

where the constant C_S only depends on the reach of ∂X.

One observes in practice a better convergence with a speed in $O(h)$. The proof has a similar flavor than the one of the δ-VCM stability. The main differences are the following: since we want to relate the parameters r and R and make them tend to 0, we have to localize the calculations. Furthermore, the numerical error due to the digitalization has to be taken into account. Using a local version of the Weyl's tube formula, we bound locally the volume of the symmetric difference of some offsets.

2.5 PERSPECTIVES

Curvature measures robust to outliers We have noticed with Frédéric Chazal, David Cohen-Steiner and Quentin Mérigot that the curvature measure stability theorem might be generalized with the distance to the measure. Indeed, the regularity result on the offset and double offset of compact set with positive μ-reach can be straightforwardly generalized to distance-like functions (instead of distance functions). More precisely, if $\delta : \mathbb{R}^d \to \mathbb{R}$ is a distance-like function such that $\|\nabla\delta(x)\| > \mu$ for $x \in \delta^{-1}([r, R])$ then the reach of $\delta^{-1}([r, +\infty])$ is greater than

a strictly positive constant. This can be used to show that if a distance like function δ is close to the distance function d_K of a compact set, then $\delta^{-1}([r, +\infty])$ has positive reach for an appropriate r. One may then proceed similarly as in [6] to show that the curvature measures are robust to outliers.

Stable sharp edge reconstruction The idea is to get a method which allows one to reconstruct a surface from a point cloud corrupted with outliers without oversmoothing its sharp features. Suppose we are given a projection that smoothes sharp edges, for example a projection corresponding to a convolved distance function, such as a distance to a measure, and that this projection is corrected so as to reinforce sharp edges. Then one wants to rebuild a distance-like function that preserves these sharp edges.

More precisely, given a projection map $\mathrm{p} : \mathbb{R}^d \to \mathbb{R}^d$ defined H^d almost everywhere, we want to consider the following optimization problem

$$\min_{\delta} \int_{\mathbb{R}^d} \|\frac{1}{2}\nabla\psi_\delta(x) - \mathrm{p}(x)\|^2 d\mathcal{H}^d(x), \tag{2.7}$$

where $\psi_\delta(x) := \|x\|^2 - \delta^2(x)$ and the infimum is taken over all the distance-like functions. Remark that the semiconcavity condition for δ^2 is almost a convex constraint. In general, the discretization of this kind of problem is not straightforward. For example, the space of piecewise linear convex functions on regular grids of the square is not dense in the space of convex functions on the square [CLM01]. One may proceed with geometric methods similarly to [MO14].

Chapter 3

Reflector problem and numerical optimal transport

The reflector problem is motivated by concrete applications in which one wants to light precisely in certain directions. It appears for example naturally in the context of automotive and aerospace industries for the design of car beams where one wants to light in specific directions with a given intensity. The problem consists in designing a reflector surface that is going to reflect a light source, emitted for example by a bulb, to a prescribed light intensity in the space of directions.

In the particular case where the light source is punctual, namely when the light is only emitted by one point, the reflector problem is well posed, has been extensively studied and is referred as the *far-field reflector problem*. The inputs are the description of the light distribution emitted by a punctual light source located at the origin and a desired target distribution of light at infinity, that is, on the sphere of directions. When the two light distributions can be modeled by a probability density μ on the source sphere and a probability density ν on the target sphere, the far-field reflector problem can be formulated as a generalized Monge-Ampère equation on the sphere. This equation is a fully non-linear elliptic partial differential equation. L.A Caffarelli and V. Oliker proved the existence of weak solutions to this equation in a preprint from 1994 (published in 2008 [CO08]), and the uniqueness has also been determined under different conditions on the densities [Wan96, GW98].

Semi-discrete Monge-Ampère equation The approach of L. A. Caffarelli and V. Oliker to show the existence of a weak solution to the far field reflector problem is geometric [CO08] and works as follows: they approximate the target probability measure ν by a sequence of discrete measures $\nu_N = \sum_i \alpha_i \delta_{y_i}$ supported on a finite set of directions $Y = \{y_1, \dots, y_N\}$. They show the existence of a solution to the (semi-discrete) far field reflector problem between μ and ν_N, and show that this solution converges to a solution of the original problem as N tends to infinity.

For the semi-discrete problem between μ and ν_N, they build a surface composed of patches of N confocal paraboloids of revolution. Denote by $P(y, \lambda)$ the

convex hull of a paraboloid of revolution focused at the origin with direction y and focal distance λ. It is well known that any ray of light emanating from the focal point is reflected by the surface $\partial P(y, \lambda)$ in the direction y. Caffarelli and Oliker ensure there exist focal distances $\lambda_1, \ldots, \lambda_N$ such that the surface $\mathcal{R} = \partial(\cap_{1 \leq i \leq N} P(y_i, \lambda_i))$ solves the far field reflector problem: for every i, the amount of light reflected by $\mathcal{R}$ in the direction y_i is exactly α_i [CO08] .

They also propose an algorithm based on this *Supporting paraboloids* approach [CKO99]. Given a desired precision error ε, this algorithm constructs in $\mathbb{R}^3$ a solution in N^2/ε steps. At each step, the algorithm requires the computation of the intersection of N confocal paraboloids.

Optimal transport The far field reflector problem was shown in 2003 to be equivalent to an optimal transport problem on the sphere [GO03, Wan04]. This new formulation allows to reformulate the reflector problem as a linear programming problem, as already noticed by X. J. Wang [Wan04]. Furthermore, it also opens the door to a concave maximization formulation, using Kantorovich duality. This concave formulation is similar to an approach suggested by Aurenhammer, Hoffmann and Aronov [AHA98] to solve the quadratic optimal transport problem in the plane between a measure with density and a finitely supported measure. Quentin Mérigot also used this approach in a multiscale algorithm to compute the optimal transport in the plane for the quadratic cost [Mér11].

Similar inverse problems in geometric optics. The far-field reflector problem is related to the intersection of solid confocal paraboloids, but can also be handled using union of solid confocal paraboloids [GO03]. In the *near field reflector problem*, where one wants to illuminate points in the space instead of directions, reflector surfaces are made of patches of ellipsoids and can be built as union or intersections of solid ellipsoids [Oli03, KO97]. Using a radial parameterization, each of these computations is equivalent to the computation of a decomposition of the unit sphere into cells, that are not necessarily connected.

Contributions. With Pedro Machado de Manhães and Quentin Mérigot, we worked on the numerical resolution of the reflector problem in the semi-discrete setting [10].

— We show that the cells on the sphere for the four types of reflectors (union or intersection of confocal paraboloids or ellipsoids) can be computed by intersecting a certain power diagram with the unit sphere.

— We show that the complexity bounds of these four diagram types on the sphere are different. In the case of intersection of solid confocal paraboloids in $\mathbb{R}^3$, the complexity of the intersection diagram is $O(N)$. This is in contrast with the $\Omega(N^2)$ complexity of the intersection of a power diagram with a paraboloid in $\mathbb{R}^3$ [BK03]. In the case of the union and intersection of solid confocal ellipsoids, we recover this $\Omega(N^2)$ complexity. Finally, the case of the union of paraboloids is very different from the case of the intersection of paraboloids. Indeed, in the latter case, the corresponding cells on the sphere are connected, while in the former case the number of connected component

of a single cell can be $\Omega(N)$. The complexity of the diagram in this case is unknown.

— We propose an algorithm for computing the intersection of a power diagram with the unit sphere. This algorithm uses the exact geometric computation paradigm, implying that the combinatorics of the cells is exact and does not depend on numerical approximations. It can be applied to the four types of unions and intersections. It is optimal for the union and intersection of ellipsoids, but its optimality for the case of intersection of paraboloids is open.

— We use our algorithm for the numerical resolution of the far-field reflector problem. Using a known optimal transport formulation [Wan04, GO03] and similar techniques to [AHA98], we cast this problem into a concave maximization problem.

Together with our PhD student André Julien, co-advised with Dominique Attali and Quentin Mérigot, we have also proposed heuristics that take into account industrial design constraints on the reflector surface [1].

3.1 INTERSECTION OF CONFOCAL PARABOLOIDS OF REVOLUTION

Because of their optical properties, finite intersections of solid paraboloids of revolutions with the same focal point play a crucial role in the far-field reflector problem. We show that the geometry and the combinatorics of the paraboloid intersection can be obtained by intersecting a power diagram in $\mathbb{R}^d$ with the unit sphere, which is very useful for the numerical computation.

Paraboloid intersection diagram A paraboloid of revolution in $\mathbb{R}^d$ with focal point at the origin is uniquely defined by its focal distance λ and its direction, described by a unit vector y. We denote by $P(y, \lambda)$ the convex hull of such a paraboloid. Given a family $Y = (y_i)_{1\leq i\leq N}$ of unit vectors and a family $\lambda = (\lambda_i)_{1\leq i\leq N}$ of *positive* focal distances, we denote by $\mathcal{R}_Y^\lambda = \partial(\cap_{1\leq i\leq N} P(y_i, \lambda_i))$ the boundary of the intersection of the solid paraboloids $(P(y_i, \lambda_i))_{1\leq i\leq N}$.

DEFINITION 3.1. The *paraboloid intersection diagram* associated to a family of solid paraboloids $(P(y_i, \lambda_i))_{1\leq i\leq N}$ is a decomposition of the unit sphere into N cells defined by:

$$\mathrm{PI}_Y^\lambda(y_i) := \mathrm{p}_{\mathcal{S}^{d-1}}(\mathcal{R}_Y^\lambda \cap \partial P(y_i, \lambda_i))$$

where $\mathrm{p}_{\mathcal{S}^{d-1}}$ is the radial projection onto the sphere.

Power diagram formulation The power diagram is a well known tool from computational geometry that we have already used in the context of geometric inference. We recall that it associates to any weighted point cloud (P, ω) of $\mathbb{R}^d$ a decomposition of the space into power cells defined for every points p of P by:

$$\mathrm{Pow}_P(p) = \{x \in \mathbb{R}^d; \forall q \in P, \|x - p\|^2 + \omega_p \leq \|x - q\|^2 + \omega_q\}.$$

It can be efficiently computed using for example the C++ library CGAL [Cga]. We show here that it can be used to compute the paraboloid intersection diagram on the sphere. More precisely

Proposition 3.2 ([10]). *Let $(P(y_i,\lambda_i))_{1\le i\le N}$ be a family of confocal paraboloids. One has*

$$\forall i \in \{1,\dots,N\} \quad \mathrm{PI}_Y^\lambda(y_i) = \mathcal{S}^{d-1} \cap \mathrm{Pow}_P^\omega(p_i),$$

where the points and weights are given by $p_i = -(\lambda_i^{-1}/2)y_i$ and $\omega_i = -\lambda_i^{-1} - \lambda_i^{-2}/4$.

Proof. The proof is straightforward and is using the radial parametrization of the paraboloids. The boundary surface $\partial P(y_i,\lambda_i)$ can be parameterized in spherical coordinates by the radial map $u \in \mathcal{S}^{d-1} \mapsto \rho_{y_i,\lambda_i}(u)\ u$, where $\rho_{y_i,\lambda_i}(u) := \frac{\lambda_i}{1-\langle y_i|u\rangle}$. For any point $u \in \mathcal{S}^{d-1}$, we have the following equivalence:

$$u \text{ belongs to } \mathrm{PI}_Y^\lambda(y_k) \iff k = \arg\min_{1\le i\le N} \frac{\lambda_i}{1-\langle y_i|u\rangle} \iff k = \arg\max_{1\le i\le N} \lambda_i^{-1} - \left\langle u|\lambda_i^{-1}y_i\right\rangle.$$

An easy computation gives:

$$\begin{aligned}\max_{1\le i\le N} \lambda_i^{-1} - \left\langle u|\lambda_i^{-1}y_i\right\rangle &= \max_{1\le i\le N} \lambda_i^{-1} - \left\|u + \tfrac{1}{2}\lambda_i^{-1}y_i\right\|^2 + \|u\|^2 + \tfrac{1}{4}\left\|\lambda_i^{-1}y_i\right\|^2 \\ &= \|u\|^2 - \min_{1\le i\le N}\left(\left\|u + \tfrac{1}{2}\lambda_i^{-1}y_i\right\|^2 - \lambda_i^{-1} - \tfrac{1}{4}\lambda_i^{-2}\right).\end{aligned}$$

This implies that a unit vector u belongs to the paraboloid intersection cell $\mathrm{PI}_Y^\lambda(y_i)$ if and only if it lies in the power cell $\mathrm{Pow}_P^\omega(p_i)$. □

Complexity of the paraboloid intersection diagram in $\mathbb{R}^3$ The paraboloid intersection diagram in $\mathbb{R}^3$ contains edges, circular edges and faces, as illustrated in Figure 3.1. The study of the complexity of this diagram strongly relies on the following proposition [CO08].

Proposition 3.3. *Let $P(y,\lambda)$ and $P(z,\mu)$ be two confocal paraboloids and $\mathcal{R} = \partial\Big(P(y,\lambda)\cap P(z,\mu)\Big)$. Then the orthogonal projection of $\mathcal{R}\cap\partial P(y,\lambda)$ onto the plane orthogonal to y is a disc.*

Let $\mathcal{R}_Y^\lambda = \partial(\cap_{1\le i\le N}\partial P(y_i,\lambda_i))$ be the reflector surface associated to the family of N paraboloids and let $\mathcal{R}_i = \mathcal{R}_Y^\lambda \cap \partial P(y_i,\lambda_i)$ be the part of the reflector corresponding to the paraboloid $P(y_i,\lambda_i)$. The previous proposition implies that the orthogonal projection of $\mathcal{R}_i$ onto the plane orthogonal to y_i is an intersection of $N-1$ discs, thus is convex. Hence $\mathcal{R}_i$ and $\mathrm{PI}_Y^\lambda(y_i)$ are connected, and the number of faces of the paraboloid intersection diagram is less than N. Using Euler's formula, one can then prove the following theorem.

Theorem 3.4 ([10]). *Let $(P(y_i,\lambda_i))_{1\le i\le N}$ be a family of solid paraboloids of $\mathbb{R}^3$. Then the number of edges, vertices and faces of its paraboloid intersection diagram is in $O(N)$.*

We show that the computation complexity of the paraboloid intersection diagram amounts to a sorting algorithm of N reals, thus leading to the following result:

Proposition 3.5 ([10]). *The complexity of the computation of the paraboloid intersection diagram is $\Omega(N\log(N))$, even under an assumption of genericity.*

3.2 OTHER TYPES OF UNION AND INTERSECTIONS

Other types of union or intersection of quadrics appear in non-imaging optic problems. In the far-field reflector case, instead of building a reflector surface as the boundary of the intersection of filled confocal paraboloids, one can also consider the boundary of the union of filled confocal paraboloids [GO03]. In the *near field reflector problem*, where one wants to illuminate points in the space instead of directions (as in the far-field reflector problem) [KO97], one considers solutions made of patches of ellipsoids. It is therefore natural to consider intersection or union of ellipsoids. As for the paraboloids intersection, we show that the geometry and the combinatorics can be obtained by intersecting a power diagram in $\mathbb{R}^d$ with the unit sphere.

Union of confocal paraboloids of revolution Let $\mathcal{RU}_T^\lambda := \partial\Big(\bigcup_{1\le j\le N} P(y_j,\lambda_j)\Big)$ denote the boundary of the union of paraboloids. This surface can be parameterized over the sphere $\mathcal{S}^{d-1}$, and one defines the *paraboloid union diagram* as the associated decomposition of the sphere into cells:

$$\mathrm{PU}_Y^\lambda(y_i) := \mathrm{p}_{\mathcal{S}^{d-1}}\left(\mathcal{RU}_T^\lambda \cap \partial P(y_i,\lambda_i)\right).$$

As before, we show that these cells can be seen as the intersection of certain power cells with the unit sphere.

Proposition 3.6 ([10]). *Given a family $(P(y_i,\lambda_i))_{1\le i\le N}$ of solid paraboloids, one has for all i,*

$$\mathrm{PU}_Y^\lambda(y_i) = \mathcal{S}^{d-1} \cap \mathrm{pow}_P^\omega(p_i),$$

where the points and weights are given by $p_i = \frac{1}{2}\lambda_i^{-1}y_i$ and $\omega_i = \lambda_i^{-1} - \frac{1}{4}\lambda_i^{-2}$.

Proposition 3.3 implies that for every i, the projection of $\mathcal{R}_i := \mathcal{RU}_Y^\lambda \cap \partial P(y_i,\lambda_i)$ onto the plane orthogonal to y_i is a finite intersection of *complements of discs*. Consequently, one cannot use the connectedness argument as in the proof of Theorem 3.4, and the complexity of the paraboloid union diagram is unknown in dimension three. Actually, we constructed an example of a family of paraboloids $(P(y_i,\lambda_i))_{0\le i\le N}$ such that the paraboloid union cell $\mathrm{PU}_Y^\lambda(y_1)$ has $\Omega(N)$ connected components.

Intersection and union of confocal ellipsoids of revolution An ellipsoid of revolution whose one focal point lies at the origin is characterized by its second focal point y and its eccentricity e in $(0,1)$. We denote by $E(y,e)$ the convex hull of such an ellipsoid of revolution. Given a family of ellipsoids $(E(y_i,e_i))_{1\le i\le N}$, we denote by $\mathcal{EI}_Y^e := \partial\Big(\bigcap_{1\le i\le N} E(y_i,e_i)\Big)$ and $\mathcal{EU}_Y^e := \partial\Big(\bigcup_{1\le i\le N} E(y_i,e_i)\Big)$ respectively the boundary of the intersection and of the union of ellipsoids. These two surfaces

can be parameterized over the unit sphere. The *ellipsoid intersection diagram* is the decomposition of the unit sphere into cells

$$\mathrm{EI}^e_Y(y_i) := \mathrm{p}_{\mathcal{S}^{d-1}}\left(\mathcal{EI}^e_Y \cap \partial E(y_i, e_i)\right).$$

Similarly, the cells of the *ellipsoid union diagram* are defined by

$$\mathrm{EU}^e_Y(y_i) := \mathrm{p}_{\mathcal{S}^{d-1}}\left(\mathcal{EU}^e_Y \cap \partial E(y_i, e_i)\right).$$

As for the paraboloids, the computation of each diagram amounts to compute the intersection of a power diagram with the unit sphere.

Proposition 3.7 ([10]). *Let $(E(y_i, e_i))_{1\leq i\leq N}$ be a family of solid confocal ellipsoids. Then*

(i) the cells of the ellipsoid intersection diagram are given by $\mathrm{EI}^e_Y(y_i) = \mathcal{S}^{d-1} \cap \mathrm{pow}^\omega_P(p_i)$, where $p_i = -\frac{e_i}{2d_i}\frac{y_i}{\|y_i\|}$ and $\omega_i = -\frac{1}{d_i} - \frac{e_i^2}{4d_i^2}$.

(ii) The cells of the ellipsoid union diagram are given by : $\mathrm{EU}^e_Y(y_i) = \mathcal{S}^{d-1} \cap \mathrm{pow}^\omega_P(p_i)$, where $p_i = \frac{e_i}{2d_i}\frac{y_i}{\|y_i\|}$ and $\omega_i = \frac{1}{d_i} - \frac{e_i^2}{4d_i^2}$.

The theorem below shows that in dimension three the complexity of these diagrams can be quadratic in the number of ellipsoids. This is in sharp contrast with the case of the paraboloid intersection diagram, where the complexity is linear in the number of paraboloids.

Theorem 3.8 ([10]). *In $\mathbb{R}^3$, there exists a configuration of confocal ellipsoids of revolution such that the number of vertices and edges in the ellipsoid intersection diagram (resp. the ellipsoids union diagram) is $\Omega(N^2)$.*

3.3 COMPUTING THE INTERSECTION OF A POWER DIAGRAM WITH A SPHERE

We have a robust and efficient algorithm to compute the intersection between a power diagram of a weighted point set (P, ω) in $\mathbb{R}^3$ and the unit sphere $\mathcal{S}^2$. This algorithm is implemented using the Computational Geometry Algorithms Library (CGAL) [Cga], and bears some similarity to [BK03, Del08]. Our algorithm provides the exact combinatorial structure of the diagram on the sphere for points whose coordinates and weights are rational.

Note that the intersection diagram has complex combinatorics. If one assumes that the weighted points are given by a paraboloid intersection diagram, Proposition 3.3 shows that the cells on the sphere are connected. But even in this case, the intersection between two adjacent cells on the sphere can have multiple connected components. Consequently, one cannot hope to be able to reconstruct these cells from the adjacency graph (i.e., the graph that contains the points in P as vertices, and where two vertices are connected by an arc if the two cells intersect in a non-trivial circular arc), even in this simple case. In general, the cells of the intersection diagram can be disconnected and they can have holes, as shown in Figure 3.1. We prove the following for our algorithm:

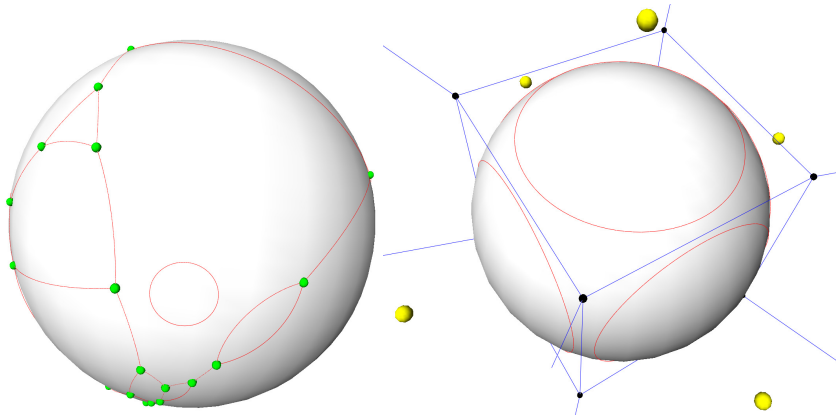

Figure 3.1: **Examples of diagram on the sphere.** *Left: an intersection diagram containing faces with no vertices, faces with holes and faces with two vertices or more. Right: a diagram corresponding to the intersection of a cube and a sphere; there are seven faces, six faces with no vertices, and a face with no vertices and six holes.*

Theorem 3.9 ([10]). *There is an $O(N \log N + C)$ algorithm for obtaining the intersection diagram of a set P of N weighted points in $\mathbb{R}^3$, where C is the complexity of the power diagram of P.*

From Theorem 3.8, the size of the output in the worst case for the intersection (or union) of confocal ellipsoids is $\Omega(N^2)$. This implies that our algorithm is optimal for computing an ellipsoid intersection (or union) diagram. The optimality of the algorithm for the paraboloid intersection diagram is an open problem.

3.4 NUMERICAL RESOLUTION AND SEMI-DISCRETE OPTIMAL TRANSPORT

We consider a discrete probability measure $\mu_N = \sum_{1 \le i \le N} \alpha_i \, \delta_{y_i}$ supported on the finite set of points $Y = (y_1, \ldots, y_N)$ of the unit (target) sphere, and a probability density ρ on the unit (source) sphere. The far-field reflector problem consists in finding a vector of non-negative focal distances $(\lambda_i)_{1 \le i \le N}$, such that

$$\forall i \in \{1, \ldots, N\}, \quad \rho(\mathrm{PI}_Y^\lambda(y_i)) = \alpha_i, \tag{FF}$$

where for a subset X of the sphere, $\rho(X) := \int_X \rho(u) \mathrm{d}u$ is the weighted area of X. Since all the incident rays of the cell $\mathrm{PI}_Y^\lambda(y_i)$ are reflected to the direction y_i, this means that the measure received by y_i is exactly α_i.

Semi-discrete optimal transport formulation It was noticed in 2003 that the far field reflector problem can be seen as an optimal transport problem on the sphere for the cost $c : \mathcal{S}^{d-1} \times \mathcal{S}^{d-1} \to \mathbb{R}$ given by $c(x, y) = -\log(1 - \langle x | y \rangle)$. In the semi-discrete setting, the cells $(\mathrm{PI}_Y^\lambda(y_i))_{1 \le i \le N}$ on the sphere correspond to the c-subdifferential of the dual variable $\psi : Y \to \mathbb{R}$, where $\psi(y_i) = \log(\lambda_i)$, also called Laguerre cells, as expressed by the following lemma.

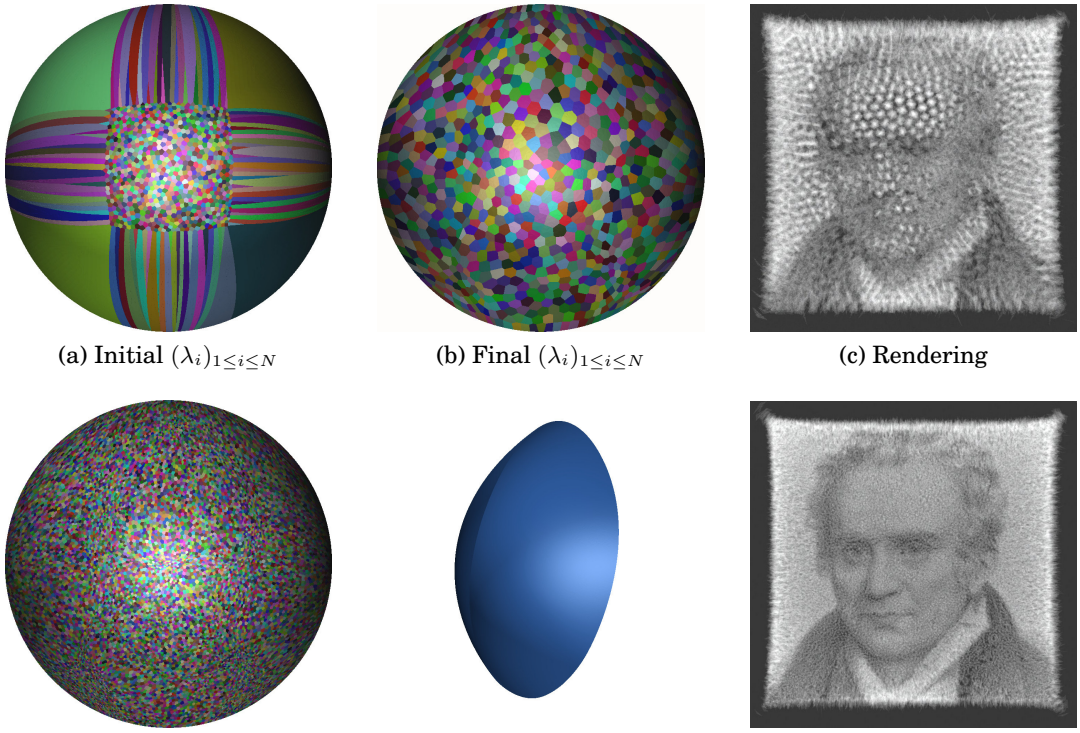

(a) Initial $(\lambda_i)_{1\leq i\leq N}$ (b) Final $(\lambda_i)_{1\leq i\leq N}$ (c) Rendering

(d) Final $(\lambda_i)_{1\leq i\leq N}$ (e) Reflector (f) Rendering

Figure 3.2: **Numerical computation.** *Calculations were done with $N = 1000$ paraboloids for the first row and $N = 15000$ paraboloids for the second row. (a) Paraboloid intersection diagram for an initial $(\lambda_i)_{1\leq i\leq N}$. (b,d) Final intersection diagram after optimization. (e) Reflector surface defined by the intersection of paraboloids. (c,f) Simulation of the illumination at infinity from a punctual light source lighting uniformly $\mathcal{S}^2_-$, using* LUXRENDER*, a physically accurate raytracer engine.*

Lemma 3.10. *The cells of the paraboloid intersection diagram are given by*

$$\mathrm{PI}_Y^\lambda(y_i) = \{x \in \mathcal{S}^{d-1},\ c(x, y_i) + \psi_i \leq c(x, y_j) + \psi_j \quad \forall j\},$$

where $c(x, y) = -\log(1 - \langle x|y\rangle)$ *and* $\psi_i := \log(\lambda_i)$.

Proof. The proof is straightforward and is using the radial parameterization of paraboloids. Let x be a point of the unit sphere $\mathcal{S}^{d-1}$. Then

$$\begin{aligned} x \in \mathrm{PI}_Y^\lambda(y_i) \quad &\iff i \in \arg\min_j \tfrac{\lambda_j}{1-\langle x|y_j\rangle} \\ &\iff i \in \arg\min_j \log(\lambda_j) - \log(1 - \langle x|y_j\rangle) \\ &\iff i \in \arg\min_j \psi_j + c(x, y_j) \end{aligned}$$

□

Using the Kantorovitch functional, the far-field reflector problem can be transformed into the maximization of a concave functional, combining ideas from [Wan04, GO03, AHA98].

Theorem 3.11 ([10]). *A vector of focal distances $(\lambda_i)_{1\leq i\leq N}$ solves the far-field reflector problem* (FF) *if and only if the vector $\psi := (\psi_i)_{1\leq i\leq N}$ defined by $\psi_i = \log(\lambda_i)$ is a global maximizer of the following $\mathcal{C}^1$ concave function:*

$$\Phi(\psi) := \left[\sum_{i=1}^{N} \int_{\mathrm{PI}_Y^{\exp\psi}(y_i)} (c(u, y_i) + \psi_i)\rho(u)\mathrm{d}u\right] - \sum_{i=1}^{N} \psi_i\alpha_i \tag{3.1}$$

where $c(u, v) := -\log(1 - \langle u|v\rangle)$ and with the convention $\log(0) = -\infty$. Moreover, the gradient of the function Φ is given by

$$\nabla\Phi(\psi) := (\rho(\mathrm{PI}_Y^{\exp(\psi)}(y_i)) - \alpha_i)_{1\leq i\leq N}. \tag{3.2}$$

The implementation of the maximization of the functional Φ follows closely [Mér11]. We rely on a quasi-Newton method, which only requires being able to evaluate the value of Φ and the value of its gradient at any point ψ, as given by Equations (3.1)–(3.2). The computations of these values are performed in two steps. First, we compute the boundary of the paraboloid intersection cells $\mathrm{PI}_Y^{\exp(\psi)}(y_i)$, using the algorithm described in Section 3.3. These cells are then tessellated, and the integrals in Equations (3.1)–(3.2) are evaluated numerically using a simple Gaussian quadrature. In the experiments illustrated in Figure 3.2, we constructed the measure $\sum_i \alpha_i\delta_{y_i}$ so as to approximate a picture of Gaspard Monge (projected on a part of the half-sphere $\mathcal{S}^2_+ := \mathcal{S}^2 \cap \{z \geq 0\}$). The density ρ is constant in the half-sphere $\mathcal{S}^2_-$ and vanishes in the other half. To the best of our knowledge, the only other numerical implementation of this formulation of the far-field reflector problem has been proposed in [CKO99]. The authors develop an algorithm, called *Supporting paraboloids* which bears resemblance to Bertsekas' auction algorithm for the assignment problem [BE88]. Using the quasi-Newton approach presented above, and the algorithm developed in Section 3.3, we solve this problem for 15,000 paraboloids in less than 10 minutes on a desktop computer.

3.5 INDUSTRIAL DESIGN CONSTRAINTS

In the previous section, we constructed a reflector surface S parameterized over the sphere. However, for applications, the surface S also needs to satisfy certain design constraints:

1. The surface S should be the graph of a function over a fixed convex domain $\Omega \subseteq \mathbb{R}^2 \times \{0\}$. More precisely, for every u in Ω, the ray joining $(u, -\infty)$ to $(u, +\infty)$ should intersect the surface S exactly once.
2. The surface S should be convex, in the sense that it is contained in the boundary of a convex domain of $\mathbb{R}^3$.

In addition to aesthetic reasons, these constraints are useful for building physical moulds for the reflectors, in particular for car lights. The convexity constraint allows one to mill the mould exactly. Furthermore, it creates a reflector surface for which the chemical vapor deposition is easier [CBC77]. The graph constraint is a natural constraint that appears for the construction of car beams. To be

more precise, a high beam is in general decomposed into several "pillows", each pillow being a reflector surface whose orthogonal projection onto a given plane is a simple two dimensional domain, such as a rectangle [CCO99]. It is therefore natural to model the surface of each pillow by the graph of a function over a planar domain. The whole reflector, composed of several pillows, is then also the graph of a function. One may notice that this property allows one to be able to remove the mould after the fabrication of the reflector.

Although supported paraboloid methods allow to find a solution to the reflector problem, the solution does not satisfy the graph constraint. Some caustics design methods can deal with the graph constraints, but they are based on non-deterministic non-convex optimization methods, and do not guarantee the fact that the generated surface satisfies the convexity constraint.

Together with Julien André, Dominique Attali and Quentin Mérigot, we proposed an heuristic method that iteratively improves the optical properties of the surface patch while adhering strictly to the design constraints. This method relies on a fixed-point algorithm which alternates between the resolution of a discrete optimal transport that produces a radially parametrized surface, and the parameterization of this solution by the graph of a function over the domain $\Omega \subset \mathbb{R}^2 \times \{0\}$.

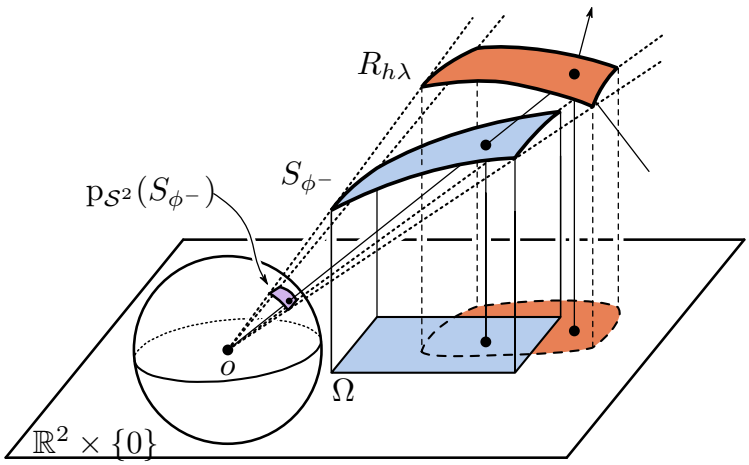

Figure 3.3: When rays from the origin in directions $\mathrm{p}_{\mathcal{S}^2}(S_{\phi^-})$ strike $R_{h\lambda}$, they define a patch whose orthogonal projection onto the plane $\mathbb{R}^2 \times \{0\}$ does not necessarily coincides with Ω.

The algorithms is illustrated in Figure 3.3. The inputs are a source measure μ and the discrete target measure ν_N on the sphere $\mathcal{S}^2$. We are also given a rectangular domain Ω of $\mathbb{R}^2 \times \{0\}$ and denote by U the set of nodes of a regular grid of Ω. For every function $\phi : U \to \mathbb{R}$ defined on the grid, we encode both the value of the function $\phi(u)$ and of its gradient $\nabla\phi(u)$ at nodes u.

Main steps of the algorithm We start by computing an initial function $\phi : U \to \mathbb{R}$, whose graph is a surface S_ϕ. We then iterate the following steps:

— We put $\phi^- := \phi$.

— We compute a discrete measure μ_M supported on M points (where M is the number of nodes of U) that approximates the restriction of the measure μ to

the radial projection $\mathrm{p}_{\mathcal{S}^2}(S_{\phi^-})$ of S_ϕ onto the unit sphere.

— We solve the far field reflector problem between the two discrete measures μ_M and μ_N (it is a linear programming problem). The result provides the parameterization of a reflector surface R_λ defined up to an homothety.

— We find the scale parameter h such that the orthogonal projection of the reflector $R_{h\lambda}$ onto $\mathbb{R}^2 \times \{0\}$ best fits the domain Ω.

— We compute a discrete function $\phi : U \to \mathbb{R}$ whose graph approximates $R_{h\lambda}$.

We iterate this process until $\|\phi - \phi^-\|$ is less than an error parameter ε.

In practice a fixed point is attained after 3 or 4 steps. The solution satisfies the design constraints and can handle complicated target measures, which may be supported on convex or non convex sets.

3.6 PERSPECTIVES

The far field reflector problem is an optimal transport problem on the sphere for the cost $c(x, y) = -\log(1 - \langle x|y\rangle)$. The Laguerre cells on the sphere correspond to the c-subdifferential of the dual function $\psi : Y \to \mathbb{R}$, where $\psi(y_i)$ is the logarithm of the focal distance λ_i. Grégoire Loeper showed that if a cost c satisfies the classical Ma-Trudinger-Wang (MTW) regularity condition, then the c-subdifferentials are convex in a particular chart [Loe09]. Using this property, the algorithm of supporting paraboloids could be extended to optimal transport problems involving a cost function c that satisfies this MTW condition [Kit12]. For this algorithm to be practical, one needs to compute efficiently the Laguerre cells. I mention here some of the perspectives and ongoing works.

Efficient computation of Laguerre cells Together with Pedro Machado and Quentin Mérigot, we are investigating the computation of the Laguerre cells for costs satisfying the MTW condition. Since the Laguerre cells are connected, we believe that a randomized incremental algorithm could be used to calculate the Laguerre cells in $O(N \log(N))$ operations in dimension 2.

Newton Algorithm for semi-discrete optimal transport problems The numerical resolution of an optimal transport problem in the semi-discrete setting amounts to the maximization of a concave function Φ. In the far field reflector problem, we have used a quasi-Newton algorithm. We are investigating, together with Quentin Mérigot and Jun Kitagawa the analysis of a damped Newton algorithm when the cost satisfies the MTW condition. In that case, the convexity of the Laguerre cells in some charts may insure that one can lower bound explicitly the first non vanishing eigenvalue of the hessian of Φ. We have preliminary results in this direction.

Refractor problem The refractor problem is an optimal transport problem on the sphere for the cost $c(x, y) = -\log(1 - \kappa \langle x|y\rangle)$ [GH09]. This cost satisfies the MTW condition when $\kappa > 1$, but it does not when $\kappa < 1$. The refractor surface is the boundary of the intersection of confocal ellipsoids with constant eccentricity

κ. The Laguerre cells on the sphere are also obtained as the intersection of power cells with the unit sphere. We can adapt our approach here to numerically build refractors.

Chapter 4

Convex Integration Theory and Smooth Fractals

In this chapter, we present the construction of an isometric embedding of the square flat torus in the ambient space that led to the discovery of the notion of smooth fractals. This work was announced in the *Proceedings of the National Academy of Sciences* [2] in 2012 and has been well diffused and popularized since then. It is the result of a multidisciplinary work together with Vincent Borrelli, Said Jabrane and Francis Lazarus that was initiated in 2006. At that time, Vincent Borrelli, who knew well the h-principle and the *Convex Integration theory* was thinking that it was possible to implement the Convex Integration theory so as to get explicit constructions of isometric embeddings of Riemannian manifolds in Euclidean spaces. We decided all together to work on that problem and to try to realize a construction of an embedding of the square flat torus in the three dimensional space. To this end, we had to adapt the Convex Integration theory of Gromov so as to make it implementable. The computational and theoretical aspects are intimately related and had to be developed simultaneously. The discovery of smooth fractals is a consequence of this multidisciplinary work, where the implementation and the theory mutually enriched each other. We only provide in this chapter the main ideas of this work, whose details can be found in [4].

A map f from a Riemannian manifold (M^n, g) into a Euclidean space $\mathbb{E}^q = (\mathbb{R}^q, \langle .,. \rangle)$ is an isometry if it preserves length, that is the length of every C^1 curve $\gamma : [a, b] \to M^n$ is equal to the length of its image $f \circ \gamma$. More formally, f is an isometry if the pullback of the inner product is the initial metric: $f^*\langle .,. \rangle = g$. Suppose that, in some local coordinate system, the metric is given by $g = \sum_{i,j}^n g_{ij} \mathrm{d}x_i \mathrm{d}x_j$, then the isometric condition $f^*\langle .,. \rangle = g$ is equivalent to a non linear PDE system

$$\langle \frac{\partial f}{\partial x_i}, \frac{\partial f}{\partial x_j} \rangle = g_{ij}, \quad 1 \leq i \leq j \leq n$$

of $s_n = \frac{n(n+1)}{2}$ equations. It was conjectured by Schlaefli [Sch73] in 1873 that any n-dimensional Riemannian manifold can be locally isometrically embedded in $\mathbb{E}^{s_n}$.

In the years 1926-1927, Janet and Cartan proved that the above PDE system has a solution if the dimension of the ambient space is at least s_n and (M^n, g) is an analytic Riemannian manifold.

In 1954, Nash surprised the mathematical community by breaking down the barrier of the Janet dimension, considering maps with only C^1 regularity [Nas54]. Precisely, he proved that any *strictly short* global embedding $f_0 : (M^n, g) \to \mathbb{E}^q$, i.e., an embedding that strictly shortens distances: $f_0^*\langle .,. \rangle < g$, can be deformed into a true C^1 global isometric embedding f provided that $q \geq n+2$. Moreover, the embedding f can be required to be arbitrarily close to the initial map f_0 for the sup norm. But its C^1 regularity cannot be improved to C^2 in general since the curvature tensor would then provide obstructions to the existence of isometric maps. Shortly after, the theorem of Nash was extended by Kuiper to the codimension 1 [Kui55].

The result of Nash and Kuiper has many counterintuitive consequences, one of them concerning the flat torus. The square flat torus $\mathbb{E}^2/\mathbb{Z}^2$ is the quotient of the Euclidean 2-plane by the lattice $\mathbb{Z}^2$. Its Gaussian curvature is obviously identically equal to zero. A classical argument shows that any C^2 complete compact surface in $\mathbb{E}^3$ has a point with positive Gaussian curvature. From Theorema Egregium it ensues that there is no C^2 isometric embedding of any flat torus. However, Nash-Kuiper Theorem implies that the square flat torus admits a C^1 isometric embedding into $\mathbb{E}^3$.

The result of Nash and Kuiper, as well as other geometric results, was revisited in the 70's and 80's by Gromov. He introduced the h-principle that states that many *partial differential relations* reduce to topological problems [GR70, Gro86] and he developed several tools to solve partial differential relations, one of them being the Convex Integration theory. Using this theory, it is possible to build a sequence of embeddings of the square flat torus that converges to an isometric embedding [EM02]. However this approach is too generic to be implemented directly.

Contributions. We adapted the Convex Integration theory to the *differential relation for isometries* so as get an algorithm for the construction of an embedding of the square flat torus in $\mathbb{E}^3$. In particular, we had the following contributions:

— We proposed a one-dimensional Convex Integration formula that captures the natural geometric notion of a corrugation.

— Mimicking the initial approach of Nash and Kuiper, we built a sequence of embeddings of the square flat torus in $\mathbb{E}^3$ that is converging to an isometric embedding. Guided by computational constraints, we adapted and simplified previous approaches: our construction takes into account the periodicity of the torus and is global at each iteration, whereas previous constructions were only local.

— We provided images of an embedding of the square flat torus in the ambient space. This visualization, as well as the simplification of the construction, led us to discover the notion of *Smooth Fractals*, which is related to the geometric structure of the Gauss map (*i.e.* the normal vector field) of the limit isometric embedding. We show that this Gauss map can be obtained as an

infinite product of rotations applied to the Gauss map of an initial embedding. Although the coefficients of the rotations are intrinsically complicated, the asymptotic behavior of this product is fairly simple and bears a formal similarity with the Weierstrass function.

We start by explaining in the first section the one dimensional Convex Integration process, which is a key ingredient of our process. We give in Section 4.2 the spirit of our construction of an isometric embedding of the square flat torus, and present in Section 4.3 the asymptotic behavior of its Gauss map.

4.1 ONE-DIMENSIONAL CONVEX INTEGRATION AND CORRUGATIONS

Convex Integration is intrinsically a one dimensional process. In this section, we show how to apply it to curves for the differential relation of isometries.

Differential relation. Let $I := [0,1]$ be an interval and suppose that for every $x \in I$ we are given a subset $\mathcal{R}_x$ of vectors of $\mathbb{R}^d$. The disjoint union $\mathcal{R} = \cup_{x\in I}\mathcal{R}_x$ is called a *differential relation*. A *solution* of $\mathcal{R}$ is a C^1 curve $f : I \to \mathbb{R}^d$ such that $f'(x) \in \mathcal{R}_x$ for all $x \in I$. In other words, a differential relation expresses a condition on the derivative of a curve that depends on the considered parameter. (In a more general setting, the differential relation depends on the parameter and the image point on the curve [EM02].)

Differential relation of isometries. Given a speed function $r : I \to \mathbb{R}_+^*$, the *differential relation of isometries* for curves is determined by $\mathcal{R}_x = \{y \in \mathbb{R}^d,\ \|y\| = r(x)\}$. This means that a curve f is a solution of $\mathcal{R}$ if its speed is given by $f'(x) = r(x)$ for every $x \in I$. Starting from an initial parameterized curve $f_0 : I \to \mathbb{E}^d$ whose speed is strictly less than r, the Convex Integration process is going to generate a parameterized curve $f : I \to \mathbb{E}^d$ whose speed equals r (*i.e.* f is a solution of $\mathcal{R}$). The length of f is therefore controlled.

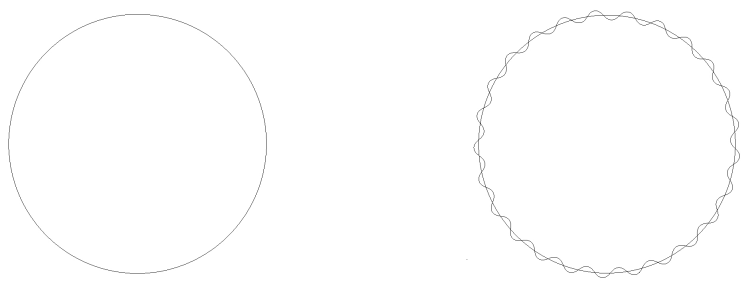

Figure 4.1: Convex Integration process. Left: initial parameterized curve f_0. Right: parameterized curve f obtained by the Convex Integration process applied to f_0 (with $N = 25$ oscillations) drawn on top of the curve f_0

4.1.1 — Convex Integration process

We detail here the Convex Integration process for a general differential relation $\mathcal{R}$. Given a C^1 curve $f : I \to \mathbb{R}^d$, Convex Integration often allows us to construct a solution of $\mathcal{R}$ that is close to f for the sup norm. We will first introduce the construction and then will say to which f and $\mathcal{R}$ it applies. The first step of the process is to define for fixed $x \in I$ a C^1 one-parameter family of loops $h(x, \cdot) : \mathbb{R}/\mathbb{Z} \to \mathcal{R}_x$ so that $f'(x)$ is the average of $h(x, \cdot)$:

$$\forall x \in I, \quad f'(x) = \int_0^1 h(x, u)\mathrm{d}u. \tag{4.1}$$

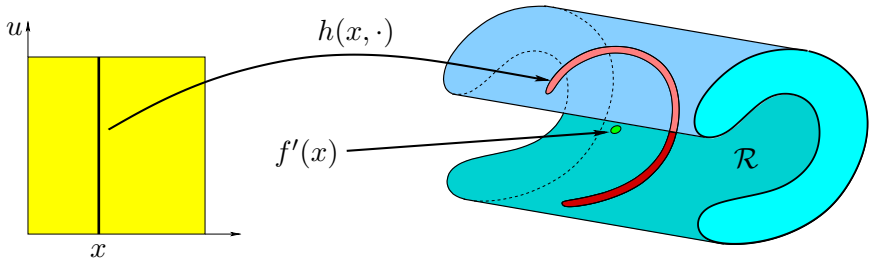

Figure 4.2: The loop $h(x, \cdot)$ is shown as a (red) thick curve contained in the differential relation $\mathcal{R}$ (in blue) and surrounding $f'(x)$. In this figure the differential constraint sets $\mathcal{R}_x$ are all parallel.

In practice, we first choose a path whose average is $f'(x)$. The loop $h(x, \cdot)$ is then obtained by travelling along this path in both directions (see Fig. 4.2). The curve f is said to be *strictly short* if $f'(x)$ is interior to the convex hull of $\mathcal{R}_x$ for all $x \in I$. When $\mathcal{R}$ is open and path connected, this is a necessary and sufficient condition for h to exist [EM02].

In the second step of the process we simply define $F_N : I \to \mathbb{R}^d$ by

$$F_N(t) := f(0) + \int_0^t h(x, \{Nx\})\mathrm{d}x, \tag{4.2}$$

where N is a positive integer and $\{Nx\}$ is the fractional part of Nx. Remark that $F_N'(x) = h(x, \{Nx\})$ and therefore F_N satisfies by construction the differential relation $\mathcal{R}$, namely $F_N'(x) \in \mathcal{R}_x$ for every x. Intuitively, F_N is obtained by integrating h along a periodic curve with period $1/N$ (see Fig. 4.3). When N is large enough, the restriction of h to each period is close to a single loop $h(x, \cdot)$ and its integral is close to $f'(x)$. Summing over the N periods, we see that F_N is roughly equal to a Riemann sum of f', hence to f. This is formally stated in the following lemma.

Lemma 4.1 (C^0-density [EM02][2]). *Let f, h, N, and F_N be defined as above. Then F_N is a solution of $\mathcal{R}$ and*

$$\|F_N - f\|_\infty \leq \frac{K(h)}{N},$$

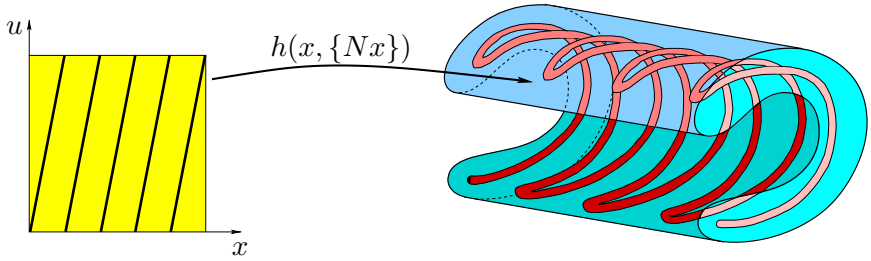

Figure 4.3: Because the parameter u belongs to $S^1 = \mathbb{R}/\mathbb{Z}$, the horizontal edges of the left square domain must be glued to produce a cylindrical domain. The path $x \mapsto (x, \{Nx\})$ winds N times around that cylinder.

where $K(h)$ only depends on the C^1-norm of h.

4.1.2 — Our choice of loops $h(s, \cdot)$ for the isometries differential relation

As far as the isometric embedding problem is concerned, we deal with closed differential relations for which $\mathcal{R}_s$ is a sphere of radius $r(s)$ in $\mathbb{R}^d$, for some strictly positive function $r : I \to \mathbb{R}_+^*$. In other words, the relation $\mathcal{R}$ constrains the norm of the derivative. In this case, a curve f is short if and only if $\|f'(s)\| \leq r(s)$, for all $s \in I$. Suppose that f' is never zero and let $\mathbf{n} : I \to \mathbb{R}^d$ be a vector field normal to f. We choose the loop $h(s, \cdot)$ with image in the circle of radius $r(s)$, intersection of $\mathcal{R}_s$ with the plane spanned by $\mathbf{t}(s) := f'(s)/\|f'(s)\|$ and $\mathbf{n}(s)$, and set

$$h(s, u) = r(s)(\cos(\alpha_s \cos(2\pi u))\mathbf{t}(s) + \sin(\alpha_s \cos(2\pi u))\mathbf{n}(s)) \tag{4.3}$$

with $\alpha_s := J_0^{-1}(\|f'(s)\|/r(s))$ (see Fig. 4.4). Here J_0 is the Bessel function of 0 order restricted to the interval $[0, z]$, where $z \approx 2.4$ is the smallest positive root of J_0. The choice of α_s guarantees the identity (4.1).

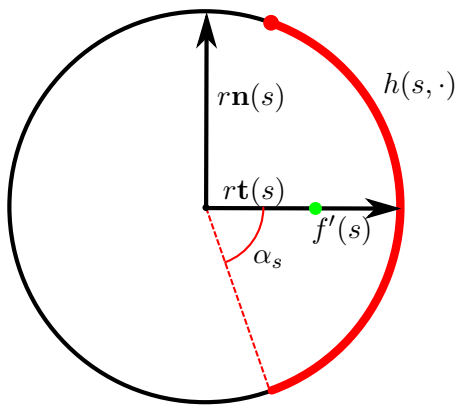

Figure 4.4: The loop $h(s, \cdot)$ starts from the top of the (red) thick arc, sweeps the arc and comes back to its starting point.

As noted in [2], our Convex Integration formula (4.3) captures the natural geometric notion of a corrugation. Indeed, in the planar case $n = 2$ the signed curvature measure $\mu := k\mathrm{d}s = k(t)\|F'(t)\|\mathrm{d}t$ of the resulting curve F given by (4.2)

is connected to the signed curvature measure $\mu_0 := k_0 \mathrm{d}s$ of the initial curve f by the following simple formula

$$\mu := \mu_0 + \big(\alpha' \cos(2\pi N t) - 2\pi N \alpha \sin(2\pi N t)\big)\, \mathrm{d}t.$$

Our Convex Integration formula thus modifies the curvature in the simplest way by sine and cosine terms with frequency N.

Loosely speaking, the Convex Integration process amounts to replace the function f_0 by a function f that oscillates a lot, but whose derivative is close in average to the derivative of f_0. This phenomenon can be seen in Figure 4.12, where the derivative of f corrugates a lot and has in average the same direction that the derivative of f_0. We say that f is a *corrugated map* that has been obtained by applying a *corrugation* to the map f_0. As a consequence, the curve f stays close to the curve f_0, as stated in the C^0-density lemma.

4.2 CONSTRUCTION OF AN EMBEDDING OF THE SQUARE FLAT TORUS

In this section, we give a brief overview of our construction of an embedding of the square flat torus in the Euclidean space $\mathbb{E}^3$, whose details can be found in [2]. Starting from a strictly short embedding $f_0 : (\mathbb{R}^2/\mathbb{Z}^2, \langle .|. \rangle_{\mathbb{E}^2}) \to \mathbb{E}^3$, namely an embedding that shortens distances, our aim is to build an isometric embedding

$$f : (\mathbb{R}^2/\mathbb{Z}^2, \langle .|. \rangle_{\mathbb{E}^2}) \to \mathbb{E}^3.$$

The first naive idea is to apply a one dimensional Convex Integration process along curves that foliate the torus, as illustrated on Figure 4.5. On each curve along which the Convex Integration process is applied one can recover exactly the metric condition. However the metric is perturbed in transverse directions. The idea is then to apply the Convex Integration process in other directions so as to reduce the isometric default everywhere.

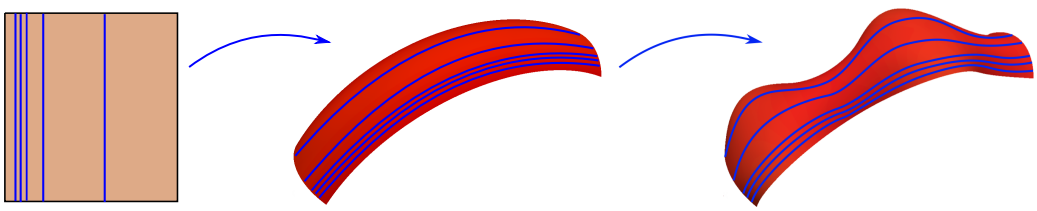

Figure 4.5: Convex Integration along a family of lines. Left: a family of segments that foliate the torus. Middle: images by f_0 of the family of segments. Right: Convex Integration is performed along each segment

4.2.1 — Reduction of the isometric default: a salve

The isometric default of f_0 is measured by the field of bilinear forms $\Delta(\cdot,\cdot) := \langle .|. \rangle_{\mathbb{E}^2} - f_0^* \langle \cdot|\cdot \rangle_{\mathbb{E}^3}$. As usual, $f_0^* \langle \cdot|\cdot \rangle_{\mathbb{E}^3} = \langle df_0(\cdot)|df_0(\cdot) \rangle_{\mathbb{E}^3}$ denotes the pull-back of the Euclidean inner product by f_0. Since f_0 is strictly short, this isometric default Δ

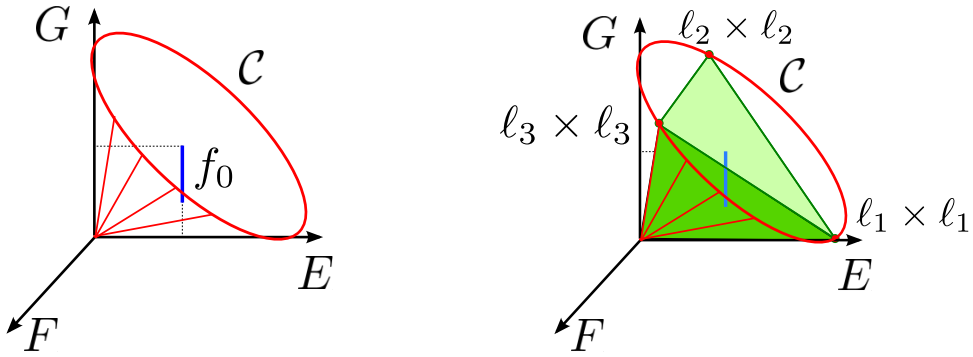

Figure 4.6: The space of symmetric bilinear forms is identified with $\mathbb{R}^3$. Left: cone $\mathcal{C}$ of metrics in red. Right: polyhedral cone $\overline{\mathcal{C}}$ that lies inside the cone of metrics

is a *metric*, *i. e.*, a map from the square flat torus into the positive cone $\mathcal{C}$ of inner products of the plane

$$\mathcal{C} = \left\{ E\, e_1^* \times e_1^* + F\, (e_1^* \times e_2^* + e_2^* \times e_1^*) + G e_2^* \times e_2^* \mid EG - F^2 > 0, E > 0, G > 0 \right\},$$

where (e_1, e_2) is the canonical basis of $\mathbb{E}^2$. Here we use the notation $\ell_1 \times \ell_2(U, V) := \ell_1(U)\ \ell_2(V)$ for any vectors U and V in the plane and linear forms ℓ_i. Not that squares of linear forms $\ell \times \ell$ lie on the boundary on this cone. By convexity, there exist linear forms of the plane $\ell_1, ..., \ell_S$, $S \geq 3$, such that $\Delta = \sum_{j=1}^{S} \rho_j \ell_j \times \ell_j$ for non-negative functions ρ_j. By a convenient choice of the initial map f_0 and of the ℓ_j's, the number S can be set to three. In practice we set the linear forms $\ell_j(\cdot) := \langle U(j)/\|U(j)\| | \cdot \rangle_{\mathbb{E}^2}$ to the normalized duals of the following constant vector fields

$$U(1) := e_1,\ U(2) := \frac{1}{5}(e_1 + 2e_2),\ U(3) := \frac{1}{5}(e_1 - 2e_2).$$

As an initial map we choose a standard parametrization of a geometric torus whose isometric default Δ belongs to the polyhedral cone spanned by the $\ell_j \times \ell_j$'s, $j \in \{1, 2, 3\}$, see Figure 4.6:

$$\overline{\mathcal{C}} = \left\{ \sum_{j=1}^{3} \rho_j \ell_j \times \ell_j \mid \rho_1 > 0, \rho_2 > 0, \rho_3 > 0 \right\}.$$

We now to apply the Convex Integration process along flow lines that foliate the square torus, successively in the directions $U(1)$, $U(2)$ and $U(3)$. In theory and also numerically, it does not work if the corrugations are performed along segments directed by the $U(i)$'s. We have to integrate along particular flow lines as shown in Figure 4.7. Furthermore, each corrugated map is not defined on the whole torus, but only on a cylinder, and we have to "merge" its boundary. We do not give the complete description of the construction. For more details, one may refer to [2]. The first, second and third Convex Integration processes depend respectively on three oscillation numbers N_1, N_2 and N_3. We denote by F_{N_1,N_2,N_3}

the resulting embedding. After the three corrugations, the isometric default is reduced as stated in the following theorem.

Theorem 4.2 ([2]). *The embedding F_{N_1,N_2,N_3} that results from our construction satisfies the following properties:*

$$\|F_{N_1,N_2,N_3} - f_0\|_\infty = O(\frac{1}{N_1} + \frac{1}{N_2} + \frac{1}{N_3})$$

and

$$\| \langle .|. \rangle_{\mathbb{E}^2} - F^*_{N_1,N_2,N_3} \langle \cdot|\cdot \rangle_{\mathbb{E}^3} \|_\infty = O(\frac{1}{N_1} + \frac{1}{N_2} + \frac{1}{N_3}),$$

where $\|.\|_\infty$ denotes the supremum norm over $\mathbb{R}^2/\mathbb{Z}^2$ (of the absolute value or of any matrix norm).

Remark that the embedding F_{N_1,N_2,N_3} converges to f_0 in the sup norm sense, which implies that the pullback of the limit embedding of F_{N_1,N_2,N_3} is the initial metric $f_0^* \langle \cdot|\cdot \rangle_{\mathbb{E}^3}$. As a consequence, the embedding F_{N_1,N_2,N_3} can be as close as we want to an isometric embedding of the flat torus if we chose the N_i's large enough, but its limit when the N_is tend to infinity cannot be an isometry. We call *salve* the fact of applying three such corrugations.

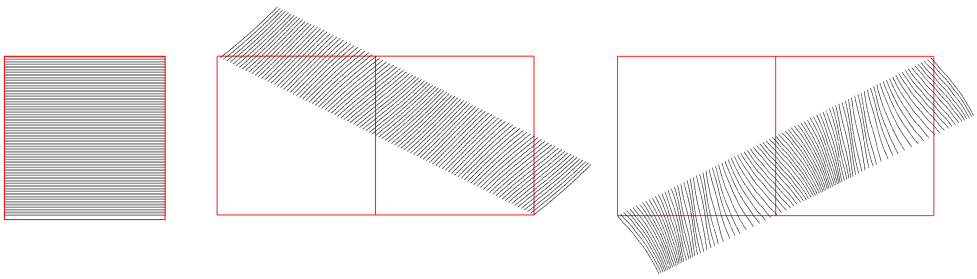

Figure 4.7: Curves that foliate the square torus and along which the Convex Integration process is performed. From left to right: the curves are associated to the directions $U(1)$, $U(2)$ and $U(3)$.

4.2.2 — A sequence of salves

As noticed above, it is not possible to reach in one salve an isometric embedding of the square flat torus in the ambient space. Mimicking Nash's approach, we consider a sequence of metrics $(g_k)_{k\geq 0}$ on the torus that is converging to the flat metric $g_\infty := \langle .|. \rangle_{\mathbb{E}^2}$. We suppose that the sequence is strictly increasing, namely for every point $x \in \mathbb{R}^2/\mathbb{Z}^2$ and any tangent vector X at the point x

$$g_k(X,X) < g_{k+1}(X,X) < \|X\|^2.$$

The key idea is to reduce iteratively the isometric default while staying strictly short at each step. We start with an initial embedding $f_0 : (\mathbb{R}^2/\mathbb{Z}^2, g_1) \to \mathbb{E}^2$ which is strictly short for the metric g_1. More precisely, we manage so that the isometric

default lies inside the polyhedral cone $\overline{\mathcal{C}}$ at every point. We can therefore apply three consecutive corrugations to f_0 to build a map $f_1 := F_{N_1,N_2,N_3}$ which is almost an isometry for the metric g_1 and which is stricly short for the metric g_2. More precisely, we guarantee that the isometric default lies again inside the polyhedral cone $\overline{\mathcal{C}}$ at every point. We repeat this process to construct f_2 from f_1 by applying again three Convex Integration steps. We pursue this process iteratively and finally build a sequence of embeddings $(f_k)_{k\geq 0}$. At each step, we guarantee that the embedding $f_k : (\mathbb{R}^2/\mathbb{Z}^2, g_k) \to \mathbb{E}^2$ is almost an isometry for the metric g_k. At the limit, we get an isometric embedding of the square flat torus.

In practice, we have to choose an oscillation number at each Convex Integration step. For this, we established the *Loop condition*, which is a sufficient theoretical condition that guarantees that the process can be iterated. We showed that this Loop condition is always satisfied if the oscillation number is chosen large enough. Hence, our algorithm consists in taking (by an exponential search and then a dichotomy) the smallest oscillation number such that the corrugated map satisfies the Loop condition.

Theorem 4.3 ([2]). *There exists an increasing sequence of metrics $(g_k)_{k\geq 1}$, such that if the corrugation numbers are chosen large enough at each corrugation, then our sequence of embeddings $(f_k)_{k\geq 0}$ C^1-converges to an isometric embedding of the square flat torus*

$$f_\infty : \mathbb{T}^2 \to \mathbb{E}^3.$$

The construction is illustrated in Figure 4.8 using the language of differential relations: the isometry to the flat metric corresponds to differential relation $\mathcal{R}_{iso}$. At each Step k, the differential relation $\mathcal{R}_k$ corresponds to ε_k-isometries to the metric g_k. Loosely speaking, the differential relation $\mathcal{R}_k$ is thickened by a parameter ε_k that is measuring the error to the metric g_k. The embedding f_k satisfies the differential relation $\mathcal{R}_k$ and remains strictly short for the differential relation $\mathcal{R}_{k+1}$. At the limit, the function f_∞ satisfies the differential relation $\mathcal{R}_{iso}$.

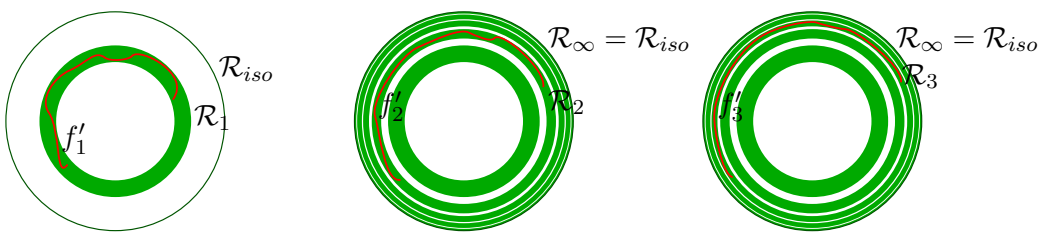

Figure 4.8: Illustration of the construction of the sequence: we consider an increasing sequence of (thick) differential relations $\mathcal{R}_k$ converging to the (thin) differential relation for isometries $\mathcal{R}_{iso}$. At each step the embedding f_k is a solution of $\mathcal{R}_k$. The limit embedding f_∞ is a solution of $\mathcal{R}_{iso}$.

Without entering into the numerous laborious details, I mention what are the main differences of our construction with previous approaches.

— We provide a Convex Integration formula (4.3) for the differential relation of isometries which is particularly simple.

— At every salve, the isometric default at every point always lies inside the same polyhedral cone spanned by only three directions. Furthermore, the directions $U(i)$ are related to fundamental domains of the torus. These two points allow us to apply Convex Integration processes globally on the torus, whereas previous approaches were only applying local Convex Integration processes.
— We keep exactly the same three directions for all the salves.

4.2.3 — Implementation

As mentioned above, at each Convex Integration process the oscillation number is imposed by the Loop condition. Our numerical experiments show that the oscillation numbers grow at least exponentially. Starting with a initial parameterization of a torus of revolution and doing only calculations on a small part of the torus, the Loop condition imposes the following oscillation numbers for the four first corrugations:

$$611, \quad 69,311, \quad 20,914,595, \quad 6,572,411,478.$$

This is far too much to be implemented in practice on the whole torus $\mathbb{R}^2/\mathbb{Z}^2$. However, the Loop condition being only a sufficient condition, we were able to reduce these numbers to

$$12, \quad 80, \quad 500, \quad 9000.$$

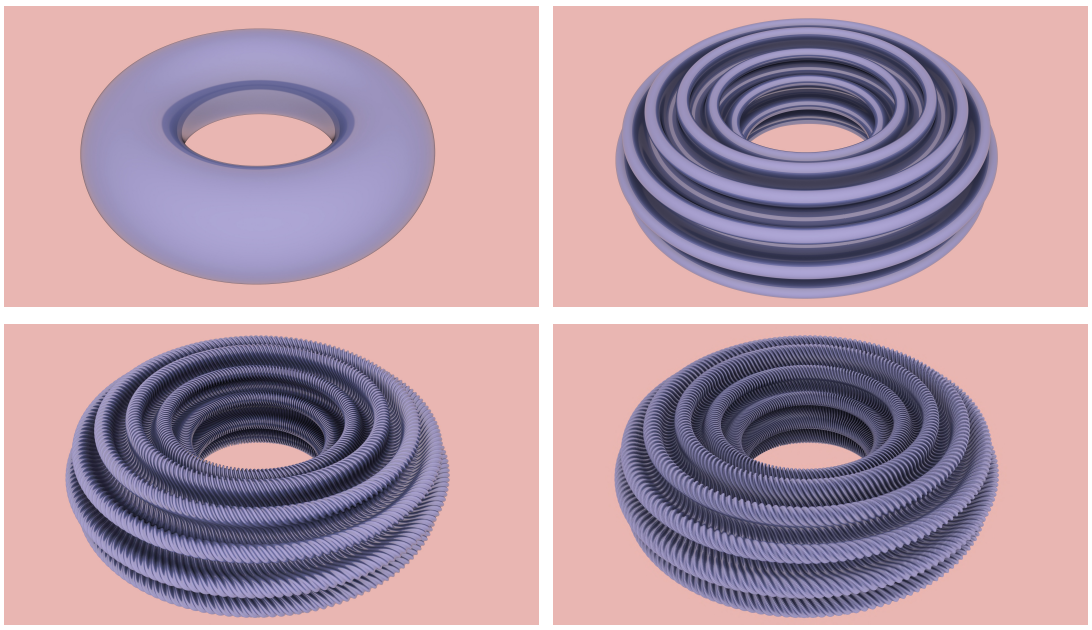

Figure 4.9: Iterative construction: initial embedding and the embeddings after respectively one, two and three corrugations

In practice, calculations were performed on a 8-core CPU (3.16 GHz) with 32 GB of RAM and parallelised C++ code. We used a $10,000^2$ grid mesh for the three first corrugations and refined the grid to 2 milliards nodes for the last corruga-

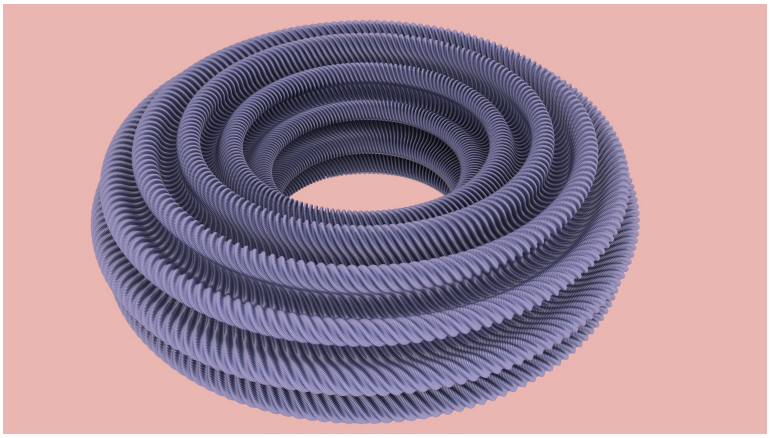

Figure 4.10: Image of an isometric embedding of the square flat torus. This image is obtained after four corrugations. Further corrugations would not be visible to the naked eye at this distance.

tion. Due to memory limitations, the last mesh was divided into 33 pieces. The computation of the final mesh took approximately two hours.

We illustrate the metric improvement by comparing the lengths of a collection of curves on the flat torus (Fig. 4.11**a**) with the lengths of their images by the fourth embedding $f_{2,1}$. The length of any curve in the collection differs by at most 10.2% with the length of its image by $f_{2,1}$. By contrast, the deviation reaches 80% when the standard torus f_0 is taken in place of $f_{2,1}$.

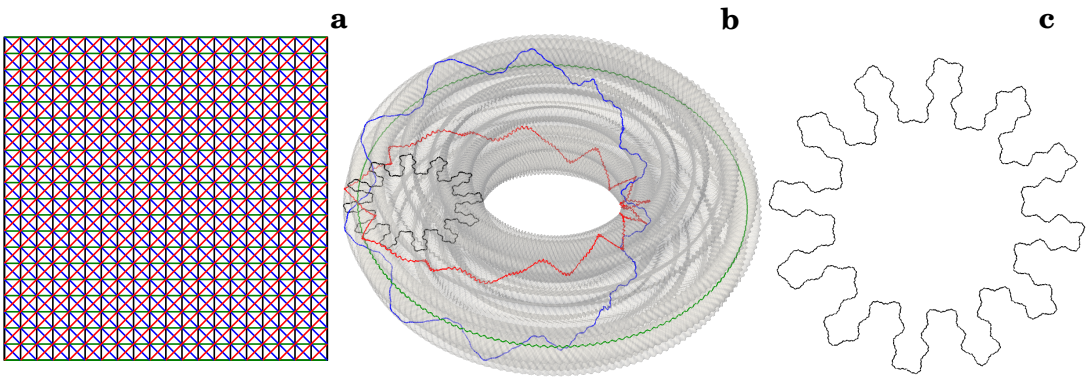

Figure 4.11: **Comparison of lengths in the parameter and image domain for the fourth corrugated map $f_{2,1}$. a**, A fundamental domain of the flat torus with four nets of meridians, parallels, main diagonals and skew diagonals, each composed of 20 curves. **b**, The images by $f_{2,1}$ of four curves, one taken in each net. **c**, A closer look at the curves evinces a fractal geometry, though the limit curves are C^1 regular.

Remark that the curve of Figure 4.11**a** seems to have a fractal behavior even though the limit curve is C^1 regular. If we zoom in this curve, we notice that the corrugations appear at each scale. We analyze this behavior in the next section.

4.3 SMOOTH FRACTALS

In this section, we show that the Gauss map $\mathbf{n}_\infty$ of the limit isometric embedding f_∞ can be approximated by an infinite product of rotation matrices. Asymptotically, this infinite product bares some similarities with the Weierstrass function and the Riesz product, that are known to have connections with fractals. We start by analyzing the iterative process of Convex Integrations in a one dimensional setting, since we have explicit formula in that case and the analogy with the Weierstrass function is obvious.

4.3.1 — Corrugation Theorem on $\mathcal{S}^1$

Let $f_0 : \mathcal{S}^1 = \mathbb{E}/\mathbb{Z} \to \mathbb{E}^2$ be a radially symmetric strictly short embedding of the circle, i.e., for every $x \in \mathcal{S}^1 : \|f_0'(x)\| < 1$. Similarly to the torus case, we thus build a sequence of corrugated maps $f_k : \mathcal{S}^1 \to \mathbb{E}^2$ that C^1-converges to a C^1-isometry $f_\infty : \mathcal{S}^1 \to \mathbb{E}^2$ (see [3] for more details on this construction). We get explicit formula for the normal vector field:

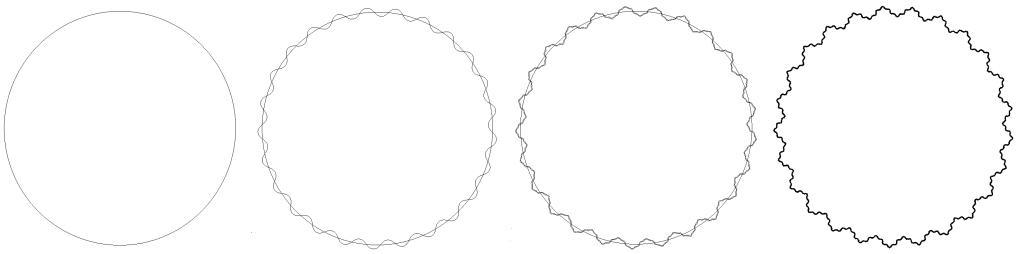

Figure 4.12: Example of a sequence of maps (f_0, f_1, f_2 and f_∞) with an exponential growth of the N_k's.

Theorem 4.4 (Corrugation Theorem on $\mathcal{S}^1$ [3])**.** *The normal map $\mathbf{n}_\infty$ of f_∞ is given by*

$$\forall x \in \mathcal{S}^1, \quad \mathbf{n}_\infty(x) = e^{iA_\infty(x)}\mathbf{n}_0(x) \quad \textit{with} \quad A_\infty(x) = \sum_{j=1}^{\infty} \alpha_j(x)\cos(2\pi N_j x).$$

Remark that the terms of the series $A_\infty(x)$ come from our Convex Integration formula (4.3). Informally, we say that the curve $f_\infty : \mathcal{S}^1 \to \mathbb{E}^2$ has a C^1 *fractal structure* as it is both a primitive of $-i\mathbf{n}_\infty$ and of class C^1. An interesting case of a C^1 fractal structure occurs when

$$A_\infty(x) = \sum_j a^j \cos(2\pi b^j x)$$

for some positive numbers a, b with $a < 1$ and $ab > 1$. Indeed, in that case, A_∞ is the well-known Weierstrass function. Although its exact value is conjectural, the Hausdorff dimension of its graph is strictly larger than one [Fal03]. It follows that the Hausdorff dimension of the graph of $\mathbf{n}_\infty$ is also strictly larger than one.

Let $\mathbf{n}_k(x) = \sum_{p\in\mathbb{Z}} a_p(k)e^{2i\pi px}$ be the Fourier expansion of the normal vector field $\mathbf{n}_k$ of the embedding f_k. Its structure is given by Lemma 4.5, is illustrated in Figure 4.13 and bares some similarities with *Riesz products* that are known to have fractal structures. We also provide in [3] an analysis of the regularity of f_∞ in terms of the speed of convergence of the oscillation numbers and of the metric.

Lemma 4.5 (Fourier expansion of $\mathbf{n}_k$ [3])**.** *We have*

$$\forall p \in \mathbb{Z}, \quad a_p(k) = \sum_{n\in\mathbb{Z}} u_n(k) a_{p-nN_k}(k-1)$$

where $u_n(k) = i^n J_n(\alpha_k)$ *(*J_n *denotes the Bessel function of order* n*).*

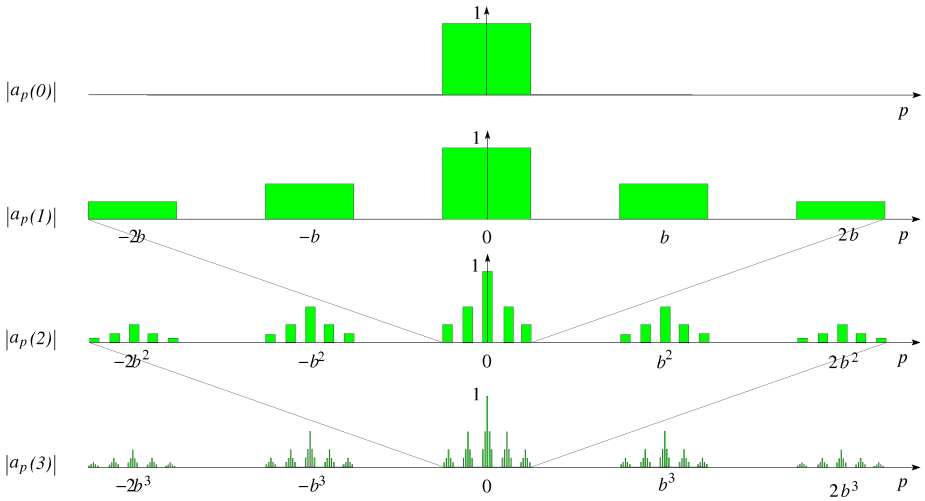

Figure 4.13: A schematic picture of the various spectra $(a_p(k))_{p\in\mathbb{Z}}$ with $N_k = b^k$.

4.3.2 — Corrugation Theorem on $\mathbb{E}^2/\mathbb{Z}^2$

Our isometric embedding of the flat torus $f_\infty : (\mathbb{R}^2/\mathbb{Z}^2, \langle .|. \rangle_{\mathbb{E}^2}) \to \mathbb{E}^3$ is obtained as the limit of a sequence

$$f_0; \quad f_{1,1}, f_{1,2}, f_{1,3}; \quad f_{2,1}, f_{2,2}, f_{2,3}; \quad f_{3,1}, f_{3,2}, f_{3,3}; \quad \dots$$

As illustrated in Figure 4.14, there is a natural orthonormal basis $(v_{k,j}^\perp, v_{k,j}, \mathbf{n}_{k,j})$ that comes with each map $f_{k,j}$ of this sequence. The vector field $v_{k,j}^\perp$ corresponds to the direction in which the Convex Integration has been performed to build $f_{k,j}$ from $f_{k,j-1}$ and $\mathbf{n}_{k,j}$ is the normal vector field of $f_{k,j}$. We denote by $\mathcal{M}_{k,j+1}(p)$ the rotation matrix that maps $(v_{k,j}^\perp, v_{k,j}, \mathbf{n}_{k,j})$ to $(v_{k,j+1}^\perp, v_{k,j+1}, \mathbf{n}_{k,j+1})$ at a point $p \in \mathbb{R}^2/\mathbb{Z}^2$. The corrugation matrix $\mathcal{M}_{k,j+1}(p)$ has intricate coefficients with integro-differential expressions. The Corrugation Theorem provides, up to an error term, a simple expression for this matrix.

Theorem 4.6 (Corrugation theorem [2, 4])**.** *Each rotation* $\mathcal{M}_{k,j+1}(p)$ *can be decomposed as the product of two rotations*

$$\mathcal{M}_{k,j+1}(p) = \mathcal{L}_{k,j+1}(p)\mathcal{R}_{k,j}(p)$$

whose asymptotic behaviors are given by

$$\mathcal{R}_{k,j}(p) = \begin{pmatrix} \cos\beta_j & \sin\beta_j & 0 \\ -\sin\beta_j & \cos\beta_j & 0 \\ 0 & 0 & 1 \end{pmatrix} + O(\epsilon_{k,j}),$$

where $\epsilon_{k,j} = \|\langle .,. \rangle_{\mathbb{E}^2} - f_{k,j}^* \langle .,. \rangle_{\mathbb{E}^3}\|_\infty$ *is the isometric default of* $f_{k,j}$ *and* β_j *is the oriented angle between* $U(j)$ *and* $U(j+1)$.

$$\mathcal{L}_{k,j+1}(p, N_{k,j+1}) = \begin{pmatrix} \cos(\theta_{k,j+1}) & 0 & \sin(\theta_{k,j+1}) \\ 0 & 1 & 0 \\ -\sin(\theta_{k,j+1}) & 0 & \cos(\theta_{k,j+1}) \end{pmatrix} + O\left(\frac{1}{N_{k,j+1}}\right)$$

where $\theta_{k,j+1} := \alpha_{k,j+1}(p)\cos(2\pi N_{k,j+1} s_{j+1}(p))$, $s_{j+1}(p) = \langle p - O | U(j+1) \rangle$ *and* $\alpha_{k,j+1}(p)$ *is a function of* p *not detailed here.*

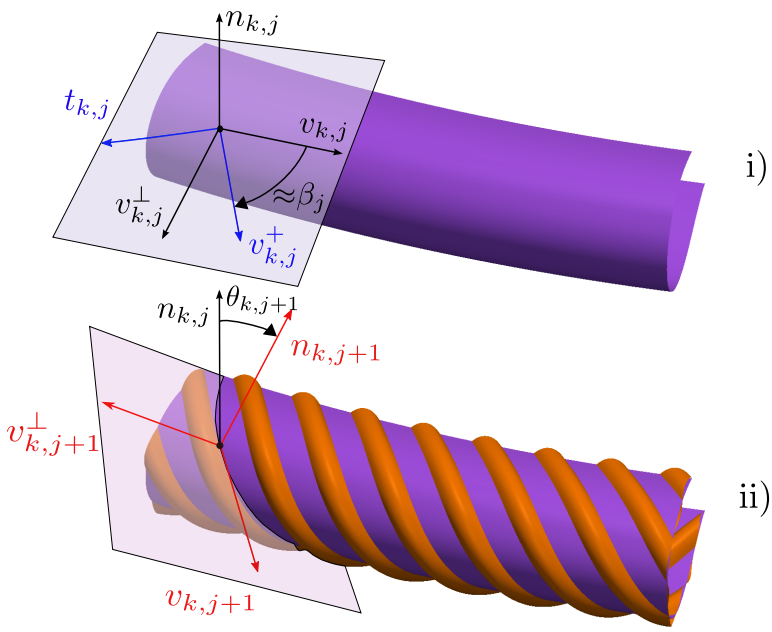

Figure 4.14: The rotation that maps the basis $(v^{\perp}_{k,j}, v_{k,j}, \mathbf{n}_{k,j})$ to $(v^{\perp}_{k,j+1}, v_{k,j+1}, \mathbf{n}_{k,j+1})$ is the composition of two rotations: i) Up to $O(\epsilon_{k,j})$, the first rotation is a rotation of angle β_j in the tangent space to $f_{k,j}(\mathbb{T}^2)$ at $f_{k,j}(p)$. ii) Up to $O\left(\frac{1}{N_{k,j+1}}\right)$, the second rotation is due to the Convex Integration process.

At each corrugation, we apply two rotations. The significance of these rotations are illustrated in Figure 4.14. Loosely speaking, the first rotation is a rotation of angle β_j in the tangent space of the embedding $f_{k,j}$. Note that β_j is the angle between the directions $U(j)$ and $U(j+1)$ of two consecutive corrugations. The error is bounded by the isometric default of the current embedding and does not depend on the salve k. The second rotation, associated to the matrix $\mathcal{L}_{k,j+1}(p, N_{k,j+1})$ is about an axis parallel to $v_{k,j+1}$. This rotation is related to the Convex Integration process and the error tends to 0 if the oscillation number $N_{k,j+1}$ tend to infinity.

4.3.3 — Asymptotic behavior of the Gauss map

The Gauss map $\mathbf{n}_\infty$ of f_∞ is given by the infinite product of matrices:

$$\begin{pmatrix} v_\infty^\perp \\ v_\infty \\ \mathbf{n}_\infty \end{pmatrix}(p) = \prod_{k=1}^{\infty}\prod_{j=1}^{3} \mathcal{M}_{k,j} \begin{pmatrix} v_0^\perp \\ v_0 \\ \mathbf{n}_0 \end{pmatrix}(p).$$

We introduce

$$M_{k,j+1} := \begin{pmatrix} \cos(\theta_{k,j+1}) & 0 & \sin(\theta_{k,j+1}) \\ 0 & 1 & 0 \\ -\sin(\theta_{k,j+1}) & 0 & \cos(\theta_{k,j+1}) \end{pmatrix} \begin{pmatrix} \cos\beta_j & \sin\beta_j & 0 \\ -\sin\beta_j & \cos\beta_j & 0 \\ 0 & 0 & 1 \end{pmatrix}$$

It follows from the Corrugation theorem that the Gauss map of f_∞ is asymptotically given by an infinite product of matrices $M_{k,j+1}$:

Theorem 4.7 (Riesz Asymptotic Behavior [4]). *There exists an increasing sequence of metrics $(g_k)_{k\geq 0}$, such that we have the following properties:*

i) The product $\prod M_k$ converges with respect to the sup norm.

ii) For every $\varepsilon > 0$, there exists $N > 0$ such that for all $n \geq N$:

$$\left\| \prod_{k=n}^{\infty}\prod_{j=1}^{3} M_{k,j} - \prod_{k=n}^{\infty}\prod_{j=1}^{3} \mathcal{M}_{k,j} \right\|_\infty \leq \varepsilon.$$

By analogy with the one-dimensional case, we call the corrugated torus f_∞ a C^1 *fractal* or a *smooth fractal*.

4.4 MORE IMAGES

Since our embedding is encoded as a three dimensional mesh, it is possible to take advantage of the existing 3D printing devices to obtain a solid representation of an embedded flat torus. Due to the resolution of those devices (about 0.1 mm), we had to limit the printing to the first three corrugations. We also present several beautiful images rendered by Damien Rohmer.

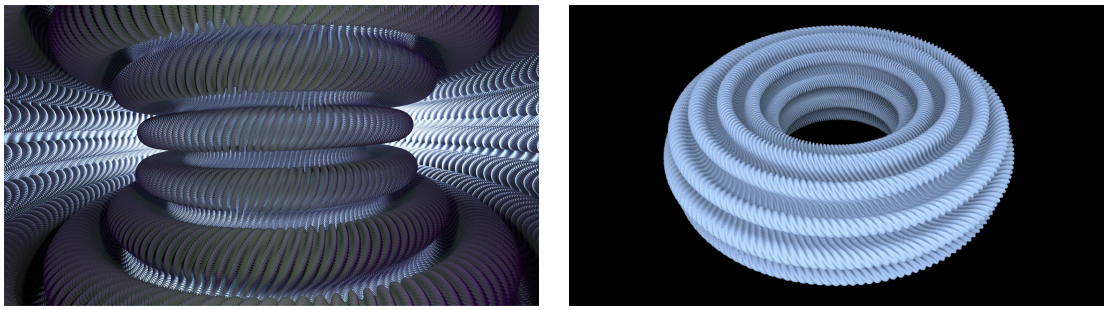

Figure 4.15: Flat torus, from the inside and from profile (rendered by Damien Rohmer)

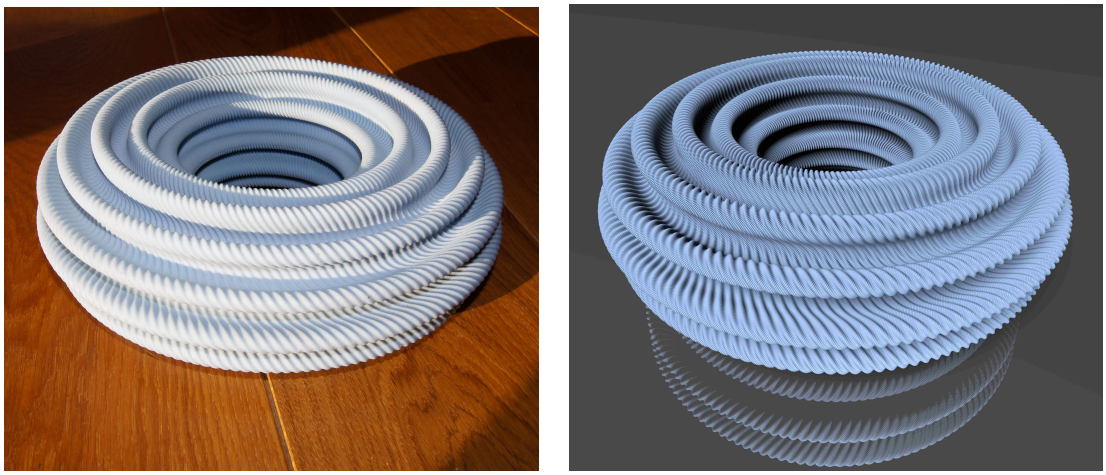

Figure 4.16: 3D printing (left) and computer renderings (right) of the map $f_{1,3}$ output by our algorithm.

4.5 PERSPECTIVES

Convex Integration is a tool for solving underdeterminated differential systems. I mention here some of the ongoing works and perspectives directly related to Convex Integration.

Nash-Kuiper spheres We have seen that the existence of a C^1 isometric embedding of the square flat torus in $\mathbb{E}^3$ is a consequence of the Nash-Kuiper Theorem. This theorem has other counter-intuitive examples, such as the *Nash-Kuiper sphere*: it is possible to isometrically embed the unit sphere $\mathcal{S}^2$ of the Euclidean space inside the ball $B(O,r)$ of radius $r < 1$ centered at the origin, for any value of r. Together with the present members of the HEVEA project, namely Evangelos Bartzos, Vincent Borrelli, Roland Denis, Francis Lazarus and Damien Rohmer, we are working on the realization of Nash-Kuiper spheres.

In our approach, we start with an initial C^1 map $f_0 : \mathcal{S}^2 \to B(O,r) \subset \mathbb{R}^3$ which is shortening distances. The map f_0 is defined as follows: we cut $\mathcal{S}^2$ into three pieces, two small spherical caps centered at the poles and a complementary equatorial belt $\mathcal{B} \subset \mathcal{S}^2$; by construction, the map f_0 vertically translates each cap into $B(O,r)$ and the restriction of f_0 to the equatorial belt is shortening distances. Since the restriction of f_0 to each cap is an isometry, we just have to build an isometry on the belt $\mathcal{B}$. Mimicking the torus case, the idea is to build iteratively a sequence of corrugated maps $f_k : \mathcal{B} \to B(O,r)$ that is converging to an isometric map $f_\infty : \mathcal{B} \to B(O,r)$ and such that $f_\infty : \mathcal{S}^2 \to B(O,r)$ is of class C^1.

Note that we cannot directly apply the construction used for the torus. At each step k, the image of $\partial\mathcal{B}$ by the map f_k is prescribed and has already the desired length. Hence the map f_k is not strictly short on the boundary of $\mathcal{B}$ and we cannot apply directly the Convex Integration process. Together with the Hevea team, we are handling this boundary condition in the Convex Integration process and have already results on the realization of Nash-Kuiper spheres.

Effective Convex Integration The actual implementation of Convex Integration is numerically too complicated to be used in practice in different applications, where one wants to build isometries. In particular, it is not possible to compute locally f_k without having to calculate the whole embeddings f_j, for $j < k$. This global construction is one of the main limitation for getting an efficient algorithm. I am planning to investigate a numerically efficient Convex Integration process for the differential relation of isometries, by considering a local construction based on a piecewise linear Convex Integration process [BZ95].

Bibliography

[AB99] Nina Amenta and Marshall Bern. Surface reconstruction by voronoi filtering. *Discrete & Computational Geometry*, 22(4):481–504, 1999.

[ACSTD07] Pierre Alliez, David Cohen-Steiner, Yiying Tong, and Mathieu Desbrun. Voronoi-based variational reconstruction of unoriented point sets. In *Symposium on Geometry processing*, volume 7, pages 39–48, 2007.

[AHA98] F. Aurenhammer, F. Hoffmann, and B. Aronov. Minkowski-type theorems and least-squares clustering. *Algorithmica*, 20(1):61–76, 1998.

[BE88] D.P. Bertsekas and J. Eckstein. Dual coordinate step methods for linear network flow problems. *Mathematical Programming*, 42(1):203–243, 1988.

[BK03] Jean-Daniel Boissonnat and Menelaos I. Karavelas. On the combinatorial complexity of euclidean Voronoi cells and convex hulls of d-dimensional spheres. In *Proceedings of the fourteenth annual ACM-SIAM symposium on Discrete algorithms*, SODA '03, pages 305–312, Philadelphia, PA, USA, 2003. Society for Industrial and Applied Mathematics.

[BZ95] Yuriy Dmitrievich Burago and Viktor Abramovich Zalgaller. Isometric piecewise-linear embeddings of two-dimensional manifolds with a polyhedral metric into \mathbbr^3. *Algebra i analiz*, 7(3):76–95, 1995.

[CBC77] F. Cork, D.F. Bettridge, and P.C. Clarke. Method of and mixture for aluminizing a metal surface, February 22 1977. US Patent 4,009,146.

[CCO99] M.A. Campos, M. Cejnek, and M. Olivik. Automotive tail lamp with large rake angle, September 21 1999. US Patent 5,954,427.

[CCSL09a] Frédéric Chazal, David Cohen-Steiner, and André Lieutier. Normal cone approximation and offset shape isotopy. *Computational Geometry*, 42(6):566–581, 2009.

[CCSL09b] Frédéric Chazal, David Cohen-Steiner, and André Lieutier. A sampling theory for compact sets in euclidean space. *Discrete & Computational Geometry*, 41(3):461–479, 2009.

[CCSM10] Frédéric Chazal, David Cohen-Steiner, and Quentin Mérigot. Boundary measures for geometric inference. *Foundations of Computational Mathematics*, 10(2):221–240, 2010.

[CCSM11] Frédéric Chazal, David Cohen-Steiner, and Quentin Mérigot. Geometric inference for probability measures. *Foundations of Computational Mathematics*, 11(6):733–751, 2011.

[Cga] CGAL, Computational Geometry Algorithms Library. http://www.cgal.org.

[CKO99] L Caffarelli, S. Kochengin, and VI Oliker. On the numerical solution of the problem of reflector design with given far-field scattering data. *Contemporary Mathematics*, 226:13–32, 1999.

[CL05] Frédéric Chazal and André Lieutier. Weak feature size and persistent homology: computing homology of solids in rn from noisy data samples. In *Proceedings of the twenty-first annual symposium on Computational geometry*, pages 255–262. ACM, 2005.

[Cla90] Frank H Clarke. *Optimization and nonsmooth analysis*, volume 5. Siam, 1990.

[CLM01] Philippe Choné and Hervé VJ Le Meur. Non-convergence result for conformal approximation of variational problems subject to a convexity constraint. 2001.

[CO08] LA Caffarelli and VI Oliker. Weak solutions of one inverse problem in geometric optics. *Journal of Mathematical Sciences*, 154(1):39–49, 2008.

[CSM06] David Cohen-Steiner and Jean-Marie Morvan. Second fundamental measure of geometric sets and local approximation of curvatures. *Journal of Differential Geometry*, 74(3):363–394, 2006.

[Del08] C. Delage. CGAL-based first prototype implementation of moebius diagram in 2D, 2008.

[DS06] Tamal K Dey and Jian Sun. Normal and feature approximations from noisy point clouds. In *FSTTCS 2006: Foundations of Software Technology and Theoretical Computer Science*, pages 21–32. Springer, 2006.

[Ede93] Herbert Edelsbrunner. The union of balls and its dual shape. In *Proceedings of the ninth annual symposium on Computational geometry*, pages 218–231. ACM, 1993.

[EM02] Y. Eliashberg and N. Mishachev. *Introduction to the h-principle*, volume 48 of *Graduate Studies in Mathematics*. A.M.S., Providence, 2002.

[Fal03] K. Falkoner. *Fractal Geometry*. Wiley, 2003.

[Fed59] Herbert Federer. Curvature measures. *Transactions of the American Mathematical Society*, pages 418–491, 1959.

[Fed69] Herbert Federer. *Geometric measure theory*. Springer, 1969.

[Fu85] Joseph Fu. Tubular neighborhoods in euclidean spaces. *Duke Mathematical Journal*, 52(4):1025–1046, 1985.

[Fu93a] Joseph Fu. Convergence of curvatures in secant approximations. *Journal of Differential Geometry*, 37(1):177–190, 1993.

[Fu93b] Joseph HG Fu. Curvature of singular spaces via the normal cycle. In *Differential geometry: geometry in mathematical physics and related topics (Los Angeles, CA, 1990), Proc. Symp. Pure Math*, volume 54, pages 211–221, 1993.

[Fu94] Joseph Fu. Curvature measures of subanalytic sets. *American Journal of Mathematics*, pages 819–880, 1994.

[GH09] Cristian E Gutiérrez and Qingbo Huang. The refractor problem in reshaping light beams. *Archive for rational mechanics and analysis*, 193(2):423–443, 2009.

[GL95] A. Gross and L. Latecki. Digitizations preserving topological and differential geometric properties. *Comput. Vis. Image Underst.*, 62(3):370–381, 1995.

[GMM13] Leonidas Guibas, Dmitriy Morozov, and Quentin Mérigot. Witnessed k-distance. *Discrete & Computational Geometry*, 49(1):22–45, 2013.

[GO03] T Glimm and V Oliker. Optical design of single reflector systems and the monge–kantorovich mass transfer problem. *Journal of Mathematical Sciences*, 117(3):4096–4108, 2003.

[GR70] M. Gromov and V. Rokhlin. Embeddings and immersions in riemannian geometry. *Russian Math. Survey*, 5:1–57, 1970.

[Gro86] M. Gromov. *Partial Differential Relations*. Springer-Verlag, 1986.

[Gro93] Karsten Grove. Critical point theory for distance functions. In *Proc. of Symposia in Pure Mathematics*, volume 54, 1993.

[GW98] Pengfei Guan and Xu-Jia Wang. On a monge-ampere equation arising in geometric optics. *J. Differential Geom*, 48(2):205–223, 1998.

[HPW06] Klaus Hildebrandt, Konrad Polthier, and Max Wardetzky. On the convergence of metric and geometric properties of polyhedral surfaces. *Geometriae Dedicata*, 123(1):89–112, 2006.

[Kit12] Jun Kitagawa. An iterative scheme for solving the optimal transportation problem. *Calculus of Variations and Partial Differential Equations*, pages 1–21, 2012.

[KO97] Sergey A Kochengin and Vladimir I Oliker. Determination of reflector surfaces from near-field scattering data. *Inverse Problems*, 13(2):363, 1997.

[KS98] Ron Kimmel and James A Sethian. Computing geodesic paths on manifolds. *Proceedings of the National Academy of Sciences*, 95(15):8431–8435, 1998.

[Kui55] N. Kuiper. On C^1-isometric imbeddings. *Indag. Math.*, 17:545–555, 1955.

[Lac06] J.-O. Lachaud. *Espaces non-euclidiens et analyse d'image : modèles déformables riemanniens et discrets, topologie et géométrie discrète*. Habilitation à diriger des recherches, Université Bordeaux 1, Talence, France, 2006.

[Lat97] L. J. Latecki. 3D well-composed pictures. *Graphical Models and Image Processing*, 59(3):164–172, May 1997.

[LCG98] L. J. Latecki, C. Conrad, and A. Gross. Preserving topology by a digitization process. *Journal of Mathematical Imaging and Vision*, 8(2):131–159, mar 1998.

[Lie04] André Lieutier. Any open bounded subset of rn has the same homotopy type as its medial axis. *Computer-Aided Design*, 36(11):1029–1046, 2004.

[Loe09] G. Loeper. On the regularity of solutions of optimal transportation problems. *Acta mathematica*, 202(2):241–283, 2009.

[LYZ+10] Y.-S. Liu, J. Yi, H. Zhang, G.-Q. Zheng, and J.-C. Paul. Surface area estimation of digitized 3d objects using quasi-monte carlo methods. *Pattern Recognition*, 43(11):3900 – 3909, 2010.

[Mér11] Q. Mérigot. A multiscale approach to optimal transport. In *Computer Graphics Forum*, volume 30, pages 1583–1592. Wiley Online Library, 2011.

[Mil93] J Milnor. Euler characteristic and finitely additive steiner measures, from: Collected papers vol. 1. *Publish or Perish*, 1993.

[MO14] Quentin Mérigot and Edouard Oudet. Handling convexity-like constraints in variational problems. *arXiv preprint arXiv:1403.2340*, 2014.

[MOG11] Quentin Merigot, Maks Ovsjanikov, and Leonidas Guibas. Voronoi-based curvature and feature estimation from point clouds. *Visualization and Computer Graphics, IEEE Transactions on*, 17(6):743–756, 2011.

[Mou03] Ayman Mourad. *Description topologique de l'architecture fibreuse et modélisation mécanique du myocarde*. PhD thesis, Institut National Polytechnique de Grenoble-INPG, 2003.

[MS05] Facundo Mémoli and Guillermo Sapiro. Distance functions and geodesics on submanifolds of \r^d and point clouds. *SIAM Journal on Applied Mathematics*, 65(4):1227–1260, 2005.

[MT04] Jean-Marie Morvan and Boris Thibert. Approximation of the normal vector field and the area of a smooth surface. *Discrete & Computational Geometry*, 32(3):383–400, 2004.

[Nas54] J. F. Nash. C^1-isometric imbeddings. *Ann. of Math.*, 60(3):383–396, 1954.

[NSW08] Partha Niyogi, Stephen Smale, and Shmuel Weinberger. Finding the homology of submanifolds with high confidence from random samples. *Discrete & Computational Geometry*, 39(1-3):419–441, 2008.

[Oli03] V.I. Oliker. Mathematical aspects of design of beam shaping surfaces in geometrical optics. *Trends in Nonlinear Analysis*, pages 193–224, 2003.

[Pav82] T. Pavlidis. *Algorithms for graphics and image processing*. Computer science press, 1982.

[PC05] Gabriel Peyré and Laurent Cohen. Geodesic computations for fast and accurate surface remeshing and parameterization. In *Elliptic and Parabolic Problems*, pages 157–171. Springer, 2005.

[Pet07] Anton Petrunin. Semiconcave functions in alexandrov's geometry. *Surveys in differential geometry*, 11:137–201, 2007.

[PTSB01] Valérie Pham-Trong, Nicolas Szafran, and Luc Biard. Pseudo-geodesics on three-dimensional surfaces and pseudo-geodesic meshes. *Numerical Algorithms*, 26(4):305–315, 2001.

[RR86] Jaroslaw R Rossignac and Aristides AG Requicha. Offsetting operations in solid modelling. *Computer Aided Geometric Design*, 3(2):129–148, 1986.

[RZ03] Jan Rataj and Martina Zähle. Normal cycles of lipschitz manifolds by approximation with parallel sets. *Differential Geometry and its Applications*, 19(1):113–126, 2003.

[RZ05] Jan Rataj and Martina Zähle. General normal cycles and lipschitz manifolds of bounded curvature. *Annals of Global Analysis and Geometry*, 27(2):135–156, 2005.

[Sch73] L. Schlaefli. Nota alla memoria del sig. beltrami, sugli spazii di curvatura constante. *Ann. di mat., 2nd série*, (5):170–193, 1870-1873.

[Ser82] J. Serra. *Image analysis and mathematical morphology*. Academic Press, 1982.

[SK05] P. Stelldinger and U. Köthe. Towards a general sampling theory for shape preservation. *Image and Vision Computing*, 23(2):237–248, 2005.

[SLS07] P. Stelldinger, L. J. Latecki, and M. Siqueira. Topological equivalence between a 3d object and the reconstruction of its digital image. *IEEE Transactions on Pattern Analysis and Machine Intelligence*, 29(1):126–140, 2007.

[Str79] Daniel D Streeter. Gross morphology and fiber geometry of the heart. *Handbook of physiology*, pages 61–112, 1979.

[Wan96] Xu-Jia Wang. On the design of a reflector antenna. *Inverse problems*, 12(3):351, 1996.

[Wan04] X.J. Wang. On the design of a reflector antenna ii. *Calculus of Variations and Partial Differential Equations*, 20(3):329–341, 2004.

[Wey39] Hermann Weyl. On the volume of tubes. *American Journal of Mathematics*, pages 461–472, 1939.

[Win82] Peter Wintgen. Normal cycle and integral curvature for polyhedra in riemannian manifolds. *Differential Geometry. North-Holland Publishing Co., Amsterdam-New York*, 1982.

[Zäh86] Martina Zähle. Integral and current representation of federer's curvature measures. *Archiv der Mathematik*, 46(6):557–567, 1986.